Study of multi-muon events produced in p\bar{p} interactions at \sqrt{s}=1.96 TeV

Aaltonen, Timo

2010

Aaltonen , T , Mehtälä , P , Orava , R , Mäki , T , Saarikko , H , Österberg , K & CDF Collaboration 2010 , ' Study of multi-muon events produced in p\bar{p} interactions at \sqrt{s}=1.96 TeV ' , European Physical Journal C. Particles and Fields , vol. 68 , no. 1-2 , pp. 109-118 . https://doi.org/10.1140/epjc/s10052-010-1336-0

http://hdl.handle.net/10138/24605
https://doi.org/10.1140/epjc/s10052-010-1336-0

FERMILAB-PUB-08-046-E

Study of multi-muon events produced in $p\bar{p}$ collisions at $\sqrt{s} = 1.96$ TeV

T. Aaltonen,[21] J. Adelman,[11] B. Álvarez González,[9] S. Amerio[x],[35] D. Amidei,[28] A. Anastassov,[31] J. Antos,[12] G. Apollinari,[15] A. Apresyan,[39] T. Arisawa,[44] A. Artikov,[13] W. Ashmanskas,[15] P. Azzurri[aa],[37] W. Badgett,[15] B.A. Barnett,[23] V. Bartsch,[25] D. Beecher,[25] S. Behari,[23] G. Bellettini[y],[37] D. Benjamin,[14] I. Bizjak[dd],[25] C. Blocker,[6] B. Blumenfeld,[23] A. Bocci,[14] V. Boisvert,[40] G. Bolla,[39] D. Bortoletto,[39] J. Boudreau,[38] A. Bridgeman,[22] L. Brigliadori,[35] C. Bromberg,[29] E. Brubaker,[11] J. Budagov,[13] H.S. Budd,[40] S. Budd,[22] S. Burke,[15] K. Burkett,[15] G. Busetto[x],[35] P. Bussey[k],[19] K. L. Byrum,[2] S. Cabrera[u],[14] C. Calancha,[26] M. Campanelli,[29] F. Canelli,[15] B. Carls,[22] R. Carosi,[37] S. Carrillo[m],[16] B. Casal,[9] M. Casarsa,[15] A. Castro[w],[5] P. Catastini[z],[37] D. Cauz[cc],[42] V. Cavaliere[z],[37] S.H. Chang,[24] Y.C. Chen,[1] M. Chertok,[7] G. Chiarelli,[37] G. Chlachidze,[15] K. Cho,[24] D. Chokheli,[13] J.P. Chou,[20] K. Chung,[10] Y.S. Chung,[40] C.I. Ciobanu,[36] M.A. Ciocci[z],[37] A. Clark,[18] D. Clark,[6] G. Compostella,[35] M.E. Convery,[15] J. Conway,[7] M. Cordelli,[17] G. Cortiana[x],[35] C.A. Cox,[7] D.J. Cox,[7] F. Crescioli[y],[37] C. Cuenca Almenar[u],[7] J. Cuevas[r],[9] J.C. Cully,[28] D. Dagenhart,[15] M. Datta,[15] T. Davies,[19] P. de Barbaro,[40] M. Dell'Orso[y],[37] L. Demortier,[41] J. Deng,[14] M. Deninno,[5] G.P. di Giovanni,[36] B. Di Ruzza[cc],[42] J.R. Dittmann,[4] S. Donati[y],[37] J. Donini,[35] T. Dorigo,[35] J. Efron,[32] R. Erbacher,[7] D. Errede,[22] S. Errede,[22] R. Eusebi,[15] W.T. Fedorko,[11] J.P. Fernandez,[26] R. Field,[16] G. Flanagan,[39] R. Forrest,[7] M.J. Frank,[4] M. Franklin,[20] J.C. Freeman,[15] I. Furic,[16] M. Gallinaro,[41] J. Galyardt,[10] F. Garberson,[8] J.E. Garcia,[18] A.F. Garfinkel,[39] K. Genser,[15] H. Gerberich,[22] D. Gerdes,[28] V. Giakoumopoulou,[3] P. Giannetti,[37] K. Gibson,[38] J.L. Gimmell,[40] C.M. Ginsburg,[15] N. Giokaris,[3] M. Giordani[cc],[42] P. Giromini,[17] G. Giurgiu,[23] V. Glagolev,[13] D. Glenzinski,[15] N. Goldschmidt,[16] A. Golossanov,[15] G. Gomez,[9] M. Goncharov,[27] O. González,[26] I. Gorelov,[30] A.T. Goshaw,[14] K. Goulianos,[41] A. Gresele[x],[35] S. Grinstein,[20] J. Guimaraes da Costa,[20] Z. Gunay-Unalan,[29] K. Hahn,[27] S.R. Hahn,[15] B.-Y. Han,[40] J.Y. Han,[40] F. Happacher,[17] M. Hare,[43] R.M. Harris,[15] M. Hartz,[38] K. Hatakeyama,[41] S. Hewamanage,[4] D. Hidas,[14] C.S. Hill[c],[8] A. Hocker,[15] S. Hou,[1] R.E. Hughes,[32] J. Huston,[29] J. Incandela,[8] A. Ivanov,[7] E.J. Jeon,[24] M.K. Jha,[5]

S. Jindariani,[15] W. Johnson,[7] M. Jones,[39] K.K. Joo,[24] S.Y. Jun,[10] J.E. Jung,[24] D. Kar,[16] Y. Kato,[34] B. Kilminster,[15] D.H. Kim,[24] H.S. Kim,[24] H.W. Kim,[24] J.E. Kim,[24] M.J. Kim,[17] S.B. Kim,[24] Y.K. Kim,[11] L. Kirsch,[6] S. Klimenko,[16] B. Knuteson,[27] B.R. Ko,[14] D.J. Kong,[24] J. Konigsberg,[16] A. Korytov,[16] D. Krop,[11] N. Krumnack,[4] M. Kruse,[14] V. Krutelyov,[8] N.P. Kulkarni,[45] Y. Kusakabe,[44] S. Kwang,[11] A.T. Laasanen,[39] S. Lami,[37] R.L. Lander,[7] K. Lannon[q],[32] G. Latino[z],[37] I. Lazzizzera[x],[35] H.S. Lee,[11] S. Leone,[37] M. Lindgren,[15] A. Lister,[7] D.O. Litvintsev,[15] M. Loreti[x],[35] L. Lovas,[12] D. Lucchesi[x],[35] P. Lukens,[15] G. Lungu,[41] R. Lysak,[12] R. Madrak,[15] K. Maeshima,[15] K. Makhoul,[27] T. Maki,[21] P. Maksimovic,[23] A. Manousakis-Katsikakis,[3] F. Margaroli,[39] C.P. Marino,[22] V. Martin[l],[19] R. Martínez-Ballarín,[26] M. Mathis,[23] P. Mazzanti,[5] P. Mehtala,[21] P. Merkel,[39] C. Mesropian,[41] T. Miao,[15] N. Miladinovic,[6] R. Miller,[29] C. Mills,[20] A. Mitra,[1] G. Mitselmakher,[16] N. Moggi,[5] C.S. Moon,[24] R. Moore,[15] A. Mukherjee,[15] R. Mumford,[23] M. Mussini[w],[5] J. Nachtman,[15] I. Nakano,[33] A. Napier,[43] V. Necula,[14] O. Norniella,[22] E. Nurse,[25] S.H. Oh,[14] Y.D. Oh,[24] I. Oksuzian,[16] T. Okusawa,[34] R. Orava,[21] S. Pagan Griso[x],[35] E. Palencia,[15] V. Papadimitriou,[15] A.A. Paramonov,[11] B. Parks,[32] G. Pauletta[cc],[42] M. Paulini,[10] D.E. Pellett,[7] A. Penzo,[42] T.J. Phillips,[14] G. Piacentino,[37] L. Pinera,[16] K. Pitts,[22] O. Poukhov*,[13] F. Prakoshyn,[13] A. Pronko,[15] F. Ptohos[i],[15] E. Pueschel,[10] A. Rahaman,[38] N. Ranjan,[39] I. Redondo,[26] V. Rekovic,[30] F. Rimondi[w],[5] A. Robson,[19] T. Rodrigo,[9] E. Rogers,[22] S. Rolli,[43] R. Roser,[15] M. Rossi,[42] R. Rossin,[8] A. Ruiz,[9] J. Russ,[10] V. Rusu,[15] W.K. Sakumoto,[40] L. Santi[cc],[42] K. Sato,[15] A. Savoy-Navarro,[36] P. Schlabach,[15] E.E. Schmidt,[15] M.A. Schmidt,[11] M. Schmitt,[31] T. Schwarz,[7] L. Scodellaro,[9] A. Sedov,[39] S. Seidel,[30] Y. Seiya,[34] A. Semenov,[13] L. Sexton-Kennedy,[15] F. Sforza,[37] A. Sfyrla,[22] S.Z. Shalhout,[45] S. Shiraishi,[11] M. Shochet,[11] A. Sidoti,[37] A. Sisakyan,[13] A.J. Slaughter,[15] J. Slaunwhite,[32] K. Sliwa,[43] J.R. Smith,[7] A. Soha,[7] V. Sorin,[29] P. Squillacioti[z],[37] R. St. Denis,[19] D. Stentz,[31] J. Strologas,[30] G.L. Strycker,[28] J.S. Suh,[24] A. Sukhanov,[16] I. Suslov,[13] R. Takashima,[33] R. Tanaka,[33] M. Tecchio,[28] P.K. Teng,[1] K. Terashi,[41] J. Thom[h],[15] A.S. Thompson,[19] G.A. Thompson,[22] P. Ttito-Guzmán,[26] S. Tokar,[12] K. Tollefson,[29] S. Torre,[17] D. Torretta,[15] P. Totaro[cc],[42] S. Tourneur,[36] M. Trovato,[37] S.-Y. Tsai,[1] S. Vallecorsa,[18]

* Deceased

N. van Remortel[b],[21] A. Varganov,[28] E. Vataga[aa],[37] F. Vázquez[m],[16] G. Velev,[15] C. Vellidis,[3] V. Veszpremi,[39] M. Vidal,[26] R. Vidal,[15] I. Vila,[9] R. Vilar,[9] T. Vine,[25] M. Vogel,[30] G. Volpi[y],[37] R.G. Wagner,[2] R.L. Wagner,[15] T. Wakisaka,[34] S.M. Wang,[1] B. Whitehouse,[43] E. Wicklund,[15] S. Wilbur,[11] P. Wittich[h],[15] S. Wolbers,[15] C. Wolfe,[11] T. Wright,[28] X. Wu,[18] K. Yamamoto,[34] U.K. Yang[o],[11] Y.C. Yang,[24] K. Yorita,[11] T. Yoshida,[34] G.B. Yu,[40] I. Yu,[24] S.S. Yu,[15] J.C. Yun,[15] A. Zanetti,[42] X. Zhang,[22] and S. Zucchelli[w],[5]

(CDF Collaboration[†])

[1]*Institute of Physics, Academia Sinica, Taipei, Taiwan 11529, Republic of China*

[2]*Argonne National Laboratory, Argonne, Illinois 60439*

[3]*University of Athens, 157 71 Athens, Greece*

[4]*Baylor University, Waco, Texas 76798*

[5]*Istituto Nazionale di Fisica Nucleare Bologna, [w] University of Bologna, I-40127 Bologna, Italy*

[6]*Brandeis University, Waltham, Massachusetts 02254*

[7]*University of California, Davis, Davis, California 95616*

[8]*University of California, Santa Barbara, Santa Barbara, California 93106*

[9]*Instituto de Fisica de Cantabria, CSIC-University of Cantabria, 39005 Santander, Spain*

[10]*Carnegie Mellon University, Pittsburgh, PA 15213*

[11]*Enrico Fermi Institute, University of Chicago, Chicago, Illinois 60637*

[†] With visitors from [a]University of Massachusetts Amherst, Amherst, Massachusetts 01003, [b]Universiteit Antwerpen, B-2610 Antwerp, Belgium, [c]University of Bristol, Bristol BS8 1TL, United Kingdom, [d]Chinese Academy of Sciences, Beijing 100864, China, [e]Istituto Nazionale di Fisica Nucleare, Sezione di Cagliari, 09042 Monserrato (Cagliari), Italy, [f]University of California Irvine, Irvine, CA 92697, [g]University of California Santa Cruz, Santa Cruz, CA 95064, [h]Cornell University, Ithaca, NY 14853, [i]University of Cyprus, Nicosia CY-1678, Cyprus, [j]University College Dublin, Dublin 4, Ireland, [k]Royal Society of Edinburgh/Scottish Executive Support Research Fellow, [l]University of Edinburgh, Edinburgh EH9 3JZ, United Kingdom, [m]Universidad Iberoamericana, Mexico D.F., Mexico, [n]Queen Mary, University of London, London, E1 4NS, England, [o]University of Manchester, Manchester M13 9PL, England, [p]Nagasaki Institute of Applied Science, Nagasaki, Japan, [q]University of Notre Dame, Notre Dame, IN 46556, [r]University de Oviedo, E-33007 Oviedo, Spain, [s]Simon Fraser University, Vancouver, British Columbia, Canada V6B 5K3, [t]Texas Tech University, Lubbock, TX 79409, [u]IFIC(CSIC-Universitat de Valencia), 46071 Valencia, Spain, [v]University of Virginia, Charlottesville, VA 22904, [dd]On leave from J. Stefan Institute, Ljubljana, Slovenia,

[12] *Comenius University, 842 48 Bratislava, Slovakia; Institute of Experimental Physics, 040 01 Kosice, Slovakia*

[13] *Joint Institute for Nuclear Research, RU-141980 Dubna, Russia*

[14] *Duke University, Durham, North Carolina 27708*

[15] *Fermi National Accelerator Laboratory, Batavia, Illinois 60510*

[16] *University of Florida, Gainesville, Florida 32611*

[17] *Laboratori Nazionali di Frascati, Istituto Nazionale di Fisica Nucleare, I-00044 Frascati, Italy*

[18] *University of Geneva, CH-1211 Geneva 4, Switzerland*

[19] *Glasgow University, Glasgow G12 8QQ, United Kingdom*

[20] *Harvard University, Cambridge, Massachusetts 02138*

[21] *Division of High Energy Physics, Department of Physics, University of Helsinki and Helsinki Institute of Physics, FIN-00014, Helsinki, Finland*

[22] *University of Illinois, Urbana, Illinois 61801*

[23] *The Johns Hopkins University, Baltimore, Maryland 21218*

[24] *Center for High Energy Physics: Kyungpook National University, Daegu 702-701, Korea; Seoul National University, Seoul 151-742, Korea; Sungkyunkwan University, Suwon 440-746, Korea; Korea Institute of Science and Technology Information, Daejeon, 305-806, Korea; Chonnam National University, Gwangju, 500-757, Korea*

[25] *University College London, London WC1E 6BT, United Kingdom*

[26] *Centro de Investigaciones Energeticas Medioambientales y Tecnologicas, E-28040 Madrid, Spain*

[27] *Massachusetts Institute of Technology, Cambridge, Massachusetts 02139*

[28] *University of Michigan, Ann Arbor, Michigan 48109*

[29] *Michigan State University, East Lansing, Michigan 48824*

[30] *University of New Mexico, Albuquerque, New Mexico 87131*

[31] *Northwestern University, Evanston, Illinois 60208*

[32] *The Ohio State University, Columbus, Ohio 43210*

[33] *Okayama University, Okayama 700-8530, Japan*

[34] *Osaka City University, Osaka 588, Japan*

[35] Istituto Nazionale di Fisica Nucleare, Sezione di Padova-Trento,
[x] University of Padova, I-35131 Padova, Italy
[36] LPNHE, Universite Pierre et Marie
Curie/IN2P3-CNRS, UMR7585, Paris, F-75252 France
[37] Istituto Nazionale di Fisica Nucleare Pisa, [y] University of Pisa,
[z] University of Siena and [aa] Scuola Normale Superiore, I-56127 Pisa, Italy
[38] University of Pittsburgh, Pittsburgh, Pennsylvania 15260
[39] Purdue University, West Lafayette, Indiana 47907
[40] University of Rochester, Rochester, New York 14627
[41] The Rockefeller University, New York, New York 10021
[42] Istituto Nazionale di Fisica Nucleare Trieste/Udine,
[cc] University of Trieste/Udine, Italy
[43] Tufts University, Medford, Massachusetts 02155
[44] Waseda University, Tokyo 169, Japan
[45] Wayne State University, Detroit, Michigan 48201

Abstract

We report a study of multi-muon events produced at the Fermilab Tevatron collider and recorded by the CDF II detector. In a data set acquired with a dedicated dimuon trigger and corresponding to an integrated luminosity of 2100 pb^{-1}, we isolate a significant sample of events in which at least one of the muon candidates is produced outside of the beam pipe of radius 1.5 cm. The production cross section and kinematics of events in which both muon candidates are produced inside the beam pipe are successfully modeled by known QCD processes which include heavy flavor production. In contrast, we are presently unable to fully account for the number and properties of the remaining events, in which at least one muon candidate is produced outside of the beam pipe, in terms of the same understanding of the CDF II detector, trigger, and event reconstruction. Several topological and kinematic properties of these events are presented in this paper. These events offer a plausible resolution to long-standing inconsistencies related to $b\bar{b}$ production and decay.

PACS numbers: 13.85.-t, 14.65.Fy, 14.80.-j

I. INTRODUCTION

This article presents the study of events, acquired with a dedicated dimuon trigger, that we are currently unable to fully explain with our understanding of the CDF II detector, trigger, and event reconstruction. We are continuing detailed studies with a longer timescale for completion, but we present here our current findings.

This study was motivated by the presence of several inconsistencies that affect or affected measurements of the $b\bar{b}$ production at the Tevatron: (a) the ratio of the observed $b\bar{b}$ correlated production cross section to the exact next-to-leading-order (NLO) QCD prediction [1] is measured to be $R = 1.15 \pm 0.21$ when b quarks are selected via secondary vertex identification, whereas this ratio is found to be significantly larger than two when identifying b quarks through their semileptonic decays [2]; (b) sequential semileptonic decays of single b quarks are supposedly the main source of dileptons with invariant mass smaller than that of b quarks, but the observed invariant mass spectrum is not well modeled by the simulation of this process [3]; and (c) the value of $\bar{\chi}$, the average time-integrated mixing probability of b flavored hadrons, derived from the ratio of muon pairs from semileptonic decays of b and $\bar{b}$ quarks with opposite and same sign charge, is measured at hadron colliders to be significantly larger than that measured by the LEP experiments [4, 5].

The first inconsistency (a) has been addressed in a recent study of the CDF collaboration [6]. That study uses a data sample acquired with a dedicated dimuon trigger to re-measure the correlated $\sigma_{b\to\mu,\bar{b}\to\mu}$ cross section. As in previous studies [4, 7], Ref. [6] makes use of the precision tracking provided by the CDF silicon microvertex detector to evaluate the fractions of muons due to the decays of long-lived b- and c-hadrons, and to the other background contributions. The new measurement is in good agreement with theoretical expectations ($R = 1.20 \pm 0.21$), as well as with analogous measurements that identify b quarks via secondary vertex identification. However, it is also substantially smaller than previous measurements of this cross section [7, 8]. The new CDF measurement [6] requires that both trigger muons arise from particles that have decayed inside the beam pipe of 1.5 cm radius. According to the simulation, approximately 96% of the known sources of dimuons, such as Drell-Yan, Υ, Z^0, and heavy flavor production, satisfy this condition. We will show that not only the rate, but also the kinematic properties of the events that satisfy this condition are correctly modeled by the simulation of known processes. However, this ar-

ticle also presents the observation of a much larger than expected sample of events that does not satisfy this condition. This component, which was present in previous measurements in which this decay-radius requirement was not made, will be described and investigated at length in this article.

We utilize the same dimuon data set, simulated samples, and analysis tools described in Ref. [6]. Section II describes the detector systems relevant to this analysis. The data selection and Monte Carlo simulation are briefly summarized in Sec. III. Section IV investigates differences in the experimental methods used to derive $\sigma_{b\to\mu,\bar{b}\to\mu}$ in Ref. [6] and in previous measurements, and isolates a larger than expected sample of events in which at least one muon candidate is produced beyond the beam pipe. Section V connects the presence of these events to the discrepancy between the observed and predicted invariant mass spectrum of lepton pairs produced by single b quark sequential decays. The properties of these events are explored in Secs. VI and VII. Our conclusions are summarized in Sec. VIII.

II. CDF II DETECTOR AND TRIGGER

CDF II is a multipurpose detector, equipped with a charged particle spectrometer and a finely segmented calorimeter. In this section, we describe the detector components that are relevant to this analysis. The description of these subsystems can be found in Refs. [9, 10, 11, 12, 13, 14, 15, 16, 17, 18]. Two devices inside the 1.4 T solenoid are used for measuring the momentum of charged particles: the silicon vertex detector (SVXII and ISL) and the central tracking chamber (COT). The SVXII detector consists of microstrip sensors arranged in six cylindrical shells with radii between 1.5 and 10.6 cm, and with a total z coverage [1] of 90 cm. The first SVXII layer, also referred to as the L00 detector, is made of single-sided sensors mounted on the beryllium beam pipe. The remaining five SVXII layers are made of double-sided sensors and are divided into three contiguous five-layer sections along the beam direction z. The vertex z-distribution for $p\bar{p}$ collisions is approximately described by a Gaussian function with a rms of 28 cm. The transverse profile

[1] In the CDF coordinate system, θ and ϕ are the polar and azimuthal angles of a track, respectively, defined with respect to the proton beam direction, z. The pseudorapidity η is defined as $-\ln\ \tan(\theta/2)$. The transverse momentum of a particle is $p_T = p\ \sin(\theta)$. The rapidity is defined as $y = 1/2 \cdot \ln((E + p_z)/(E - p_z))$, where E and p_z are the energy and longitudinal momentum of the particle associated with the track.

of the Tevatron beam is circular and has a rms spread of $\simeq 25$ μm in the horizontal and vertical directions. The SVXII single-hit resolution is approximately 11 μm and allows a track impact parameter [2] resolution of approximately 35 μm, when also including the effect of the beam transverse size. The two additional silicon layers of the ISL help to link tracks in the COT to hits in the SVXII. The COT is a cylindrical drift chamber containing 96 sense wire layers grouped into eight alternating superlayers of axial and stereo wires. Its active volume covers $|z| \leq 155$ cm and 40 to 140 cm in radius. The transverse momentum resolution of tracks reconstructed using COT hits is $\sigma(p_T)/p_T^2 \simeq 0.0017$ $[\mathrm{GeV}/c]^{-1}$. The trajectory of COT tracks is extrapolated into the SVXII detector, and tracks are refitted with additional silicon hits consistent with the track extrapolation.

The central muon detector (CMU) is located around the central electromagnetic and hadronic calorimeters, which have a thickness of 5.5 interaction lengths at normal incidence. The CMU detector covers a nominal pseudorapidity range $|\eta| \leq 0.63$ relative to the center of the detector, and is segmented into two barrels of 24 modules, each covering 15° in ϕ. Every module is further segmented into three submodules, each covering 4.2° in ϕ and consisting of four layers of drift chambers. The smallest drift unit, called a stack, covers a 1.2° angle in ϕ. Adjacent pairs of stacks are combined together into a tower. A track segment (hits in two out of four layers of a stack) detected in a tower is referred to as a CMU stub. A second set of muon drift chambers (CMP) is located behind an additional steel absorber of 3.3 interaction lengths. The chambers are 640 cm long and are arranged axially to form a box around the central detector. The CMP detector covers a nominal pseudorapidity range $|\eta| \leq 0.54$ relative to the center of the detector. Muons which produce a stub in both the CMU and CMP systems are called CMUP muons. The CMX muon detector consists of eight drift chamber layers and scintillation counters positioned behind the hadron calorimeter. The CMX detector extends the muon coverage to $|\eta| \leq 1$ relative to the center of the detector.

The luminosity is measured using gaseous Cherenkov counters (CLC) that monitor the rate of inelastic $p\bar{p}$ collisions. The inelastic $p\bar{p}$ cross section at $\sqrt{s} = 1960$ GeV is scaled from measurements at $\sqrt{s} = 1800$ GeV using the calculations in Ref. [19]. The integrated

[2] The impact parameter d is the distance of closest approach of a track to the primary event vertex in the transverse plane.

luminosity is determined with a 6% systematic uncertainty [20].

CDF uses a three-level trigger system. At Level 1 (L1), data from every beam crossing are stored in a pipeline capable of buffering data from 42 beam crossings. The L1 trigger either rejects events or copies them into one of the four Level 2 (L2) buffers. Events that pass the L1 and L2 selection criteria are sent to the Level 3 (L3) trigger, a cluster of computers running speed-optimized reconstruction code.

For this study, we select events with two muon candidates identified by the L1 and L2 triggers. The L1 trigger uses tracks with $p_T \geq 1.5$ GeV/c found by a fast track processor (XFT). The XFT examines COT hits from the four axial superlayers and provides $r-\phi$ information in azimuthal sections of 1.25°. The XFT passes the track information to a set of extrapolation units that determine the CMU towers in which a CMU stub should be found if the track is a muon. If a stub is found, a L1 CMU primitive is generated. The L1 dimuon trigger requires at least two CMU primitives, separated by at least two CMU towers. The L2 trigger additionally requires that at least one of the muons also has a CMP stub matched to an XFT track with $p_T \geq 3$ GeV/c. All these trigger requirements are emulated by the detector simulation on a run-by-run basis. The L3 trigger requires a pair of CMUP muons with invariant mass larger than 5 GeV/c^2, and $|\delta z_0| \leq 5$ cm, where z_0 is the z coordinate of the muon track at its point of closest approach to the beam line in the $r-\phi$ plane. These requirements define the dimuon trigger used in this analysis.

Two other triggers are also utilized to acquire calibration samples used in this analysis. We use events acquired requiring a L1 CMUP primitive with $p_T \geq 4$ GeV/c accompanied by a L2 requirement of an additional track with $p_T \geq 2$ GeV/c and impact parameter $0.12 \leq d \leq 1$ mm as measured by the Silicon Vertex Trigger (SVT) [21]. The SVT calculates the impact parameter of each XFT track, with respect to the beam line, with a 50 μm resolution that includes the 25 μm contribution of the beam transverse width. Events selected with this trigger, referred to as $\mu-$SVT, are used to verify the muon detector acceptance and the muon reconstruction efficiency. We use an additional trigger, referred to as CHARM, that acquires events with two SVT tracks with $p_T \geq 2$ GeV/c and with impact parameter $0.12 \leq d \leq 1.00$ mm. In this data sample, we reconstruct $D^0 \to K^-\pi^+$ decays to measure the probability that the punchthrough of a charged hadron mimics a muon signal.

III. DATA SELECTION AND MONTE CARLO SIMULATIONS

This study starts using the same data set and analysis selection criteria employed in the measurement of the correlated $b\bar{b}$ cross section [6], that corresponds to an integrated luminosity of 742 pb^{-1}. When extending the scope of that analysis, we also use larger data sets corresponding to integrated luminosities of 1426 and 2100 pb^{-1}. The correlated $b\bar{b}$ cross section measurement selects events acquired with the dimuon trigger and which contain at least two CMUP muons with same or opposite sign charge. If events contain more than two muons that pass our selection cuts, the two with the highest transverse momenta, referred to as initial muons, are considered. Events are reconstructed offline taking advantage of more refined calibration constants and reconstruction algorithms than those used by the L3 trigger. COT tracks are extrapolated into the SVXII detector, and refitted adding hits consistent with the track extrapolation. Stubs reconstructed in the CMU and CMP detectors are matched to tracks with $p_T \geq 3$ GeV/c. A track is identified as a CMUP muon if $\Delta r\phi$, the distance in the $r-\phi$ plane between the track projected to the CMU (CMP) chambers and a CMU (CMP) stub, is less than 30 (40) cm. We require that muon-candidate stubs correspond to a L1 CMU primitive, and correct the muon momentum for energy losses in the detector. We also require the z_0 distance between two muon candidates to be smaller than 1.5 cm. We reconstruct primary vertices using all tracks with SVXII hits that are consistent with originating from a common vertex. In events in which more than one interaction vertex has been reconstructed, we use the one closest in z to the average of the muon track z_0-positions and within a 6 cm distance. We evaluate the impact parameter of each muon track with respect to the primary vertex. The primary vertex coordinates transverse to the beam direction are measured with an accuracy of approximately 3 μm [6]. Cosmic rays are removed by requiring that the azimuthal angle between muons with opposite charge is smaller than 3.135 radians. Muon pairs arising from cascade decays of a single b quark are removed by selecting dimuon candidates with invariant mass greater than 5 GeV/c^2. We also reject muon pairs with invariant mass larger than 80 GeV/c^2 that are mostly contributed by Z^0 decays. The data sample that survives these selection criteria consists of 743006 events.

In this study, data are compared to different simulated samples. The heavy flavor production is simulated with the HERWIG Monte Carlo program [22], the settings of which are described in Appendix A of Ref. [6]. Hadrons with heavy flavors are subsequently decayed

using the EVTGEN Monte Carlo program [23]. The detector response to particles produced by the above generators is modeled with the CDF II detector simulation that in turn is based on the GEANT Monte Carlo program [24].

IV. STUDY OF THE DATA SAMPLE COMPOSITION

The procedure to extract $\sigma_{b\to\mu,\bar{b}\to\mu}$ from the data is to fit the observed impact parameter distributions of the selected muon pairs with the expected impact parameter distributions of muons from various sources. To ensure an accurate impact parameter measurement, Ref. [6] requires that each muon track is reconstructed in the SVXII detector with hits in the two inner layers and in at least two of the remaining four external layers. These SVXII quality requirements reduce the data sample to 143743 events. After this selection, the dominant sources of reconstructed muons are semileptonic decays of bottom and charmed hadrons, prompt decays of quarkonia, Drell-Yan production, and muons mimicked by prompt hadrons or hadrons arising from heavy flavor decays. In the following, the sum of these contributions will be referred to as QCD production. Monte Carlo simulations are used to model the impact parameter distributions of muons from b- and c-hadron decays. The impact parameter distribution of muons from prompt sources, such as quarkonia decays and Drell-Yan production, is constructed using muons from $\Upsilon(1S)$ decays. The sample composition determined by the fit is shown in Table I. The projection of the two-dimensional impact parameter distribution is compared to the fit result in Fig. 1. After removing the contribution of muons mimicked by hadrons from heavy flavor decays, the study in Ref. [6] determines the size of $b\bar{b}$ production to be 52400 ± 2747 events. For muons with $p_T \geq 3$ GeV/c and $|\eta| \leq 0.7$, Ref. [6] reports $\sigma_{b\to\mu,\bar{b}\to\mu} = 1549 \pm 133$ pb. The ratio of this cross section to the NLO prediction (1.20 ± 0.21) is appreciably smaller than that reported in previous measurements [7, 8], and in agreement with the correlated $b\bar{b}$ cross section measurements that select b quarks via secondary vertex identification (1.15 ± 0.21) [26, 27]. This result mitigates previous inconsistencies between measurements and theoretical predictions of the correlated $b\bar{b}$ cross section.

However, a new problem arises that concerns the sample composition when the requirement that muons are accurately measured in the SVXII detector is released. The study in Ref. [6] uses very strict selection criteria, referred to as tight SVX selection in the following,

TABLE I: Number of events attributed to the different dimuon sources by the fit to the muon impact-parameter distribution in the range $0 - 0.2$ cm. The fit parameters BB, CC, and PP represent the $b\bar{b}$, $c\bar{c}$, and prompt dimuon contributions, respectively. The component BC represents events containing b and c quarks. The fit parameter BP (CP) estimates the number of events in which there is only one b (c) quark in the detector acceptance and the second muon is produced by misidentified prompt hadrons. The data correspond to an integrated luminosity of 742 pb^{-1}.

Component	No. of Events
BB	54583 ± 678
CC	24458 ± 1565
PP	41556 ± 651
BP	10598 ± 744
CP	10024 ± 1308
BC	2165 ± 693

by requiring muon tracks with hits in the first two layers of the SVXII detector, and at least in two of the remaining four outer layers. This requirement selects muon parent particles which decayed within a distance of $\simeq 1.5$ cm from the nominal beam line, or in other words inside the beam pipe. According to the simulation, approximately 96% of dimuons due to known QCD processes, such as Drell-Yan, Υ, Z^0, and heavy flavor production, satisfy this latter condition. The efficiency of the tight SVX requirements for prompt dimuons is purely geometrical, and is measured to be 0.257 ± 0.004 by using $\Upsilon(1S)$ candidates [6]. For dimuons arising from heavy flavor production, the efficiency of the tight SVX selection is determined to be 0.237 ± 0.001 by using muons from J/ψ decays after reweighting their p_T distribution to be equal to that of muons from simulated decays of heavy flavors. As shown by Fig. 2 (a), the 7% decrease of the efficiency for heavy flavors is due to a small fraction of high-p_T b hadrons decaying after the first SVXII layer. Using the sample composition determined by the fit to the muon impact parameter distribution, listed in Table I, we estimate that (24.4 ± 0.2)% of the initial data sample survives the tight SVX requirements.

Analyses performed by the CDF collaboration customarily select tracks for secondary vertexing purposes with less stringent requirements, such as tracks with hits in at least three

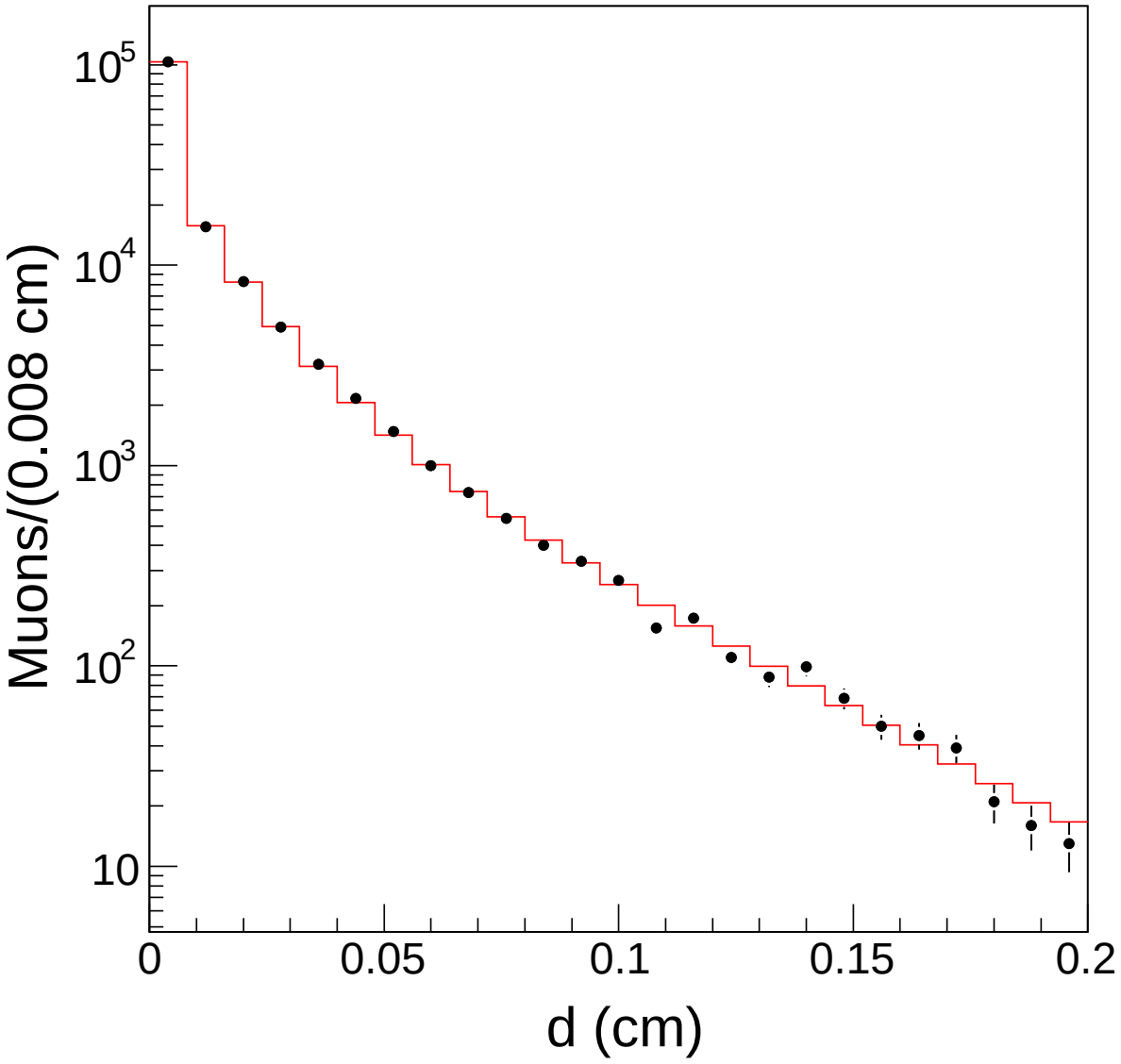

FIG. 1: The projection of the two-dimensional impact parameter distribution of muon pairs onto one of the two axes is compared to the fit result (histogram).

out of the eight layers of the SVXII and ISL detectors (referred to as loose SVX selection in the following). The latter selection accepts muons from parent particles with a decay length as long as $\simeq$ 10 cm. As shown by Fig. 2 (b), in this case the SVX selection efficiency is much higher and does not depend on the dimuon invariant mass. By using $\Upsilon(1S)$ and J/ψ candidates, we measure the efficiency of the loose SVX requirements to be 0.88 ± 0.01. The acceptance of the different SVX selections as a function of the decay length of the muon

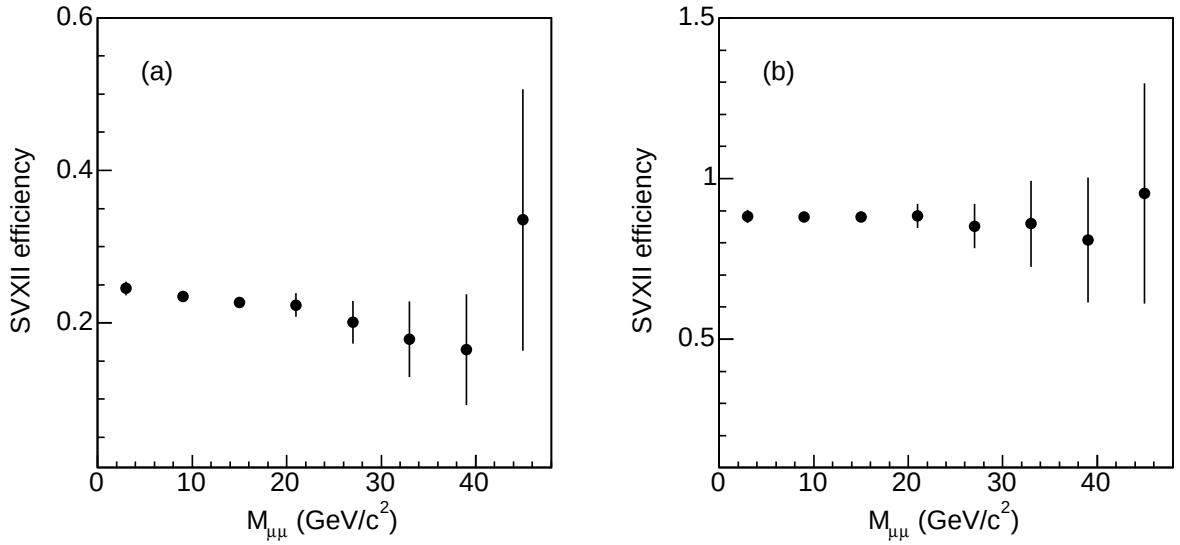

FIG. 2: Efficiency of SVX tight (a) and loose (b) selection in simulated dimuon events due to heavy flavor production (see text). The efficiency is shown as a function of the dimuon invariant mass.

parent particle is verified using cosmic muons that overlap in time with a $p\bar{p}$ collision (for this purpose we remove the request that the azimuthal angle between two initial muons be less than 3.135 radians). Cosmic muons, which are reconstructed as two back-to-back muons of opposite charge, cluster along the diagonal of the two-dimensional distribution of the muon impact parameters. As shown in Fig. 3, the loose SVX selection accepts larger decay lengths than the tight SVX selection. As shown by the scatter of the points along the $d_1 = d_2$ diagonal, both SVX selections yield rms resolutions that are negligible on a scale of the order of centimeters.

If the dimuon sample before the tight SVX selection (743006 events) had the same composition of the sample listed in Table I (143743 events), the average efficiency of the tight SVX requirements in this data set would be 0.244 ± 0.002, whereas it is found to be 0.1930 ± 0.0004. This feature suggests the presence of a large background that, unlike the QCD contribution, is significantly suppressed by the tight SVX selection. Because it went unnoticed for a long time, this background will be whimsically referred to as the ghost contribution in the following. In the assumption that the contribution of ghost events to the dimuon sample selected with tight SVX requirements is negligible, the size of the ghost sample can be estimated as the difference between the number of muon pairs prior to any SVX requirements and the number of muons passing the tight SVX selection divided by the efficiency of the tight SVX

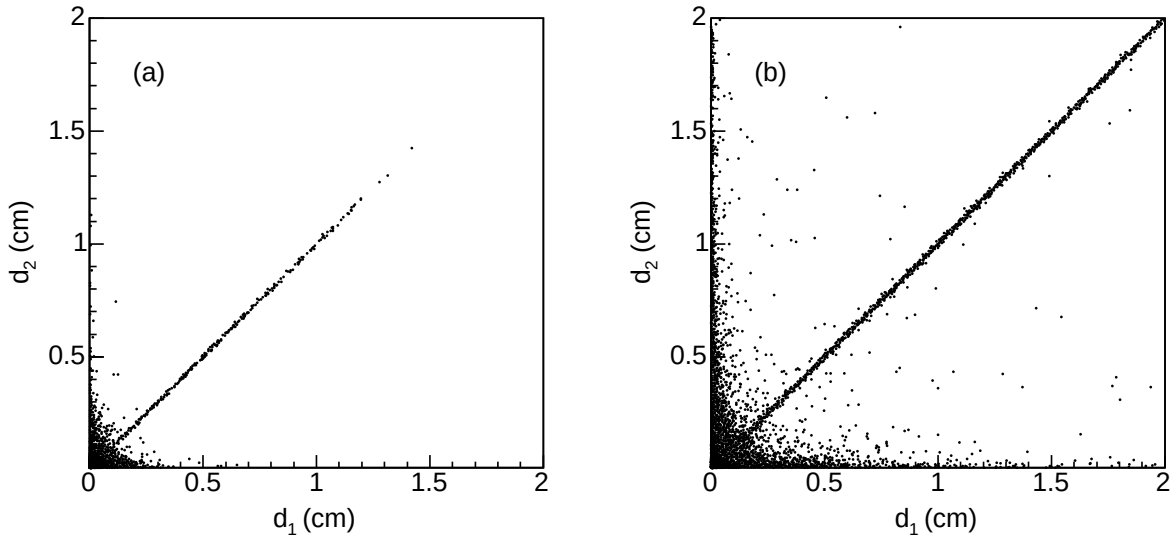

FIG. 3: Two-dimensional impact parameter distributions of muons that pass the (a) tight and (b) loose SVX requirements. Cosmic muons are reconstructed as two back-to-back muons of opposite charge and cluster along the $d_1 = d_2$ diagonal.

requirements (see Table II). In Table II, the contribution of ghost events to dimuons that pass the loose SVX requirements is determined as the difference between the numbers of events that pass the loose SVX requirements and of events that pass the tight SVX requirements, divided by the efficiency of the tight SVX requirements and multiplied by that of the loose SVX requirements. The size of the ghost sample (153895 $\pm$ 4829 events) is of a magnitude comparable to $b\bar{b}$ production (221564$\pm$11615 events). When using the loose SVX requirements, the size of the ghost sample is reduced by a factor of two, whereas 88% of the dimuons due to known processes survive (the ghost size is 72553 $\pm$ 7264 events, whereas the $b\bar{b}$ contribution is 194976 $\pm$ 10221 events). Muon pairs in the ghost sample are equally split in opposite and same sign charge combinations.

We have investigated at length the possibility that ghost muons are a consequence of the experimental conditions of the present study. The appearance of ghost events does not depend on the instantaneous luminosity nor the presence of multiple $p\bar{p}$ interactions. We have investigated in many ways the possibility that ghost events are ordinary QCD events in which one of the initial muons appears to originate beyond the beam-pipe radius because of pattern recognition problems in the SVX or COT detectors (see Appendix A). As an example, we compare yields of $D^0 \to K^-\pi^+$ (and charge-conjugate) decays in QCD and

TABLE II: Number of events that pass different SVX requirements. QCD indicates the sum of the various components listed in Table I. Ghost indicates the additional background in the data. Dimuons are also split into pairs with opposite (OS) and same (SS) sign charge.

Type	Total	Tight SVX	Loose SVX
All	743006	143743	590970
All OS		98218	392020
All SS		45525	198950
QCD	589111 ± 4829	143743	518417 ± 7264
QCD OS		98218	354228 ± 4963
QCD SS		45525	164188 ± 2301
Ghost	153895 ± 4829	0	72553 ± 7264
Ghost OS		0	37792 ± 4963
Ghost SS		0	34762 ± 2301

ghost events. We search for D^0 candidates by using tracks of opposite sign charge, with $p_T \geq 1.0$ GeV/c, $|\eta| \leq 1.1$, and contained in a 60° cone around the direction of each initial muon. The two-track systems are constrained to arise from a common space point. Track combinations are discarded if the three-dimensional vertex fit returns a χ^2 larger than 10 or if the vertex is not in the hemisphere containing the D^0 candidate. We attribute the kaon mass to the track with the same charge as the initial muon (RS combination, as expected for $B \to \mu^- D^0$ decays). We also study wrong sign combinations (WS) attributing the kaon mass to the track with opposite charge. A D^0 signal found in the WS combinations is a measure of the fraction of fake muons, whereas a D^0 signal in RS combinations found in ghost events indicates a heavy flavor contribution. As shown in Figs. 4 (a) and (b), a clear D^0 signal is observed in QCD but not in ghost events. It is our conclusion that ghost events are not due to track reconstruction failures in normal QCD events.

The unnoticed presence of a ghost contribution of this size, that is incrementally reduced by stricter SVX requirements, can help explain the inconsistencies mentioned in the introduction. The general observation is that the measured $\sigma_{b\to\mu,\bar{b}\to\mu}$ increases as the SVX requirements are made looser and is almost a factor of two larger than that measured in

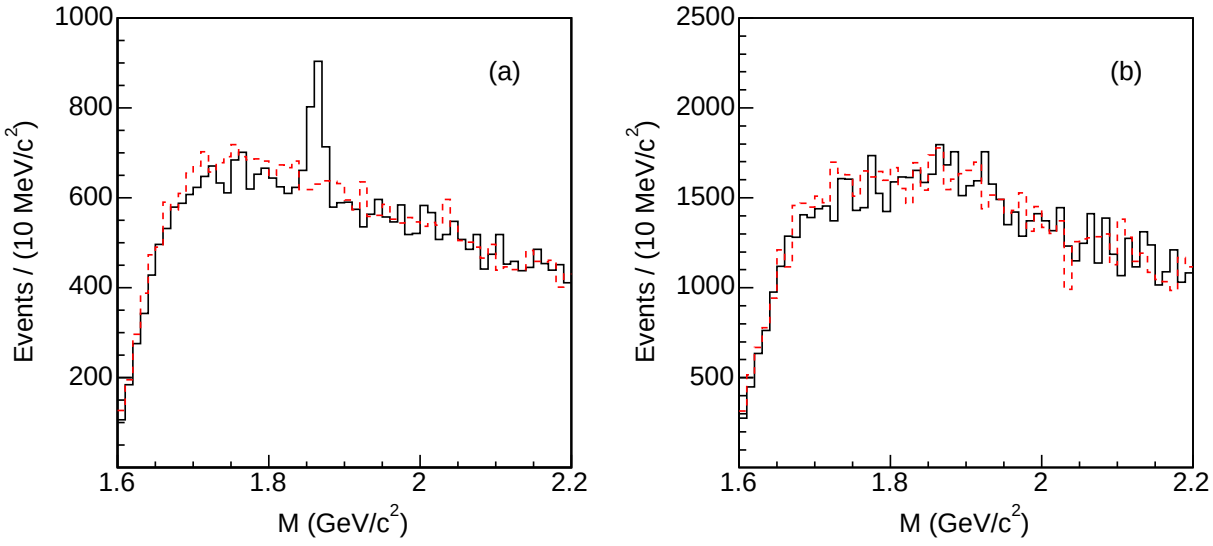

FIG. 4: Invariant mass, M, distributions of RS (histogram) and WS (dashed histogram) D^0 candidates in (a) QCD and (b) ghost events.

Ref. [6] when no SVX requirements are made [8]. As mentioned above, the magnitude of the ghost contribution is comparable to the $b\bar{b}$ contribution when no SVX selection is made and in combination would account for the measurement reported in Ref.[8]. Similarly, for the loose SVX criteria, the magnitude of the ghost contribution (72553 ± 7264 events equally split in OS and SS combinations), when added to the expected $b\bar{b}$ contribution of 194976 ± 10221 events, coincides with the cross section measurement reported in Ref.[7] and the $\bar{\chi}$ value reported in Ref.[4] since these measurements use similar sets of silicon criteria.

A. Ordinary sources of ghost events

In the following, we investigate several sources of ghost events that might not have been properly accounted for by previous experiments. Possible sources are: (a) semileptonic decays of hadrons with an unexpectedly large Lorentz boost; (b) muonic decays of particles with a lifetime longer than that of heavy flavors, such as K and π mesons; (c) decays of K^0_S mesons and hyperons; and (d) secondary interactions of prompt tracks that occur in the detector volume. In the last two cases, muons are predominantly produced by punchthrough of the secondary prongs that hit the muon detectors. Figure 5 shows the invariant mass of dimuon pairs before the tight SVX selection, and the efficiency of this selection as a function

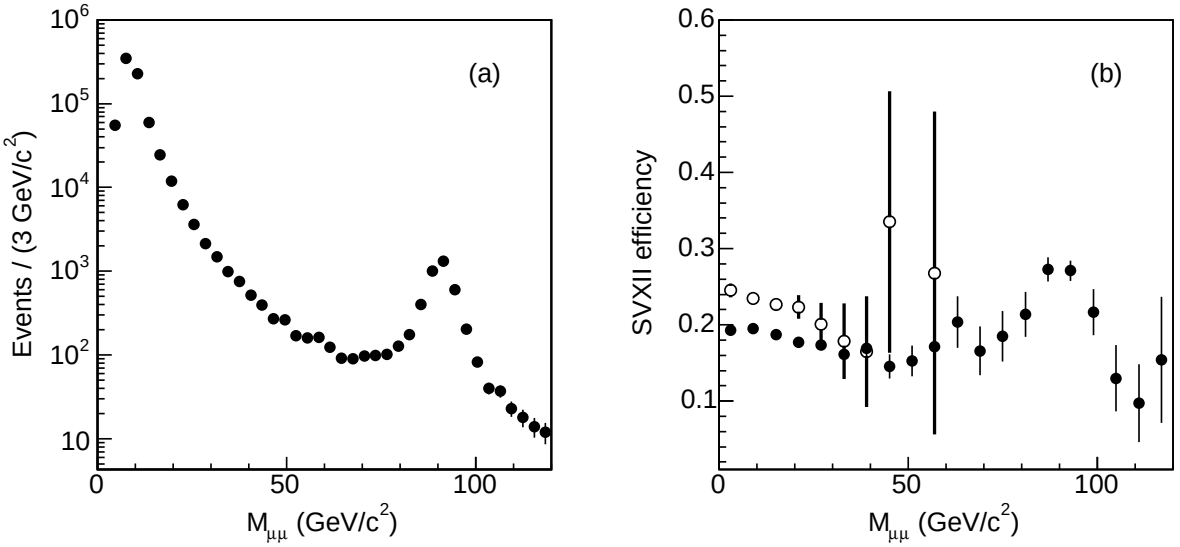

FIG. 5: Invariant mass distribution (a) of the dimuon pairs used in the study. The efficiency (b) of the tight SVX requirements as a function of the dimuon invariant mass in the data (•) is compared to that in the heavy flavor simulation (○).

of the dimuon invariant mass. The efficiency of tight SVX requirements in the data is below that in the simulation only for dimuon invariant masses smaller than 40 GeV/c^2, and then rises to the expected value of 0.257 where events are mostly contributed by prompt Z^0 decays. This feature does not favor the first hypothesis (a).

A long-lived particle contribution is suggested by the comparison of the impact parameter distribution of dimuons that pass the loose and tight SVX requirements. The request that muons pass loose SVX requirements is momentarily used to reduce the possible contribution of muons from secondary interactions occurring beyond the SVXII detector. We note that loose SVX requirements sculpt the impact parameter distribution of muons arising from the decay of objects with a lifetime much longer than that of b hadrons, such as π, K, or K^0_S mesons. Two-dimensional impact parameter distributions are shown in Fig. 6. One-dimensional distributions are shown in Fig. 7. The impact parameter distribution of muons in ghost events differs from that of the QCD contribution. According to the heavy flavor simulation [6], dimuons with impact parameter larger than 0.12 cm only arise from $b\bar{b}$ production. We fit the impact parameter distribution in Fig. 8 with the function $A\exp(-d/(c\tau))$ in the range $0.12 - 0.4$ cm. The best fit returns $c\tau = 469.7 \pm 1.3$ μm in agreement with the value 470.1 ± 2.7 μm expected for the b-hadron mixture at the Tevatron [5]. We conclude

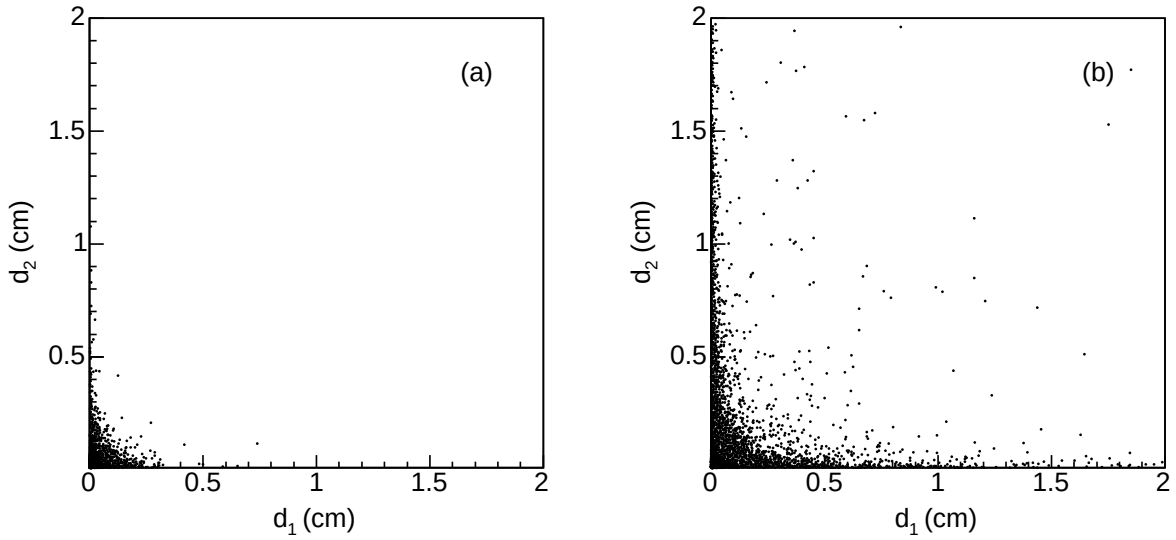

FIG. 6: Two-dimensional impact parameter distribution of dimuons that pass the (a) tight and (b) loose SVX requirements.

that the data sample selected with the tight SVX selection is not appreciably contaminated by ghost events. This supports our procedure for estimating the ghost size by assuming that the ghost contribution to events selected with tight SVX requirements is negligible. It also follows that the $b\bar{b}$ contribution to dimuons with impact parameter larger than 0.5 cm is negligible.

In ghost events, the presence of a large tail extending to high impact parameters suggests the contribution of particles with a lifetime much longer than that of b quarks, such as K^0_S, K and π mesons, and hyperons. We first investigate muons produced by pion and kaon in-flight-decays [source (b)]. As reported in Ref. [6], after having selected muon pairs with the tight SVX requirements, approximately 30% of the QCD contribution is due to prompt hadrons mimicking a muon signal. The size of the ghost sample has been estimated assuming that the efficiency of the tight SVX requirements for these tracks is the same as that for real muons. This is a reasonable assertion when fake muons are generated by hadronic punchthroughs. However, muons arising from π or K decays inside the tracking volume may yield misreconstructed tracks that are linked to hits in the SVXII detector less efficiently than real muons. We estimate this efficiency using pions and kaons produced in the large statistics heavy flavor simulation used to derive the dimuon acceptance for the $\sigma_{b\to\mu,\bar{b}\to\mu}$ measurement [6]. We use the quantity $\Delta^2 = 1/3\cdot[(\eta^h - \eta^{\rm track})^2/\sigma^2_\eta + (\phi^h - \phi^{\rm track})^2/\sigma^2_\phi + (1/p^h_T -$

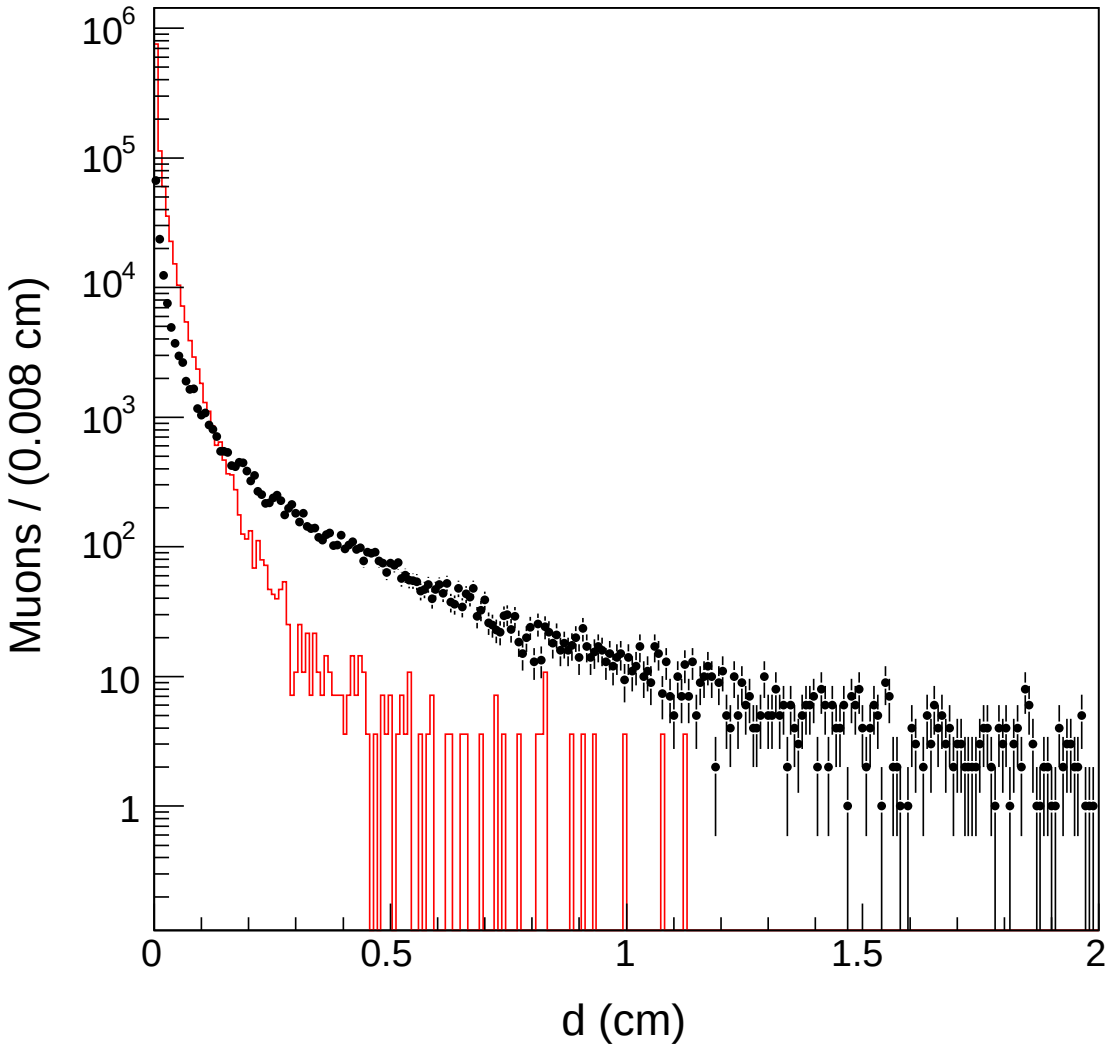

FIG. 7: Impact parameter distribution of muons contributed by ghost (•) and QCD (histogram) events. Muon tracks are selected with loose SVX requirements. The detector resolution is $\simeq 30$ μm, whereas bins are 80 μm wide.

$1/p_T^{\rm track})^2/\sigma^2_{1/p_T}]$ to measure the difference between the momentum vectors of the undecayed pions or kaons (h) and that of the closest reconstructed tracks [3]. Figure 9 shows the Δ distribution as a function of R, the decay distance from the beamline. One notes that most of the decays at radial distances $R \leq 120$ cm yield misreconstructed tracks. The numbers

[3] The assumed experimental resolutions are $\sigma_\phi[\text{rad}] = \sigma_\eta = 10^{-3}$ and $\sigma_{1/p_T} = 2 \cdot 10^{-3}$ [GeV/c]$^{-1}$.

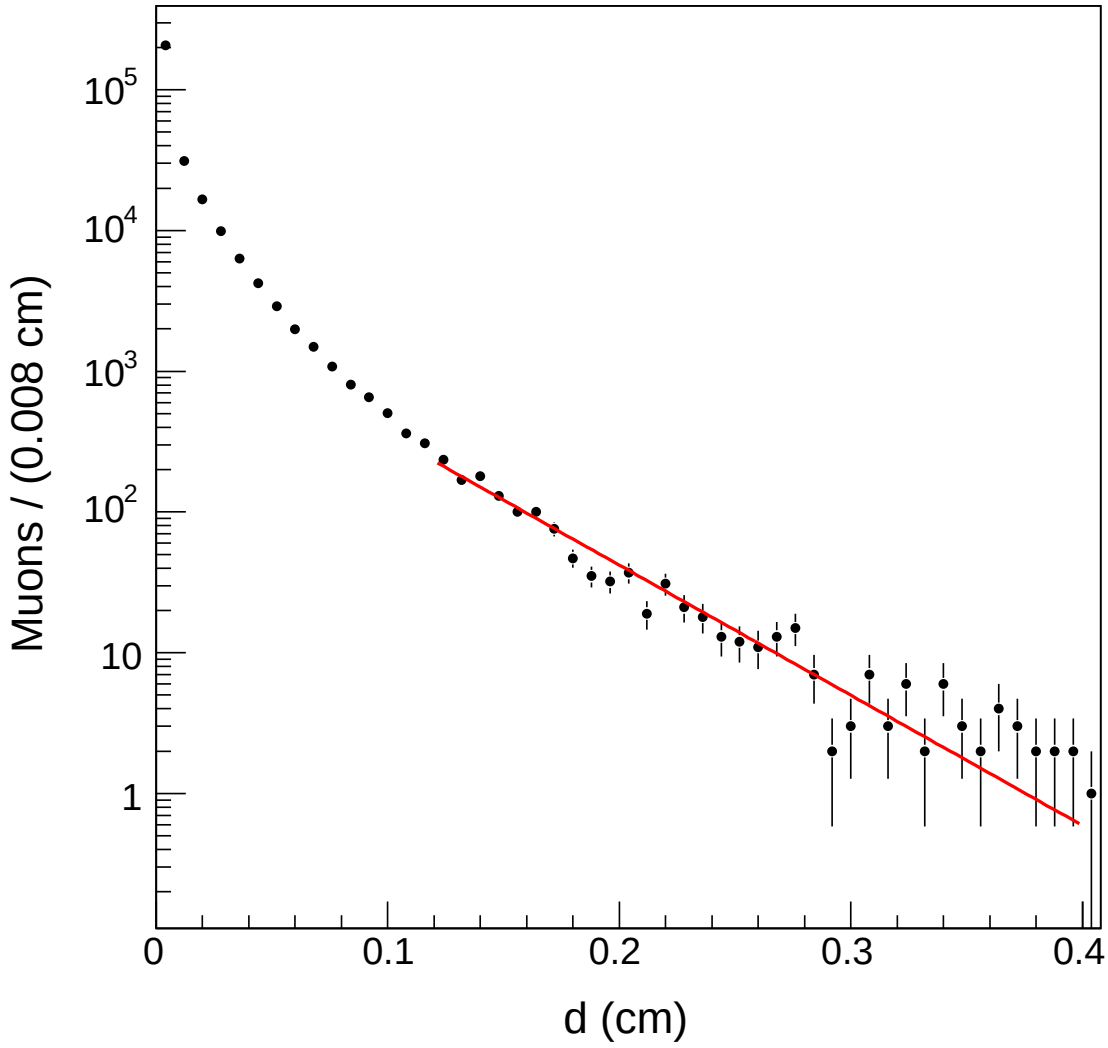

FIG. 8: Impact parameter distribution of muons that pass the tight SVX requirements. The line represents the fit described in the text.

of in-flight-decays that produce CMUP muons with $p_T \geq 3$ GeV/c, a L1 primitive, and which pass different SVX selections are listed in Table III. The efficiency of the tight SVX requirements for a single muon due to in-flight-decays (0.16 and 0.21 for π and K decays, respectively) is smaller than that for muons in QCD events ($\simeq 0.5$). The contributions of muons due to in-flight-decays to ghost events is evaluated using simulated events produced in generic-parton hard scattering [4]. In the simulation, there are 44000 track pairs per

[4] We use option 1500 of the HERWIG program to generate final states produced by hard scattering of

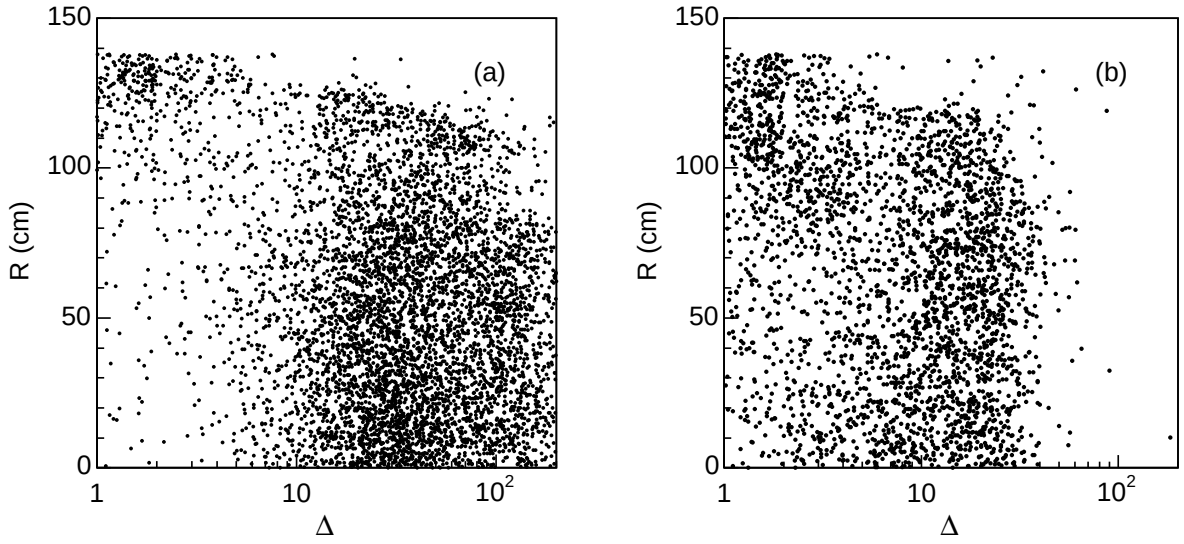

FIG. 9: Distribution of Δ (see text) as a function of the distance R of the (a) K and (b) π decay vertices from the beamline. For comparison, the analogous distribution for real muons from heavy flavor decays does not extend beyond $\Delta = 9$.

TABLE III: Number of pions and kaons corresponding to a misreconstructed track ($\Delta \geq 5$) with $p_T \geq 3$ GeV/c and $|\eta| \leq 0.7$, that decay inside the tracking volume, produce CMUP muons with a L1 primitive, and pass different SVX selections.

Selection	π	K
Tracks	2667199	1574610
In-flight-decays	14677	40561
CMUP+L1	1940	5430
Loose SVX	897	3032
Tight SVX	319	1135

CMUP pair due to $b\bar{b}$ production with the same kinematic acceptance ($p_T \geq 3$ GeV/c and $|\eta| \leq 0.7$). The ratio of the number of pions to that of kaons is approximately 5/1. Each simulated track in the kinematic acceptance is weighted with the corresponding in-flight-

partons with transverse momentum larger than 3 GeV/c [6].

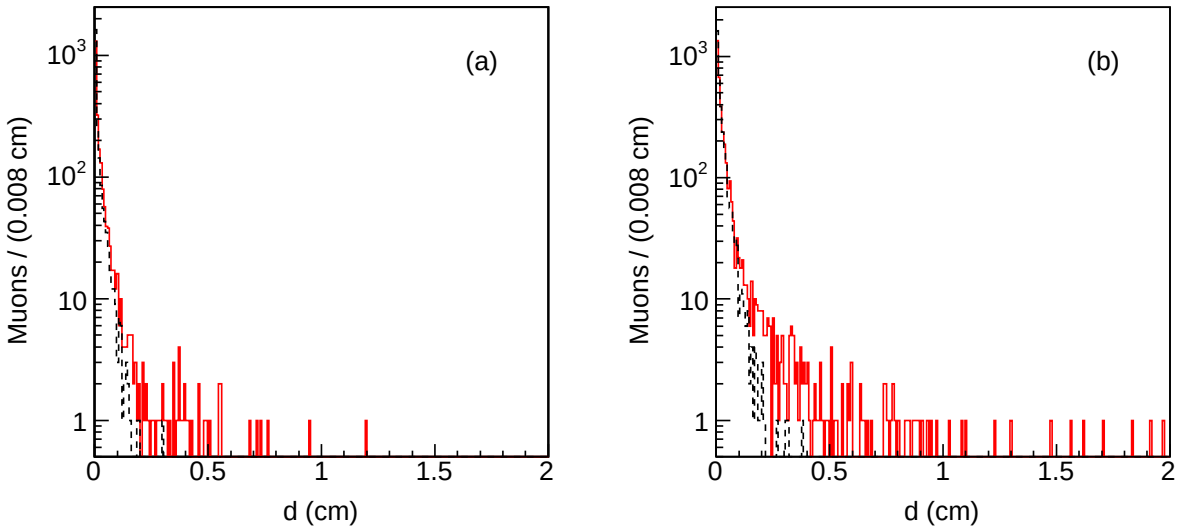

FIG. 10: Impact parameter distributions of simulated CMUP muons (histogram) that pass all analysis requirements, including the loose SVX selection, and arise from (a) pions and (b) kaon in-flight decays. The dashed histograms show the impact parameter of the parent pions and kaons.

decay probabilities of producing CMUP muons listed in Table III. Tracks are also weighted with the probabilities, measured in Ref. [6], that π or K punchthrough mimics a CMUP signal. In the latter case, the efficiency of the SVX requirement is the same as for real muons, and we ignore the cases in which both muons arise from hadronic punchthrough. Having normalized this simulation to the number of observed initial muons arising from $b\bar{b}$ production, we predict a contribution to ghost events due to in-flight-decays of pions and kaons that is 57000 events, 44% and 8% of which pass the loose and tight SVX selection, respectively. In the 25000 simulated events that pass the loose SVX selection, approximately 15000 muons arise from kaon in-flight-decays. These predictions depend on how well the HERWIG generator models generic parton hard scattering and its uncertainty is difficult to estimate. Figure 10 shows the impact parameter distribution of muons arising from in-flight-decays of pions and kaons produced in simulated $b\bar{b}$ and $c\bar{c}$ events. The number of events in Fig. 10 has to be multiplied by five in order to be compared with the data in Fig. 7. Our estimate of the number of muons arising from in-flight-decays accounts for 35% of the ghost muons, but for less than 10% of those with $d \geq 0.5$ cm.

In addition, muons in ghost events can be mimicked by the punchthrough of hadrons arising from the decay of K^0_S mesons or hyperons [source (c)]. We have searched the dimuon

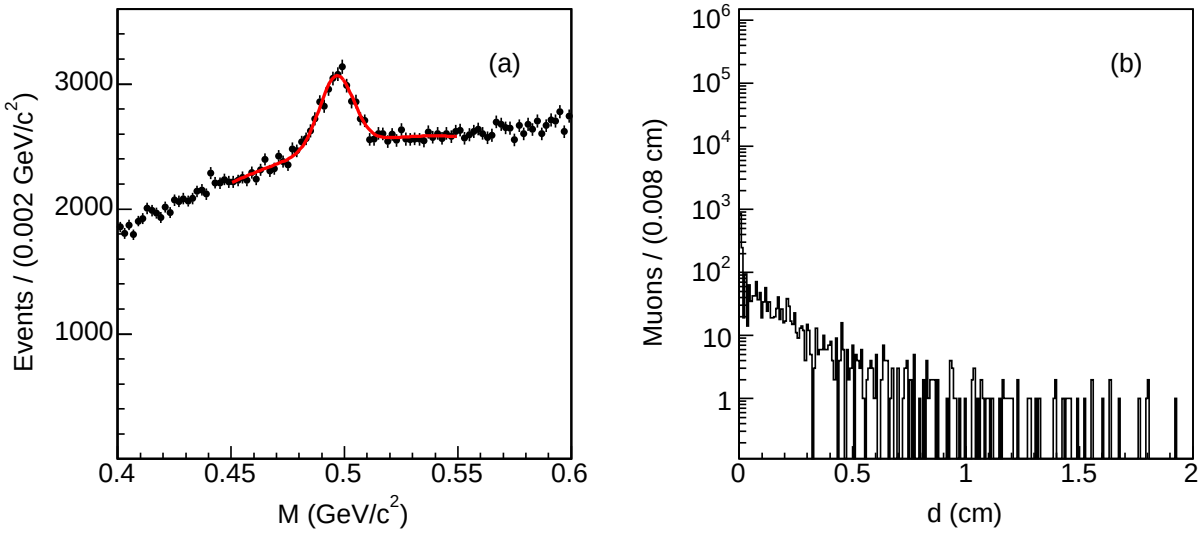

FIG. 11: Distributions of (a) the invariant mass of pairs of initial muons and opposite sign tracks and of (b) the impact parameter of initial muons, produced by K^0_S decays, that pass the loose SVX selection. The solid line represents a fit described in the text. In the impact parameter distribution, the combinatorial background is removed with a sideband subtraction method. For comparison, the vertical scale in (b) is kept the same as in Fig. 7.

data set for $K^0_S \to \pi^+\pi^-$ decays in which a pion punchthrough mimics the muon signal. We combine all initial muon tracks with all opposite sign tracks with $p_T \geq 0.5$ GeV/c contained in a 40° cone around the direction of the initial muons. Muon-track combinations are constrained to arise from a common space point. They are discarded if the three-dimensional vertex fit returns a χ^2 larger than 10. Figure 11 (a) shows the invariant mass distribution of the K^0_S candidates reconstructed assuming that both tracks are due to pions. A fit of the data with a Gaussian function to model the signal plus a second order polynomial to model the background yields a signal of 5348 ± 225 K^0_S mesons. The impact parameter distribution of initial muons produced by K^0_S decays is shown in Fig. 11 (b). The data also contain a smaller number of cases in which the initial muon is mimicked by the products of hyperon decays. Using a similar technique, we have searched the data for $\Lambda \to p\pi^-$ decays and we find a signal of 678 ± 60 Λ baryons (see Fig. 12). Since in both case the kinematic acceptance times reconstruction efficiency is approximately 50%, source (c) ($\simeq 12000$ events) explains $\simeq 8\%$ of the ghost events.

The final source (d) of ghost events, secondary interactions in the detector volume, is

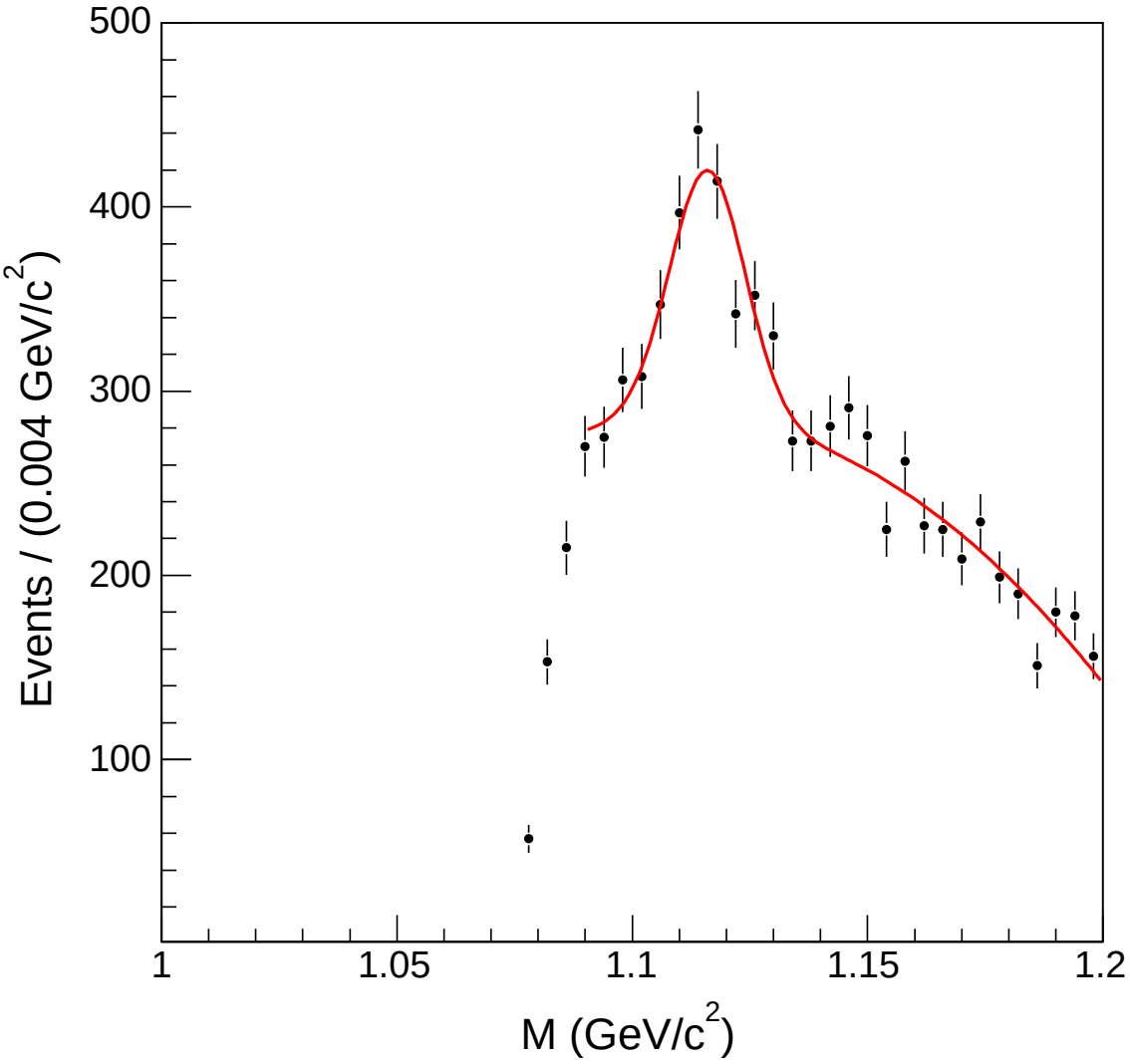

FIG. 12: Distributions of the invariant mass of pairs of initial muons and opposite sign tracks produced by Λ decays. We attribute the proton (pion) mass to the track with positive (negative) charge. The solid line represents a fit that uses a Gaussian function to model the signal and a fourth order polynomial to model the combinatorial background.

investigated using the data. We search for secondary interactions by combining initial muons with all tracks with $p_T \geq 0.5$ GeV/c contained in a 40° cone around the muon direction. Muon-track combinations are constrained to arise from a common space point. They are discarded if the three-dimensional vertex fit returns a χ^2 larger than 10. The distribution of R, the distance of a reconstructed secondary vertex from the detector origin in the plane

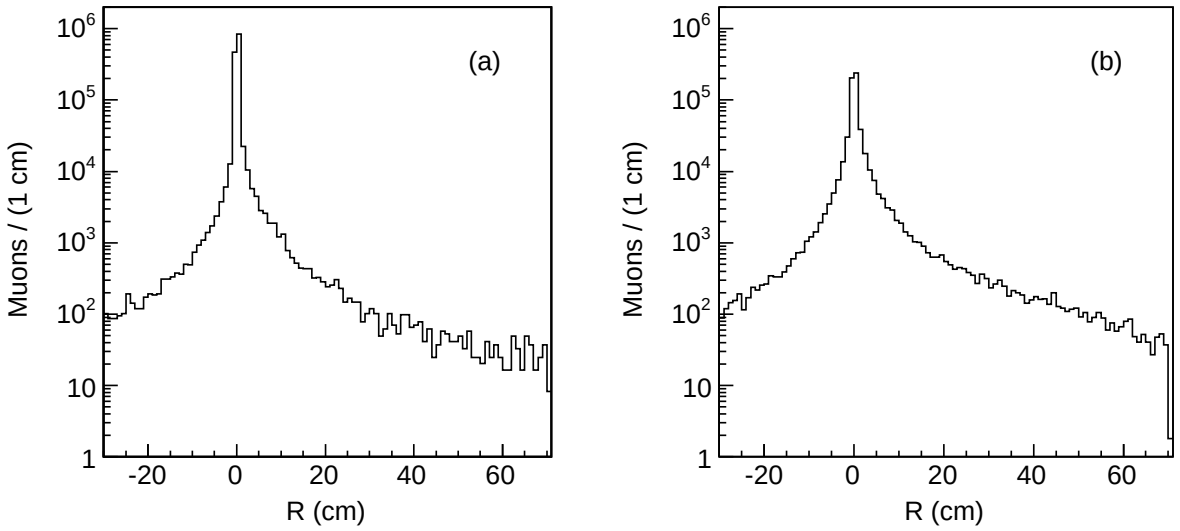

FIG. 13: Distributions of R, the signed distance of muon-track vertices from the nominal beam line for (a) QCD and (b) ghost events (see text).

transverse to the beam line, is shown in Fig. 13. The distance R is negative when the secondary vertex is in the hemisphere opposite to that containing the momentum of the muon-track system. Secondary interactions are characterized by spikes at R values where the detector material is concentrated, such as SVX supports or the COT inner support cylinder. From the absence of visible spikes, we conclude that the contribution of multi-prong secondary interactions to initial muons in ghost events is negligible. At the same time, we cannot exclude some contribution to ghost events from elastic or quasi-elastic nuclear scattering of hadronic tracks in the detector material.

Our estimate of the size of possible sources of ghost events underpredicts the observed number of ghost events by approximately a factor of two (154000 observed and 69000 accounted for). However, given the possible large uncertainty of the in-flight-decay prediction and the possible contribution of elastic or quasi-elastic nuclear scattering in the detector material, at this point of our study we cannot exclude that the ghost sample can be completely accounted for by a combination of all the above-studied background sources. Were ghost events all due to these ordinary sources, they would not contain a significant number of additional real muons. Therefore, these sources are unlikely to be the origin of the excess of low-mass dileptons reported in Ref. [3]. That study is repeated in the next section.

V. STUDY OF EVENTS THAT CONTAIN AN ADDITIONAL MUON

We begin this study with events that contain a pair of initial muons passing our analysis selection without any SVX requirements. We then search for additional tracks with $p_T \geq 2$ GeV/c and a matching stub in the CMU, CMX, or CMP muon detectors (the three detectors cover the pseudorapidity region $|\eta| \leq 1.1$). No SVX requirements are made on these additional muons. For muons with $p_T \geq 2$ GeV/c and $|\eta| \leq 1.1$, the muon detector efficiency in the heavy flavor simulation is 0.805 ± 0.008. We measure the muon detector efficiency in the data by using J/ψ candidates acquired with the μ-SVT trigger (see Ref. [6] for more details). After reweighting the kinematics of the muons from J/ψ decays to reproduce that of simulated muons from heavy flavor decays, the efficiency is measured to be 0.838 ± 0.004.

According to the heavy flavor simulation, additional real muons predominantly arise from sequential decays of single b hadrons (the $g \to b\bar{b}$ and $g \to c\bar{c}$ contributions are suppressed by the request of two initial muons with $p_T \geq 3$ GeV/c, $|\eta| \leq 0.7$, and invariant mass larger than 5 GeV/c^2). In addition, one expects a contribution of additional muons from hadrons mimicking the muon signal. In the data, 9.7% of the dimuon events contain an additional muon (71835 out of 743006 events). In events containing an $\Upsilon(1S)$ candidate, that are included in the dimuon sample, the probability of finding an additional muon is $(0.90 \pm 0.01)\%$. Of the 5348 ± 225 events with an identified K^0_S meson only 94 ± 41, $(1.7 \pm 0.8)\%$, survive the request of an additional muon in the event.

Our investigation starts with measuring the efficiency of the tight SVX requirements for initial muon pairs in events that also contain at least one additional muon. The efficiency drops from 0.193 to 0.166. If ghost events were all due to initial muons arising from π or K decays, or secondary interactions in the detector volume, this efficiency would have increased back to 0.244 because these types of source contain fewer additional muons than events with heavy flavors. For example, this is the case for events containing an $\Upsilon(1S)$ or K^0_S candidate. This observation anticipates that a fraction of the ghost events contains more additional muons than QCD events.

Following the study in Ref. [3], additional muons are paired with one of the initial muons if their invariant mass is smaller than 5 GeV/c^2. For this study, we use a larger statistics

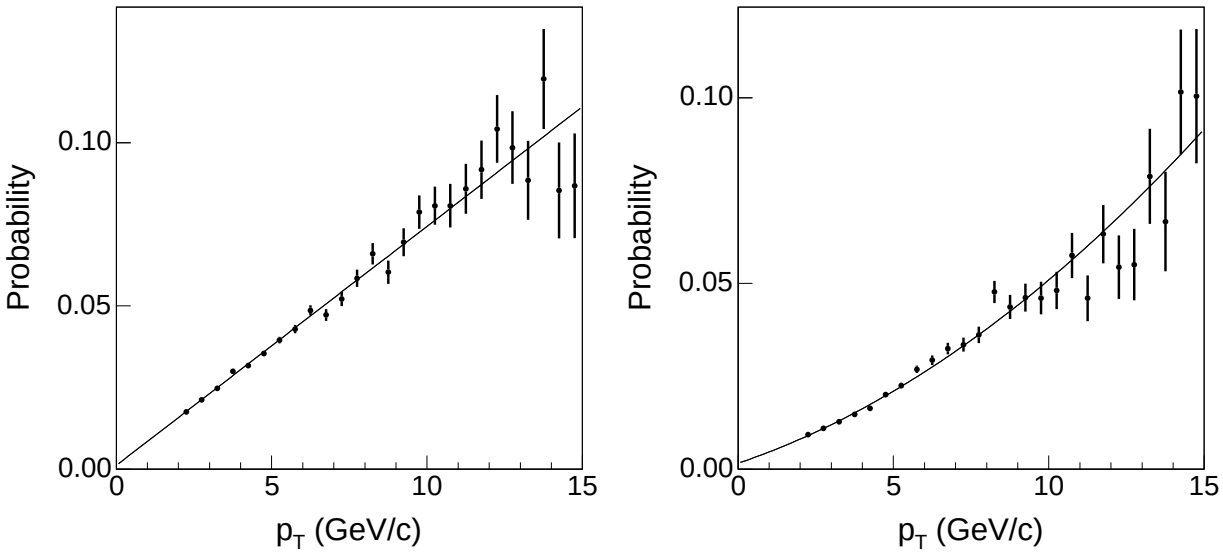

FIG. 14: Probability that a track with $|\eta| \leq 1.1$ mimics a muon signal in the CMU, CMX, or CMP detectors as a function of the kaon (left) or pion (right) transverse momentum. We have verified that these fake probabilities do not depend on the SVX requirements applied to the tracks.

data sample [5]. Following the analysis procedure of Ref. [3], we retain muon combinations with charges of opposite sign (OS). As in Ref. [3], we estimate the contribution of fake muons from the number of observed same sign (SS) muon pairs. In the case of Drell-Yan or quarkonia production, fake additional muons arise from the underlying event and one expects no charge correlation between initial and additional fake muons. However, in the simulation of heavy flavor decays, the numbers of OS and SS tracks surrounding an initial muon are not equal. These tracks come from the b- and c-quark fragmentation and decay. In the simulation, the ratio of OS to SS combinations as well as the ratio of the numbers of pion to kaon tracks is a function of the invariant mass of the muon-track pair. The CDF II detector simulation does not describe the punchthrough of hadrons. Therefore, we evaluate the fake muon contribution by weighting pion and kaon tracks in the heavy flavor simulation with the probability that hadronic punchthrough mimics a muon signal. These fake probabilities, shown in Fig. 14 as a function of the track p_T, have been measured using a sample of $D^0 \to K^-\pi^+$ decays acquired with the CHARM and μ-SVT triggers. The procedure

[5] The correlated $b\bar{b}$ cross section measurement uses 742 pb^{-1} of data in which the dimuon trigger is not prescaled as a function of the instantaneous luminosity. From the rate of dimuon events that pass the analysis selection, the luminosity of the larger data sample is estimated to correspond to 1426 pb^{-1}.

for determining these probabilities is described in detail in Appendix B of Ref. [6].

The rate of real plus fake muon pairs with small invariant mass is evaluated after rescaling the parton level cross section predicted by the HERWIG generator to match the measurements $\sigma_{b\to\mu,\bar{b}\to\mu} = 1549 \pm 133$ pb and $\sigma_{c\to\mu,\bar{c}\to\mu} = 624 \pm 104$ pb [6]. In the simulation, SS combinations due to either real or fake muon pairs are subtracted from OS combinations. In the simulation, the initial pair of muons is always arising from heavy-flavor semileptonic decays. In the data, 9% of the initial muons recoiling against a small mass dimuon are due to prompt hadrons mimicking the muon signal (relative size of the BB and BP components in Table I). In addition, 2% of these recoiling muons are due to hadrons from heavy flavor decays [6]. We account for this by increasing the rates predicted by the simulation by a factor of 1.12.

Figure 15 shows the ratio of the total number of $OS - SS$ muon pairs predicted by the above calculation to that of real $OS - SS$ dimuons from heavy flavor decays. The fake contribution is approximately 33% of that of real muons from sequential decays of single b quarks. Figure 16 compares the invariant mass spectrum of $OS - SS$ muon pairs in the data and in the heavy flavor simulation. Since the simulation is effectively normalized to the observed number of initial muon pairs, the prediction has a 3% systematic error due to the branching ratio $b \to c \to \mu$ plus a 3% uncertainty due to the absolute pion and kaon rates predicted by the simulation [6] (the systematic uncertainty of the muon detector efficiency is negligible). This systematic uncertainty is not shown in Fig. 16. The number of J/ψ mesons in the data is correctly modeled by the simulation in which J/ψ mesons only arise from $b\bar{b}$ production. The agreement between the number of observed and predicted J/ψ mesons selected without any SVX requirement supports the estimate of the efficiency of the tight SVX requirement and the resulting value of the correlated $b\bar{b}$ cross section reported in Ref. [6]. However, the data are underestimated by the simulation for invariant masses smaller than 2 GeV/c^2. The excess of 8451 ± 1274 events results from an observation of 37042 ± 389 and a prediction of 28589 ± 1213 events. The size and shape of the excess is consistent with what was first reported in Ref. [3], in which the excess was mostly observed in a high statistics $e\mu$ sample. We have an advantage with respect to the previous observation. The robustness of the prediction can be verified by comparing the observed and predicted invariant mass spectrum of dimuon pairs when the initial muons are selected with the tight SVX requirements. In this case we observe 6935 ± 154 events, whereas 6918 ± 293 are

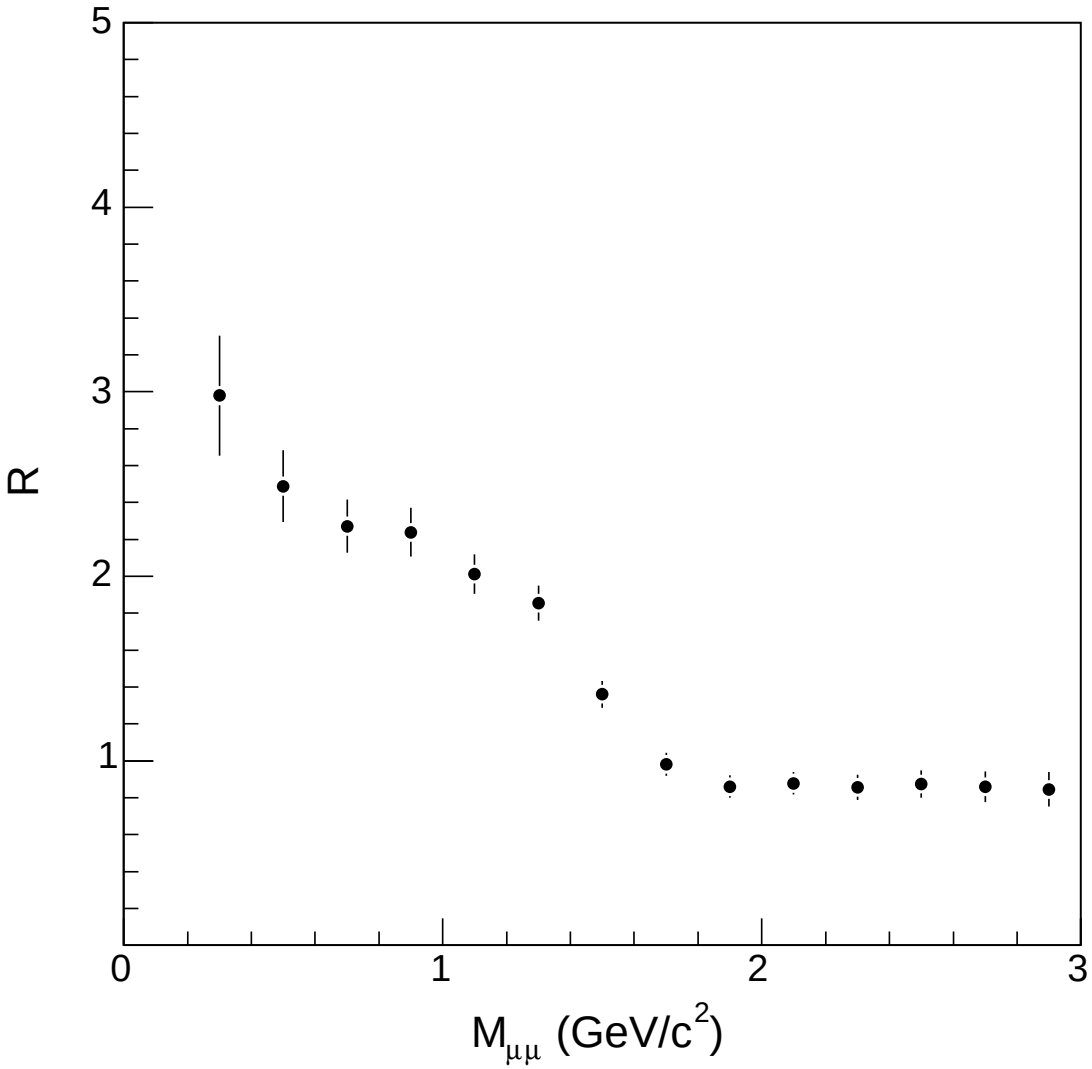

FIG. 15: Ratio R of total number of $OS - SS$ muon pairs to that of real $OS - SS$ pairs arising from heavy flavor decays as a function of the dimuon invariant mass. We use simulated events generated with the HERWIG Monte Carlo program. The generator parton-level cross sections have been scaled to match the data [6]. The number of fake muon pairs has been evaluated by weighting simulated hadronic tracks with the probability of mimicking a muon signal as measured with data. Errors are statistical only.

predicted. The corresponding invariant mass distribution is shown in Fig. 17.

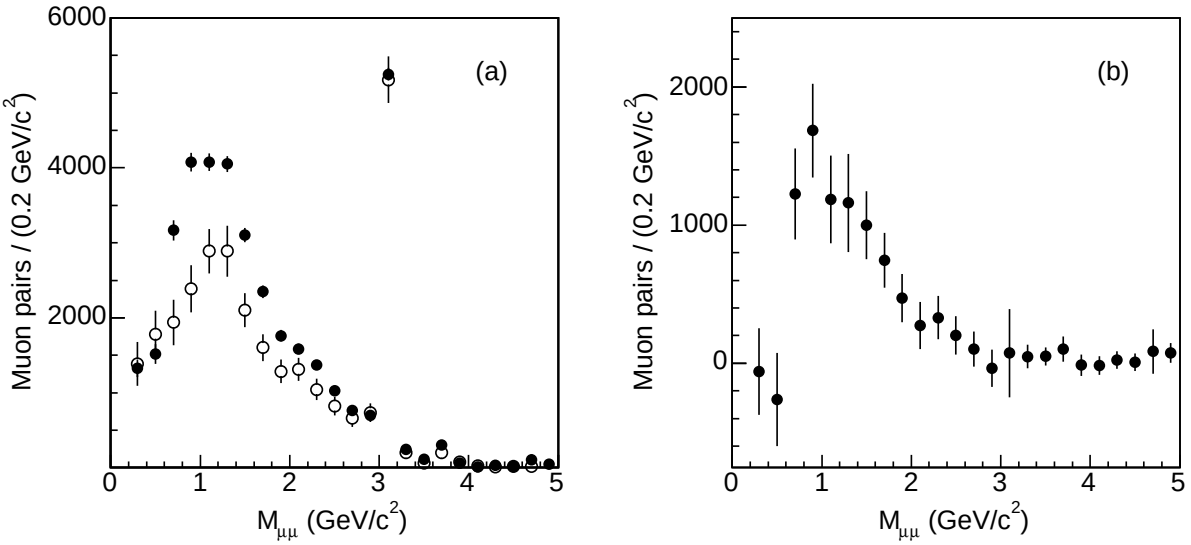

FIG. 16: The invariant mass distribution of (a) $OS - SS$ muon pairs in the data (•) is compared to the simulation prediction (○). One of the two initial muons in the event is combined with an additional muon if their invariant mass is smaller than 5 GeV/c^2. The difference (b) between data and prediction is also shown.

A. Kinematics of additional muons in ghost events

The excess of 8451 ± 1274 $OS - SS$ pairs with invariant mass smaller than 5 GeV/c^2 is a measure of the charge asymmetry of additional muons as a function of the invariant mass of the muon pair. For 1,426,571 initial dimuons, we find 94148 OS and 57106 SS combinations with an additional muon with $m_{\mu\mu} \leq 5$ GeV/c^2. A qualitative estimate predicts that 14200 SS and OS fake muon combinations are produced by the underlying event [6]. The heavy flavor simulation, which also accounts for fake muons, predicts 40899 OS and 12309 SS real plus fake combinations for a grand total of 55100 OS and 26500 SS pairs. This approximate prediction underestimates the data by 39000 OS and 30500 SS pairs. The number of the OS and SS pairs in ghost events is determined more precisely as the difference between the data and the QCD expectation. The QCD expectation is the number of muon combinations found in events in which the initial dimuons pass the tight SVX requirements divided by the SVX requirement efficiency. This study is summarized in Table IV. In ghost events, the fraction

[6] These numbers are derived from the 1% probability of finding an additional muons in events with $\Upsilon(1S)$ candidates and assuming that the underlying event is the same for all processes.

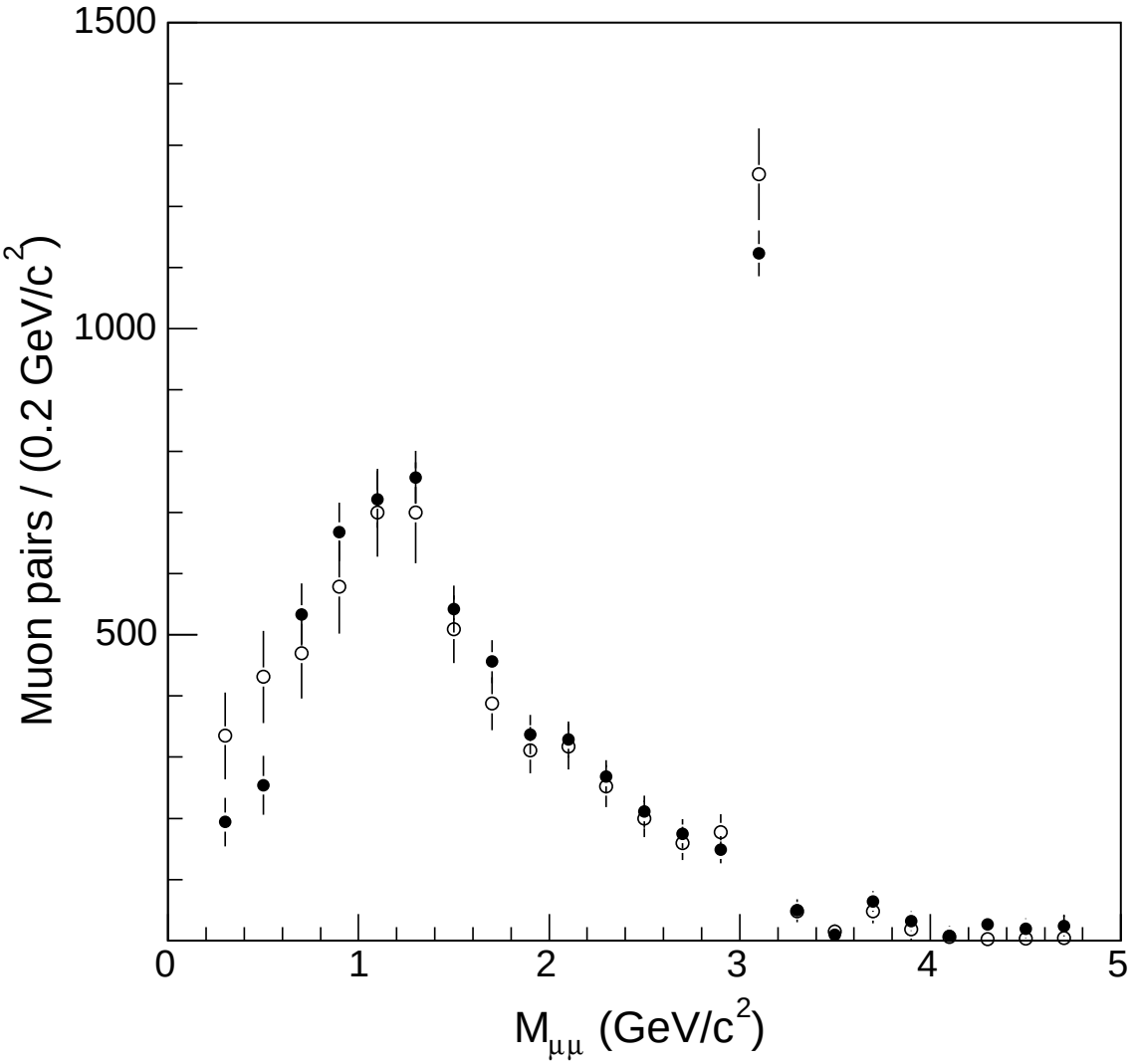

FIG. 17: The invariant mass distribution of $OS - SS$ muon pairs in the data (•) is compared to the simulation prediction (◦). Initial muons are selected using the tight SVX requirements.

of events that carries an additional real or fake muon with any charge is $(15.8 \pm 0.3)\%$, approximately a factor of two higher than in QCD events. The fraction of additional muons due to tracks mimicking a muon signal is estimated in the next section.

In order to compare with the previous measurement [3], we have analyzed dimuon pairs with $m_{\mu^+\mu^-} \leq 5$ GeV/c^2. This requirement is appropriate for selecting dimuons produced by sequential semileptonic decays of single b-quarks, but could bias the investigation of ghost events. Therefore, we search dimuon events for additional muons without any invariant mass

TABLE IV: Number of events as a function of N_c, the number of combinations of initial and additional muons. Additional muons are combined with initial muons if the pair invariant mass is smaller than 5 GeV/c^2. The numbers of events with at least one combination are split according to opposite (OS) or same (SS) charge sign. "SVX" are numbers of events that pass the tight SVX selection. QCD is the latter number divided by the efficiency of the tight SVX requirements. Ghost is the difference between the total and the QCD contributions.

Topology	Total	SVX	QCD	Ghost
$N_c \geq 0$	1426571	275986	1131090 ± 9271	295481 ± 9271
$N_c \geq 1$	141039	22981	94184 ± 772	46855 ± 772
OS	94148	15372	63000 ± 516	31148 ± 516
SS	57106	8437	34578 ± 283	22528 ± 283
$N_c \geq 2$	10215	828	3393 ± 28	6822 ± 28

cut. If the initial dimuon pair has opposite charge, we combine the additional muon with the initial muon of opposite charge (OSO combinations). If the initial muons have same charge, we randomly combine the additional muon with one of the initial muons (SSO and SSS combinations). The QCD contribution is estimated as the number of combinations in events in which initial dimuons pass the tight SVX requirements (SVX contribution) divided by the efficiency of the tight SVX requirements. As before, the ghost contribution is the difference between the data and the QCD contribution. The number of three-muon combinations is listed in Table V. Figure 18 shows the invariant mass and opening angle distribution of OSO combinations for the QCD and ghost contributions. Muon pairs due to b sequential decays, which account for most of the QCD contribution, peak at small invariant masses and small opening angles. The tail at large masses and opening angles results from fake muons with wrong charge. The distributions of analogous pairs in the ghost sample have a quite similar behaviour. However, it is important to note that combinations of initial and additional muons in ghost events have a smaller opening angle than those from sequential b decays. As shown in Fig. 19, SSO and SSS combinations have similar opening angle distributions. Therefore, it seems reasonable to restrict the study of ghost events to muons and tracks contained in a cone of angle $\theta \leq 36.8^{\circ}$, corresponding to $\cos\theta \geq 0.8$, around the

TABLE V: Numbers and types of three-muon combinations. We separate events according to the charge of the initial muons. The topology OSO is that of two opposite-charge initial dimuons; by definition, the third muon has opposite charge with respect to one of them. When initial dimuons have same sign charge, the third muon charge can have either the same (SSS) or opposite sign (SSO).

Topology	All	SVX	QCD	Ghost
OSO	90022	14497	59414 ± 487	30608 ± 487
SSO	48220	7708	31590 ± 259	16630 ± 259
SSS	28239	4139	16963 ± 139	11276 ± 139

TABLE VI: Numbers of additional muons with an angle $\theta \leq 36.8^{\circ}$ with respect to the direction of one of the initial muons. We list separately the combination of additional and initial muons with opposite (OS) and same (SS) sign charge.

Topology	All	SVX	QCD	Ghost
OS	83237	13309	54545 ± 447	28692 ± 447
SS	50233	7333	30053 ± 246	20180 ± 246

direction of each initial muon.

VI. STUDY OF MUON AND TRACK PROPERTIES IN GHOST EVENTS

The number of additional muons contained in a cone of angle $\theta \leq 36.8^{\circ}$ ($\cos\theta \geq 0.8$) around the direction of any initial muon is listed in Table VI. Figure 20 shows the two-dimensional distribution of the impact parameter of an initial muon versus that of all additional muons in a $\cos\theta \geq 0.8$ cone around its direction. The QCD contribution has been removed using events in which the primary muons pass the tight SVX requirement. The tail of the impact parameter distribution of additional muons in QCD events, shown in Fig. 21, does not extend beyond 2 mm. In contrast, as shown in Fig. 20, the impact parameter dis-

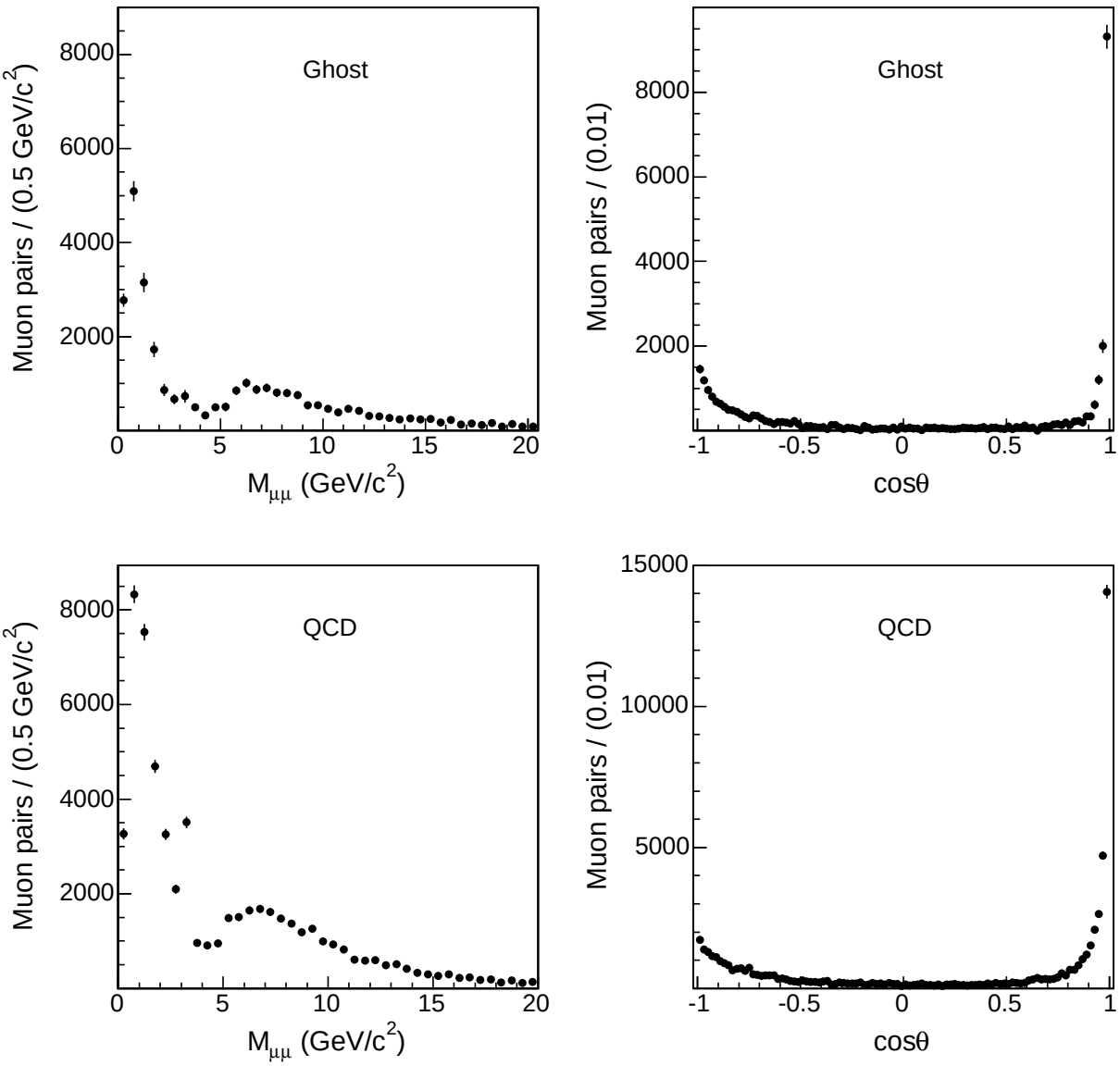

FIG. 18: Events with OS initial muon pairs and an additional muon combined with the opposite-charge initial muon. We show the invariant mass, $M_{\mu\mu}$, and opening angle, θ, distributions of these combinations for the QCD and ghost contributions.

tribution of additional muons in ghost events extends to much larger values and is consistent with that of the initial muons. However, the impact parameters of the additional and initial muons are loosely correlated (the correlation factor is $\rho_{d_p d_s} = 0.03$).

The contribution of fake muons is evaluated by weighting all tracks with $p_T \geq 2$ GeV/c, $|\eta| \leq 1.1$, and contained in a $\cos\theta \geq 0.8$ cone, with the fake probabilities shown in Fig. 14. Table VII lists the number of these tracks for QCD and ghost events. The QCD and

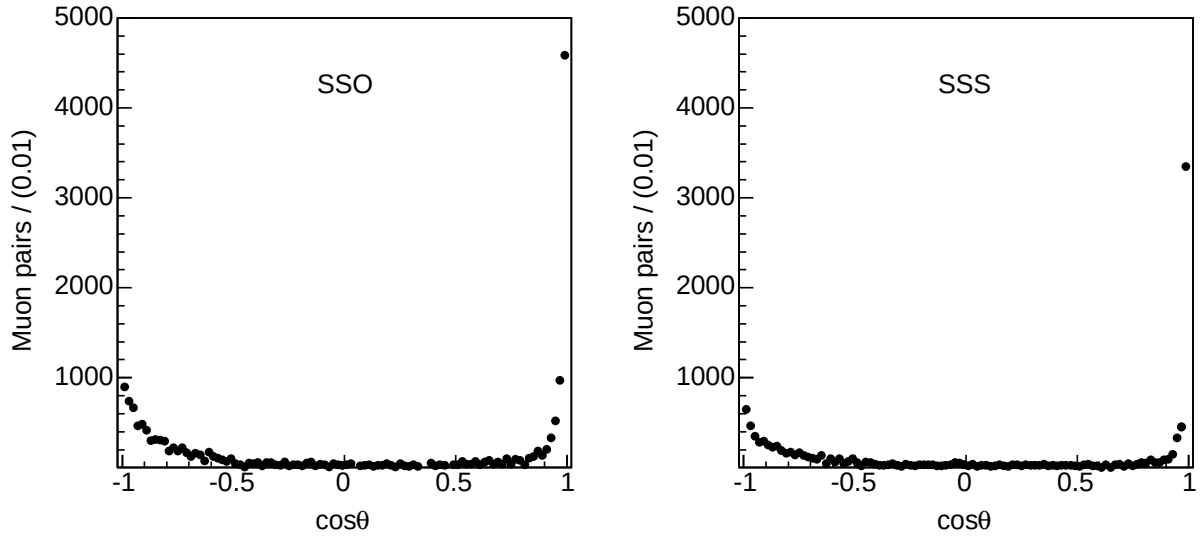

FIG. 19: Opening angle distributions of dimuon combinations for ghost events. The initial dimuons have same sign charge, and combinations of an additional and initial muons are split according to the charge of the additional muon. The plots are the projection of two-dimensional distributions in which the additional muon is combined with both initial muons.

TABLE VII: Numbers of tracks with $p_T \geq 2$ GeV/c, $|\eta| \leq 1.1$, and an angle $\theta \leq 36.8^{\circ}$ with respect to the direction of one of the initial muons. We list separately the numbers of tracks with opposite (OS) and same (SS) charge as the initial muon. Tracks associated with a muon stub are excluded.

Topology	All	SVX	QCD	Ghost
OS	1315451	207344	849770 ± 6965	465860 ± 6965
SS	893750	140238	574745 ± 4711	318004 ± 4711

ghost contributions have been previously determined to be 1131090 and 295481 events, respectively. It follows that the average number of tracks contained in a $\theta \leq 36.8^{\circ}$ cone around the direction of one of the initial muons in ghost events is 1.58 OS and 1.08 SS, twice the values measured in QCD events (0.75 OS and 0.51 SS tracks).

Table VIII compares the observed number of additional muons to the predicted number of additional fake muons in ghost events. In ghost events, the fraction of real muons with any charge is approximately four times larger than that of real muons in QCD events (9.4%

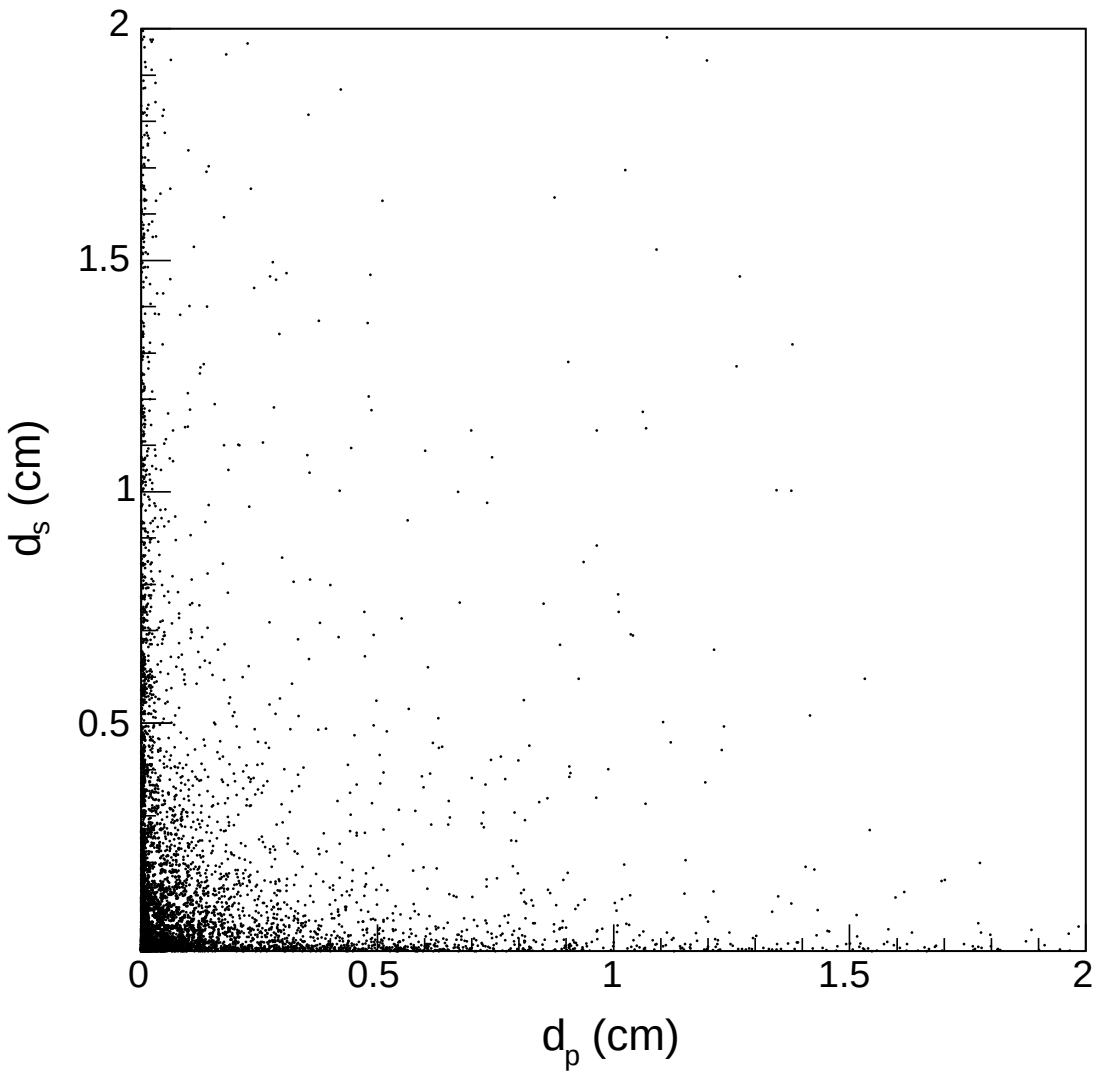

FIG. 20: Two-dimensional distribution of the impact parameter of additional muons, d_s, versus that of initial muons, d_p, for ghost events. Muons are selected with loose SVX requirements. The QCD contribution has been removed.

compared to 2.1%, as obtained from the number of $OS-SS$ dimuons listed in Table VI and the number of $OS+SS$ dimuons in ghost events after subtracting the average of the pion and kaon fake contributions listed in Table VIII, respectively). In Table VIII, the ratio of real to background muons is approximately 1. This ratio is larger than that in QCD events (0.4) which are correctly modeled by the heavy flavor simulation. As a cross-check that the difference in rates of additional muons between the QCD and ghost sample is contributed by

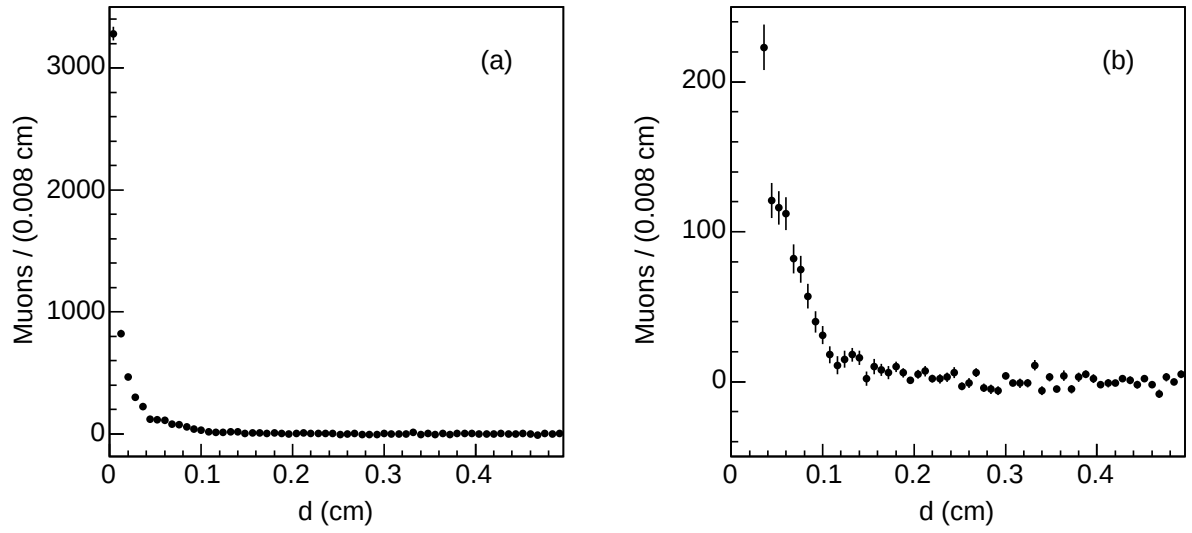

FIG. 21: Impact parameter distribution of (a) additional muons found in events in which the initial muons are selected with tight SVX requirements. The same distribution is plotted in (b) with a magnified vertical scale. Additional muons are selected without SVX requirements.

TABLE VIII: Numbers of additional muons in ghost events are compared to fake muon expectations. The fake muon prediction is evaluated by applying the fake probabilities shown in Fig. 14 to all tracks not associated to a muon stub and with $p_T \geq 2$ GeV/c, $|\eta| \leq 1.1$, and an angle $\theta \leq 36.8^{\circ}$ with respect to the direction of one of the initial muons. We list separately the numbers of muons with opposite (OS) and same (SS) sign charge as the initial muon. F_K and F_π are the numbers of fake muons predicted assuming that hadronic tracks are all kaons or all pions, respectively. For kaon tracks, the rate of predicted fake muons should be increased by 10% to also account for in-flight-decay contributions.

Topology	Observed	F_K	F_π
OS	28692 ± 447	15447 ± 210	9649 ± 131
SS	20180 ± 246	10282 ± 137	6427 ± 81

real muons, we restrict ourselves to additional muons identified as CMUP muons. In this case the contribution of fake muons is significantly reduced and is expected to be negligible [6] (see Appendix A). The numbers of additional CMUP muons and expected fakes are listed in

TABLE IX: Numbers of additional CMUP muons in QCD and ghost events. F_π is the number of fake muons in ghost events, predicted assuming that hadronic tracks are pions. If tracks are assumed to be kaons, the fake probability per track is approximately four times higher after including the in-flight-decay contribution. In QCD events, in which a large fraction of fake muons is due to kaons, the number of SS combinations underestimates the fake muon contribution to OS combinations by approximately 10%.

Topology	All	QCD	Ghost	F_π
OS	10812	7380 ± 172	3432 ± 201	216 ± 44
SS	4400	2635 ± 104	1765 ± 123	138 ± 35

Table IX. One notes that the fake contribution is much reduced at the expense of the muon acceptance that decreases by a factor of approximately five. The fraction of real additional CMUP muons is $(0.40 \pm 0.01)\%$ in QCD events, and is four times larger $(1.64 \pm 0.08)\%$ in ghost events. This result is consistent with the previous determination that uses all muon detectors.

To summarize, ghost events have the following features that differentiate them from QCD events. A $\cos\theta \geq 0.8$ cone around the direction of a primary muon contains twice as many tracks as QCD events. These cones contain a number of additional real muons that is approximately four times larger than in QCD events. Since approximately 50% of the ghost events is accounted for by ordinary contributions, the remaining fraction contains a surprisingly large number of tracks and muons with $p_T \geq 2$ GeV/c per event. The shapes of the muon impact parameter distributions in QCD and ghost events are different. Additional and initial muons in ghost events have a tail that extends well beyond that observed in the QCD events. Impact parameters of muons contained in a 36.8° cone are loosely correlated.

Figure 22 (a) shows the distribution of the number of muons found in a $\cos\theta \geq 0.8$ cone around a primary muon due to ghost events. In the plot, an additional muon increases the multiplicity by 1 when of opposite sign and by 10 when of the same sign charge as the initial muon [7]. It is clear that a small fractions of ghost events contains a very large muon

[7] As examples, the 3rd bin indicates cones with 3 muons with charge $(+--)$ or $(-++)$; and the 21st bin

multiplicity. The contribution of fake muons is estimated assuming that the large majority of the tracks in a $\cos\theta \geq 0.8$ cone are pions. We correct the distribution in Fig. 22 (a) as follows. Given an event with n muons, we loop over the tracks not associated to a muon stub and with the same kinematic properties of muon candidates and randomly generate fake muons using the probability that a pion mimics a muon signal. If m is the number of generated fake muons, we remove one event with $m + n$ muons in the distribution in Fig. 22 (a) and add one event to the bin with n muons. The fake subtraction reduces the number of $\cos\theta \geq 0.8$ cones that contain one or more additional muons from 40409 to 27539. The resulting distribution is shown in Fig. 22 (b). In conclusion, we are capable of predicting the number of additional muons in events in which the initial muons originate inside the beam pipe. In this case, the dominant sources of events are heavy flavor, Υ and Drell-Yan production, and most of the additional muons arise from sequential decays of single b quarks. In contrast, it seems difficult to account for the muon multiplicity distribution shown in Fig. 22 (b) if the ghost events were all due to ordinary sources, such as in-flight decays of pions and kaons, or hyperon decays in which the punchthrough of a hadronic prong mimics a muon signal.

A. Robustness of the fake muon prediction

It is important to further verify that such a large number of muons contained in such a small angular cone is not a detector artifact. The display of the muon chamber hits in events that contain four or more muons did not yield any indication of a detector malfunction. However, there are events in which certain areas of the muon detectors have a dense clustering of dozens of hits. In these events, some muons correspond to tracks linked to muon stubs constructed in those clusters. We estimate the muon fake rate using the probability that pions and kaons from D^0 decays mimic a muon signal. After requiring that D^0 candidates have an appreciable proper decay time in order to select D^0 mesons from b-hadron decays, a 36.8° cone around the direction of these tracks contains an average of 0.02 muons and 1.6 additional tracks with $p_T \geq 2$ GeV/c. The muon fake probability does not increase at all when using D^0 prongs accompanied by at least two tracks. However, the multiplicity in a

indicates cones with 3 muons with charge $(+++)$ or $(---)$.

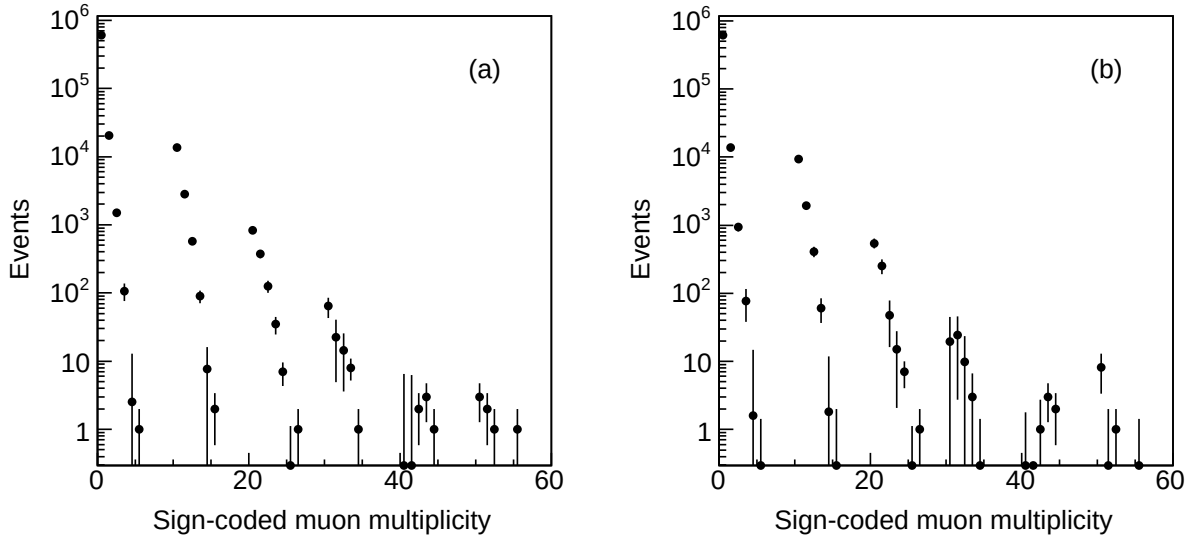

FIG. 22: Sign-coded multiplicity distribution of additional muons found in a $\cos\theta \geq 0.8$ cone around the direction of a primary muon in ghost events before (a) and after (b) correcting for the fake muon contribution. An additional muon increases the multiplicity by 1 when it has the opposite sign and by 10 when it has same sign charge as the initial muon. The background subtracted distribution is also listed in Table X.

36.8° cone around the direction of the D^0 prongs does not have the high multiplicity tail of ghost events. We do not possess a data set of a known process with a number of tracks and muons as large as in ghost events that could be used to verify the muon detector response to this type of event.

One concern is that our procedure underestimates the fake rate in multi-muon events in which hadronic tracks can take advantage of hits in the muon chambers produced by real muons or by hadronic punchthrough. Our muon selection criteria were not optimized for this type of event. A track is accepted as a muon if the distance of its projection onto a muon detector from a muon stub is $\Delta x \leq 30$, 40, and 30 cm for the CMU, CMP, and CMX detector, respectively. For CMX or CMU muons with $p_T = 2$ GeV/c, these Δx cuts correspond to the requirement that the track extrapolation and the muon stub match within 3 σ in the $r - \phi$ plane, where σ is a rms deviation that includes the effect of multiple scattering and energy loss. We have selected additional muons by adding the increasingly stricter requirements that track-stub matches are within 3 and 2 σ, respectively. The latter requirement reduces the number of multiple-muon combinations by a factor of two, but

TABLE X: Sign-coded, background subtracted, muon multiplicity in ghost events. Bins without entries are not shown. The multiplicity is not acceptance corrected because we do not know the mechanism producing ghost events. However, the detector acceptance for an additional muon with $p_T \geq 2$ GeV/c and $|\eta| \leq 1.1$ is 0.838 ± 0.004. The detector acceptance for an initial muon with $p_T \geq 3$ GeV/c and $|\eta| \leq 0.7$ is 0.506 ± 0.003.

Bin	Content	Bin	Content
0	620307 ± 3413	30	19.4 ± 25.6
1	13880 ± 573	31	24.2 ± 21.5
2	941 ± 135	32	9.8 ± 13.8
3	77 ± 39	33	3.0 ± 3.6
4	1.6 ± 13.2	34	0.00 ± 1.4
5	0.0 ± 1.4	40	-7.4 ± 9.2
10	9312 ± 425	41	-7.2 ± 7.0
11	1938 ± 173	42	1.0 ± 1.7
12	409 ± 71	43	3.0 ± 1.7
13	60 ± 23	44	2.0 ± 1.4
14	1.8 ± 10.1	50	8.1 ± 4.8
15	0.0 ± 2.0	51	0.0 ± 2.0
20	542 ± 91	52	1.0 ± 1.0
21	251 ± 61	55	0.0 ± 1.4
22	47 ± 31		
23	14.9 ± 12.8		
24	7.0 ± 3.0		
25	-3.1 ± 4.2		
26	1.0 ± 1.0		

does not affect the salient features of the multiplicity distribution in Fig. 22 (a). We have compared Δx and σ distributions of muon-track matches for the different muon detectors in QCD and ghost events (see Appendix A). These distributions, as well as the fractional

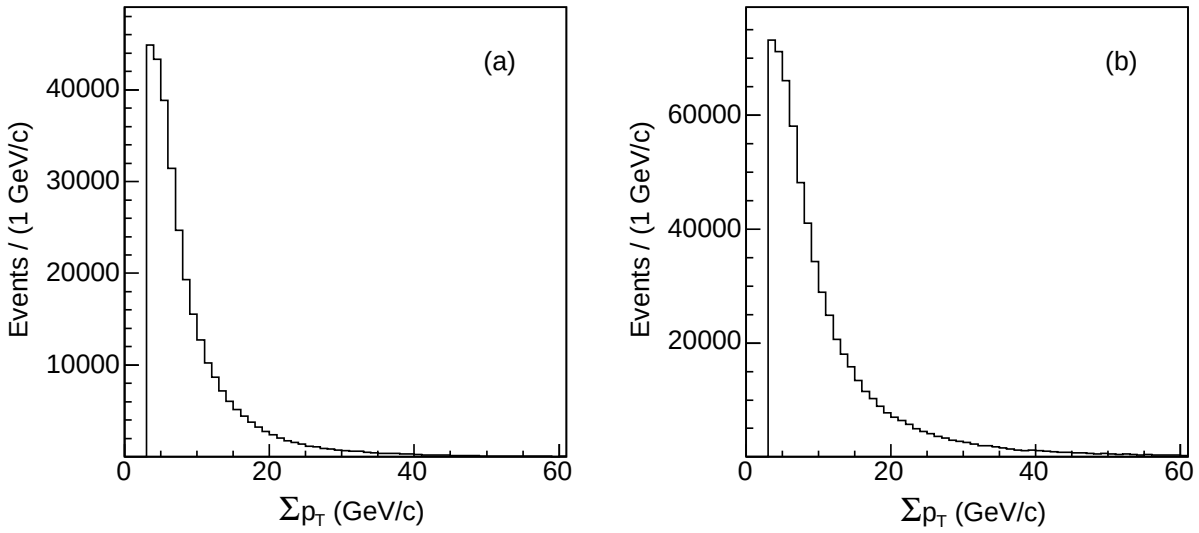

FIG. 23: Distribution of the transverse momentum carried by all tracks with $p_T \geq 1$ GeV/c contained in a 36.8° cone around an initial muon in (a) QCD and (b) ghost events.

usage of different muon detectors, in ghost events are not significantly different to those of QCD events. Since we are able to predict the rate of additional muons in QCD events, which have a larger fake muon background than ghost events, the present estimate of the fake muon contribution is an unlikely candidate to explain the large excess of additional muons in ghost events.

As shown at the beginning of Sec. V, we have identified 5348 ± 225 K^0_S candidates in the dimuon data, and 96 ± 41 of them contain at least an additional muon in the event. By applying the fake muon probability to all candidate tracks in events with a K^0_S candidate, we predict 86 ± 30 events with at least an additional fake muon, consistent with the observation.

Traditionally, searches for soft ($p_T \geq 2$ GeV/c) muons performed by the CDF collaboration estimate the fake muon contribution by using a fake probability per track [25]. One could argue that the excess of muons in ghost events were due to a breakdown of this method when applied to high E_T jets with many tracks that are not contained in the calorimeter and muon absorber. This effect was not observed in previous analyses. We would also have observed the presence of multi-muons events in the QCD contribution because, as shown in Fig. 23, the distributions of the transverse momentum carried by all tracks with $p_T \geq 1$ GeV/c and contained in a 36.8° cone are quite similar in ghost and QCD events.

The appearance of multi-muon events seems to be correlated with the presence of muons

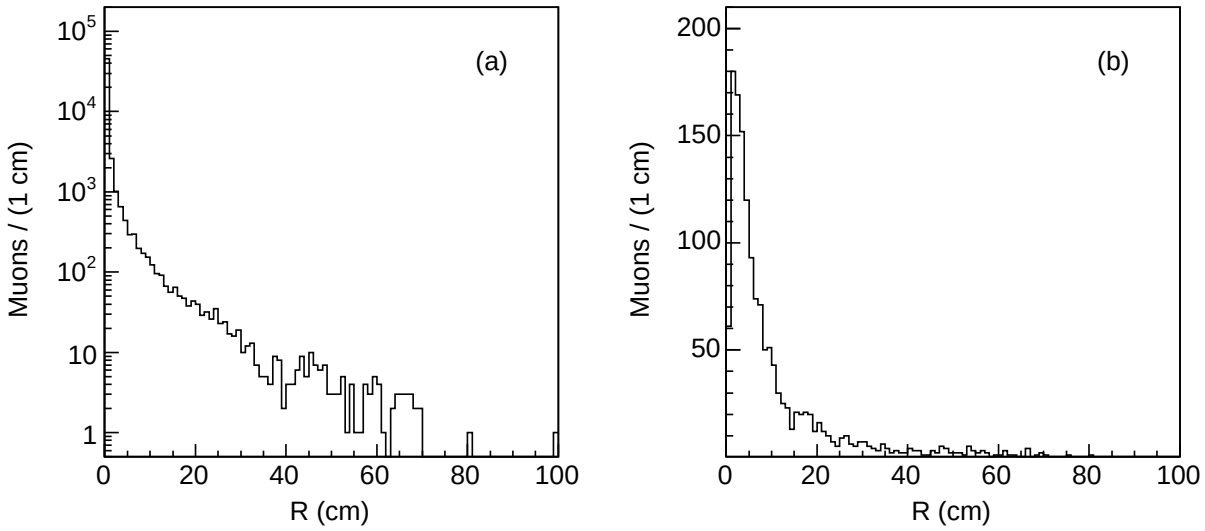

FIG. 24: Distributions of R, the distance of dimuon vertices from the nominal beam line for initial muons with impact parameter (a) smaller and (b) larger than 0.3 cm.

with large impact parameters. As discussed earlier, multi-track secondary interactions in the detector volume do not contribute significantly to the total number of ghost events. This does not exclude the possibility that the smaller number of multi-muon ghost events are due to secondary interactions in the detector volume that point into calorimeter cracks. We search for secondary interactions by combining initial muons with small and large impact parameters with all additional muons in a 36.8° cone around the muon direction. Dimuon combinations are constrained to arise from a common space point. They are discarded if the three-dimensional vertex fit returns a χ^2 larger than 10. The distribution of R, the distance of a reconstructed secondary vertex from the detector origin in the plane transverse to the beam line, is shown in Fig. 24 for initial muons with small and large impact parameters. The absence of spikes in the distributions shows that secondary interactions are not a significant source of multi-muon events.

VII. INVESTIGATION OF ADDITIONAL PROPERTIES OF MULTI-MUON EVENTS

We study the muon impact parameter distributions for the subset of ghost events in which a cone contains two or more muons. The impact parameter distribution of initial

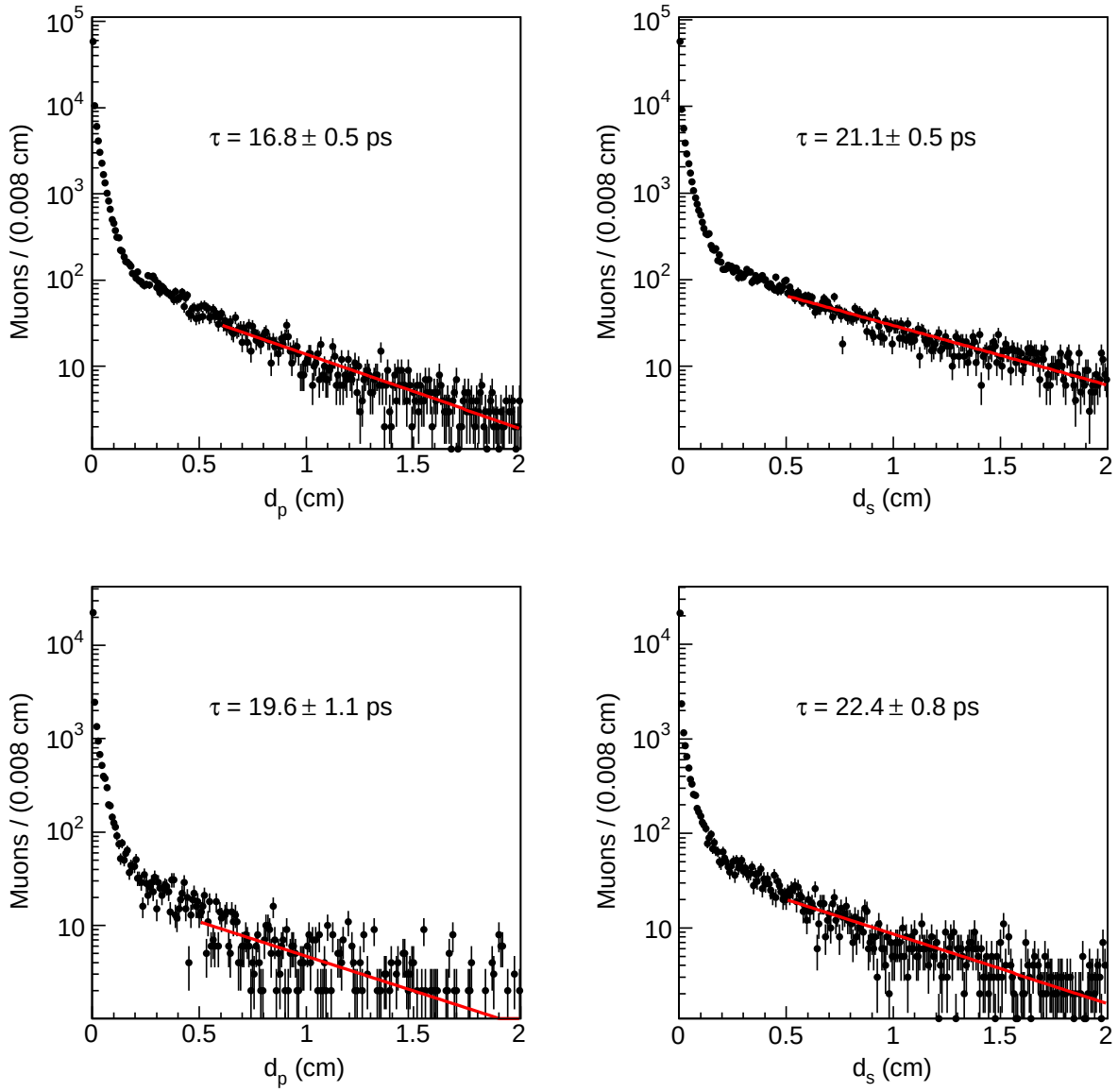

FIG. 25: Muon impact parameter distributions for events containing (top) only two muons or (bottom) more than two muons in a $\cos\theta \geq 0.8$ cone. We call d_p and d_s the impact parameter of initial and additional muons, respectively. The solid lines represent fits to the data distribution with an exponential function. The fit result is shown in each plot.

muons due to ghost events in Fig. 7 is derived using muon tracks that pass the loose SVX selection in order to minimize the possible contribution of interactions in the detector systems surrounding the SVXII detector. As mentioned earlier, this requirement sculpts the impact parameter distribution of muons arising from the decay of particles with a lifetime much larger than that of b quarks. The smaller number of events that contain two or more muons

in a $\cos\theta \geq 0.8$ cone cannot be significantly contaminated by secondary interactions, and we select these muons without any SVX requirement. The corresponding impact parameter distributions are shown in Fig. 25. In the assumption that the exponential tail at large impact parameter is produced by the decay of long-lived objects, fits with an exponential function to the impact parameter distributions of additional muons in the range $0.5-2.0$ cm return a slope of approximately 21.4 ± 0.5 ps [8]. The fits to the impact parameters of initial muons yield smaller values of the slope. The difference is understood in term of kinematic and trigger biases affecting the initial muons. As an example, Fig. 26 compares the result of fits to the impact parameter of muons and tracks corresponding to identified K^0_S decays. The fit to the track impact parameter yields a K^0_S lifetime in agreement with the PDG value of $\tau = 89.6$ ps. In contrast, the lifetime measurement using initial muons yields a much smaller lifetime value. The slope returned by the fits to the impact parameter tail of additional muons in ghost events is different from the lifetime of any known particle.

Conversely, one might wonder if the impact parameter tail is a detector effect that has not been noticed in t- and b-quark studies performed by the CDF collaboration because these analyses customarily utilize muons and tracks with impact parameters smaller than $0.1-0.2$ cm. We study the impact parameter distributions of CMUP trigger muons accompanying a $D^0 \to \pi^+ K^-$ and charge conjugate candidates. We use events acquired with the μ-SVT trigger and reconstruct D^0 candidates by attributing the kaon mass to the track with the same charge as the muon (RS combinations as expected for $\mu + D^0$ systems produced by b hadron decays). We retain combinations in which the muon plus two-track system has an invariant mass smaller than 5 GeV/c^2. No wrong-sign (WS) combinations are found. We use a sideband subtraction method to remove the combinatorial background in the invariant mass region corresponding to the D^0 signal. The impact parameter distribution of CMUP muons produced by b hadron decays, shown in Fig. 27, does not have the large tail at large impact parameters that is characteristic of initial muons in ghost events. Figure 28 is the analogous plot when muons are selected as the additional muons in this analysis ($p_T \geq 2$ GeV/c and $|\eta| \leq 1.1$). No high impact parameter tails are observed. The fraction of fake muons, measured as the number of WS combinations, is approximately 2%.

[8] The error is statistical. A study of systematic effects due to possible background contributions is beyond the scope of this pioneering study.

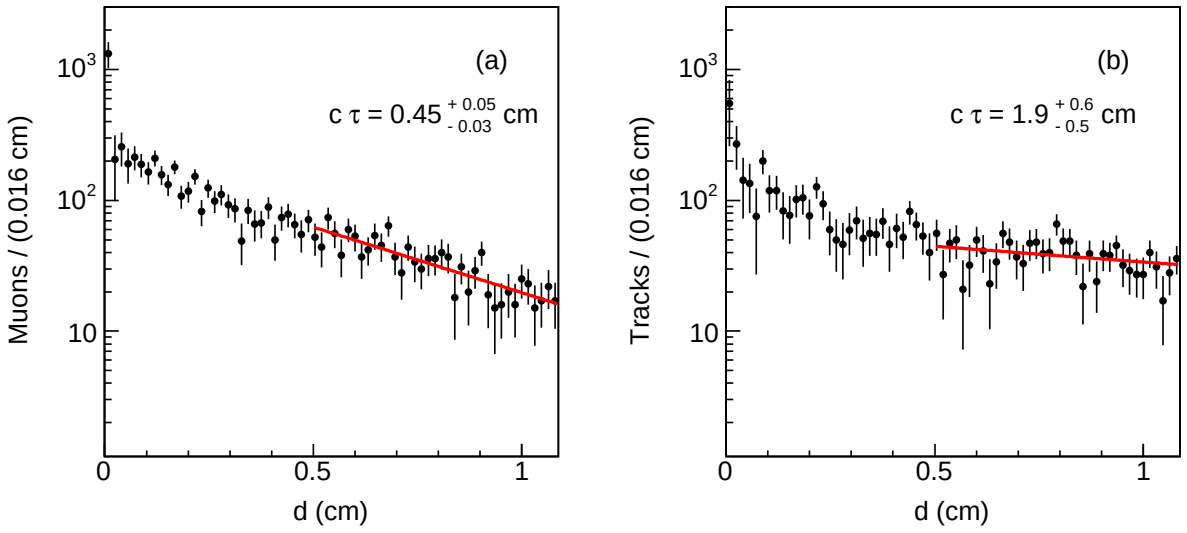

FIG. 26: Impact parameter distributions of (a) initial muons and (b) tracks of identified K^0_S decays. The combinatorial background under the K^0_S signal in Fig. 11 has been removed using a sideband subtraction method.

A. Lifetime

The fact that multi-muon events have been isolated by the request that at least one of the trigger muons originates outside of the beam pipe suggests that they could be associated with objects with lifetime much larger than that of b quarks. In the previous section, we have estimated the lifetime by using a small fraction of events in the tail of the muon impact parameter distribution. In the following, we search for a confirmation based on the entire sample of ghost data. We have seen in the previous section that the impact parameters of muons contained in the same cone are not strongly correlated. This would happen if each muon arise from the decay of a different object. Therefore, we search for secondary vertices produced by pairs of tracks with $p_T \geq 1$ GeV/c and opposite charge contained in a 36.8° cone around the direction of each initial muon. Track pairs are constrained to arise from a common space point. Combinations are discarded if the three-dimensional vertex fit returns a χ^2 larger than 10. If a track is associated with more than one secondary vertex, we discard those with lower fit probability. For each secondary vertex, we define L_{xy} as the distance between the secondary and primary event vertices projected onto the transverse momentum of the two-track system. Combinations of tracks arising from the primary vertex or from

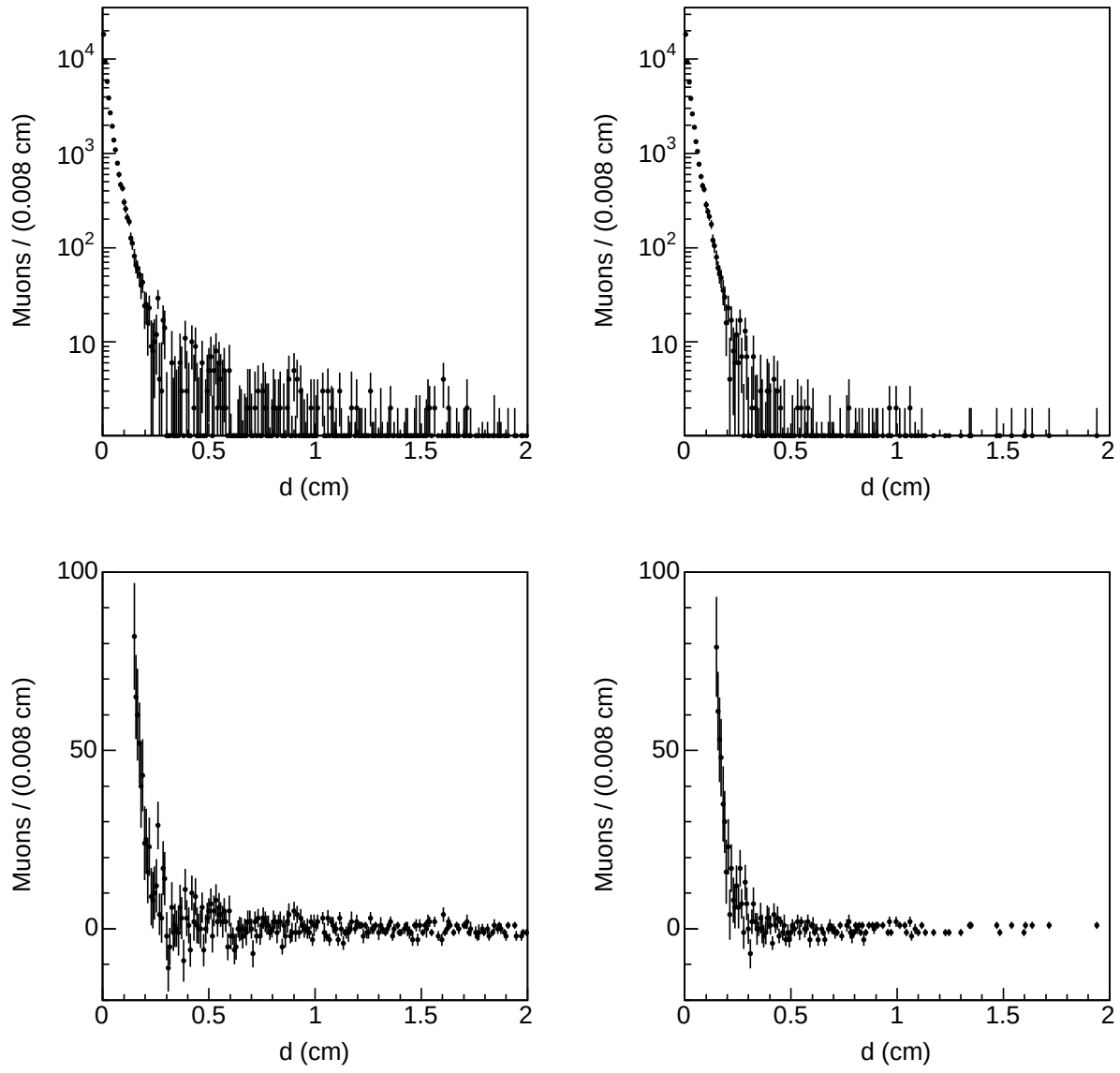

FIG. 27: Impact parameter distributions of CMUP muons which are accompanied by a D^0 meson and are selected without (left) SVX or with (right) loose SVX requirements. The bottom plots are magnified views to show distributions at large impact parameters. The contribution of the combinatorial background under the D^0 signal has been removed with a sideband subtraction method.

the decay of different objects yield a L_{xy} distribution symmetric around $L_{xy} = 0$. An excess at positive L_{xy} is a property of the decay of a long-lived object.

We use $K^0_S \to \pi^+\pi^-$ decays to verify with data the detector response in the impact parameter region populated by ghost events. We search for K^0_S decays in the dimuon dataset

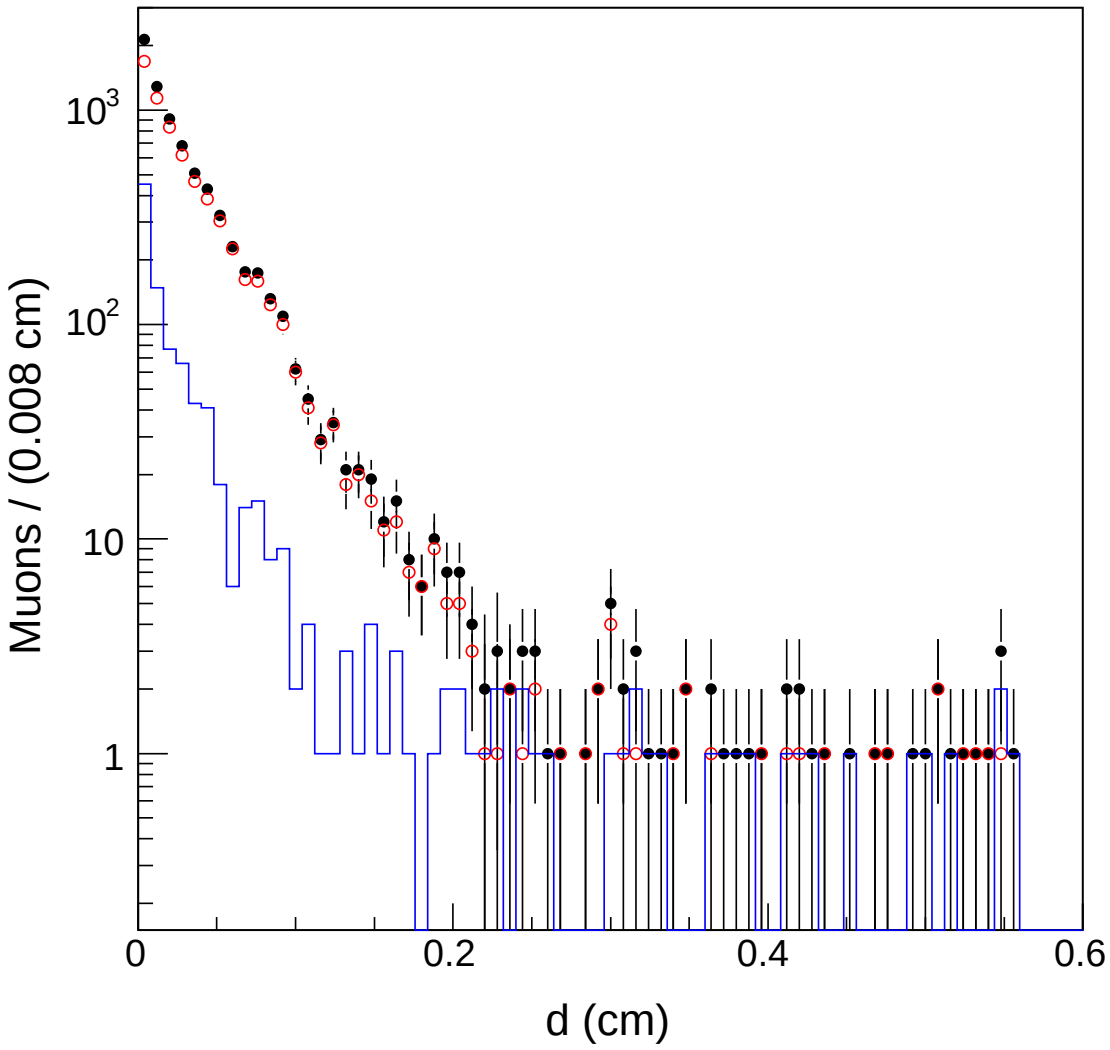

FIG. 28: Impact parameter distributions of muons accompanied by a D^0 meson and selected as the additional muons in this analysis. No SVX requirements are applied. All events (•) are compared to RS (○) and WS (histogram) combinations (see text). The contribution of the combinatorial background under the D^0 signal has been removed with a sideband subtraction method.

used for this analysis by pairing tracks of opposite charge with $p_T \geq 0.5$ GeV/c, $|\eta| \leq 1.1$, and opening angle smaller than 60°. Track combinations are constrained to arise from a common space point. Combinations are discarded if the three-dimensional vertex fit returns a χ^2 larger than 10 or the L_{xy} distance is smaller than 0.1 cm. In this case, the L_{xy} distance is also corrected for the Lorentz boost of the two-track system. Figure 29 (a) shows the

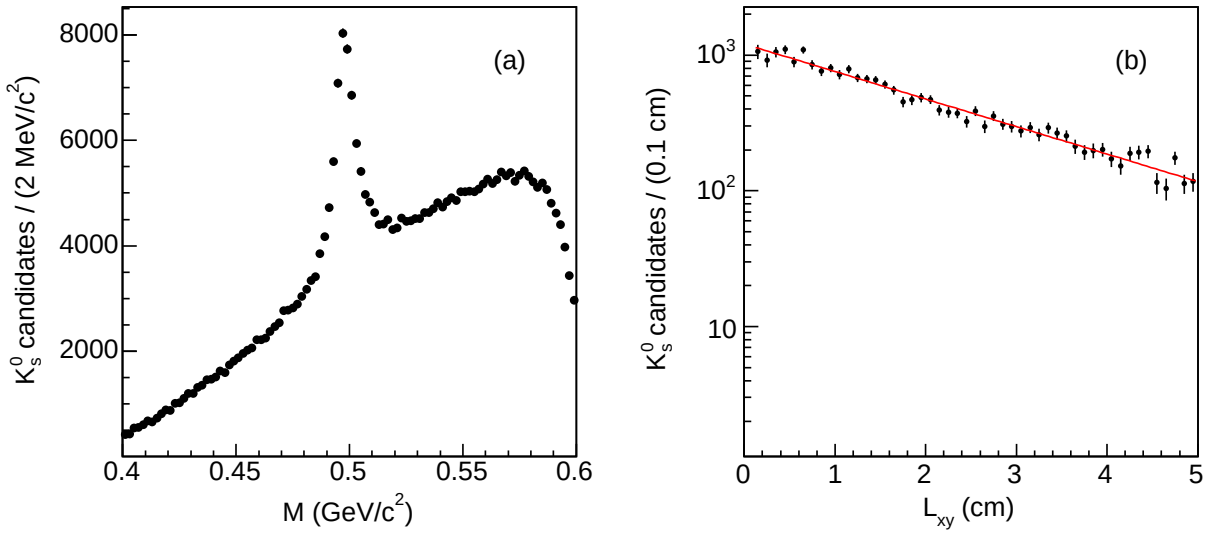

FIG. 29: Invariant mass distribution (a) of $K^0_S \to \pi^+\pi^-$ candidates. The background subtracted L_{xy} distribution of K^0_S mesons (b) is compared to the expectation based on the K^0_S measured lifetime [5].

invariant mass spectrum of the two-track systems passing this selection. The combinatorial background under the K^0_s signal, integrated from 0.486 to 0.510 GeV/c^2, is removed by subtracting the events contained in the side bands $0.474 - 0.486$ and $0.510 - 0.522$ GeV/c^2. The background subtracted L_{xy} distribution, shown in Fig. 29 (b) is consistent with the K^0_S lifetime of 89.5 ps [5].

The distributions of the number of secondary vertices reconstructed in QCD and ghost events are shown in Fig. 30. Figure 31 shows the difference between the positive and negative L_{xy} distributions of secondary vertices reconstructed in QCD and ghost events. The shape of the distribution for ghost events is consistent with the hypothesis that a small but significant fraction of them arise from the production and decay of objects with a lifetime significantly larger than that of b hadrons and smaller than that of K^0_S mesons.

B. Track multiplicity

As discussed in Sec. VI, ghost events include a sizable contribution from ordinary sources such as in-flight-decays, and K^0_S and hyperon decays. The average track multiplicity in ghost events is a factor of two larger than in QCD events. In order to study the average

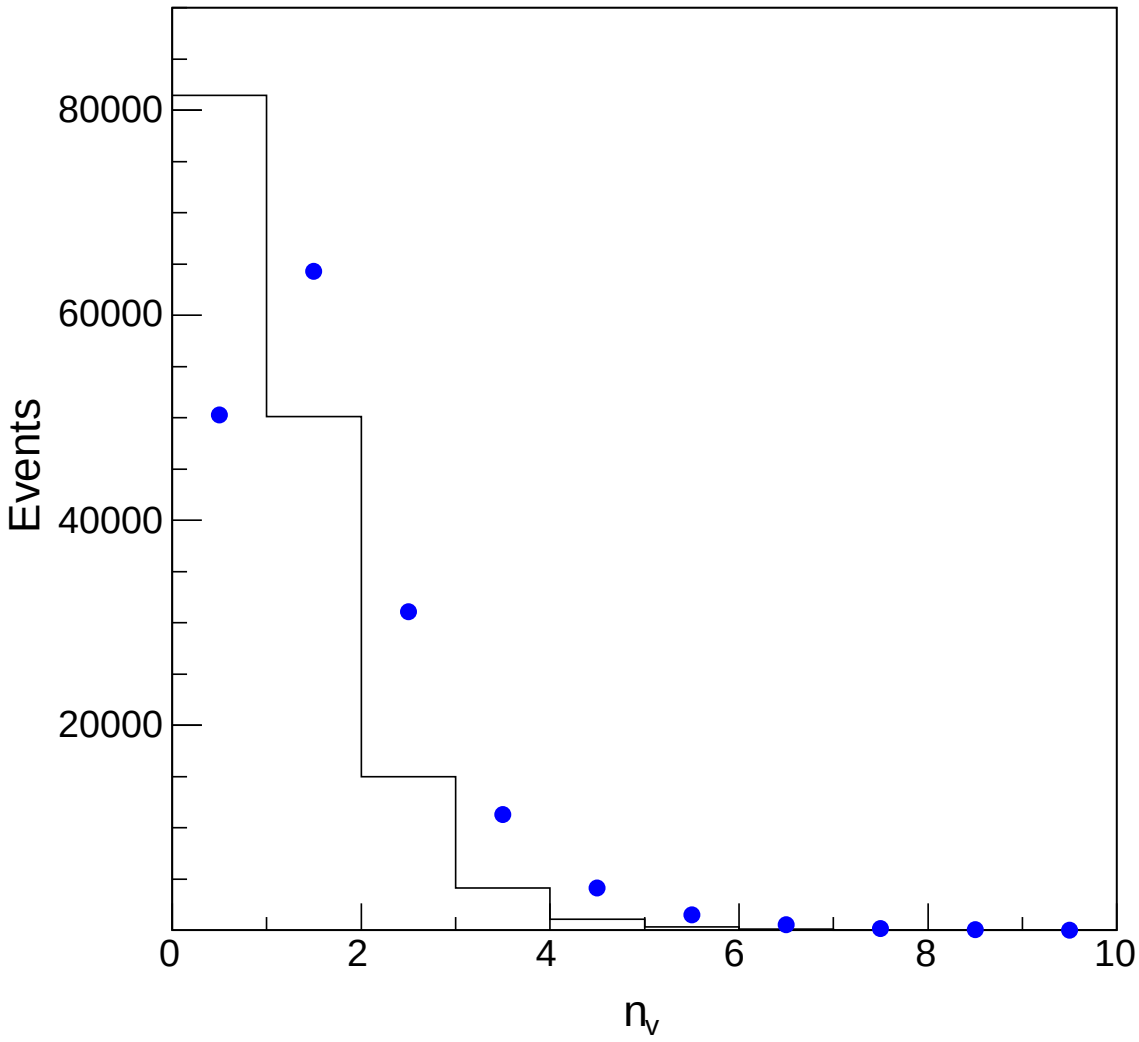

FIG. 30: Distribution of n_v, the number of reconstructed secondary vertices of opposite sign track pairs in QCD (histogram) and ghost (•) events. We use all tracks with $p_T \geq 1$ GeV/c contained in a 36.8° cone around the direction of each initial muon.

multiplicity of multi-muon events, we use events that contain at least three muons in a 36.8° cone. Figure 32 shows the average number of all tracks with $p_T \geq 2$ GeV/c contained in a 36.8° cone around a primary muon as a function of the total transverse momentum of the tracks.

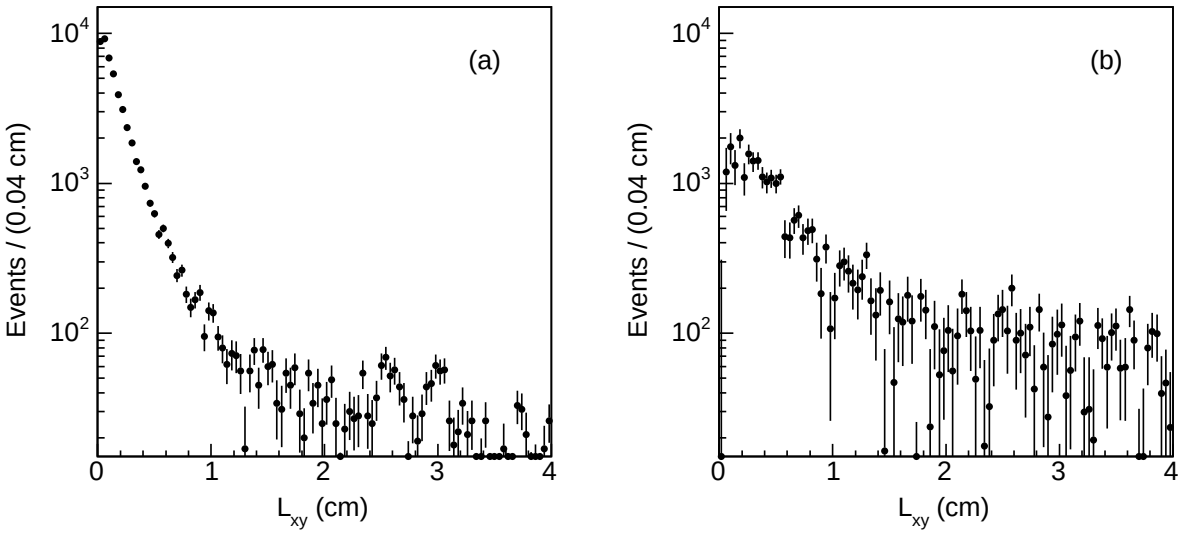

FIG. 31: Distribution of the distance L_{xy} of reconstructed secondary vertices due to long-lived decays in (a) QCD and (b) ghost events. The combinatorial background has been removed by subtracting the corresponding negative L_{xy} distributions. The data correspond to an integrated luminosity of 742 pb^{-1}.

C. Cone correlations

In the previous section, we have investigated the kinematics and topology of muons and tracks contained in a single 36.8° cone around the direction of an initial muon. In this section, we extend the investigation to the rate and properties of events in which two 36.8° cones contain a muon multiplicity larger than that of QCD events. After subtracting the QCD and fake muon contribution, in ghost events there are 27990 ± 761 cones that contain two or more muons, 4133 ± 263 cones that contain three or more muons, and 3016 ± 60 events in which both cones contain two or more muons. It follows that approximately 13% of the ghost events in which one cone contains two or more muons also contain a second cone with the same feature. In events triggered by a central jet, the fraction of events also containing an additional central jet is $10 - 15\%$ depending on the jet transverse energy [28]. Therefore, it is difficult to imagine detector effects that might produce a similar fraction of ghost events with two multi-muon cones.

The following distributions serve the purpose of showing that, when a second cone containing multi muons is found, it has the same characteristics of the first found multi-muon

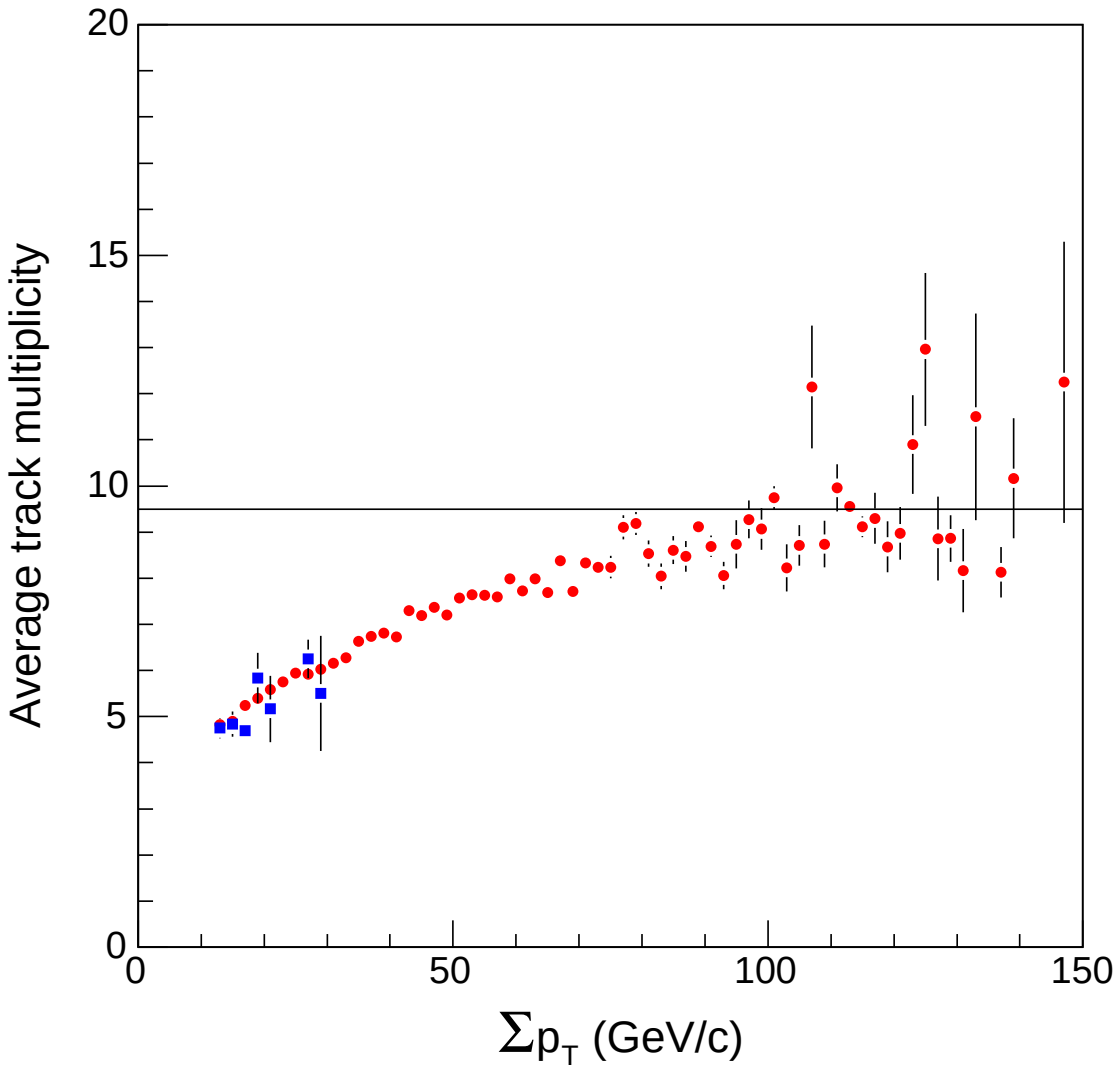

FIG. 32: Average number of tracks in a 36.8° cone around the direction of a primary muon as a function of $\sum p_T$, the transverse momentum carried by all the tracks. We use cones containing at least three muons. Data (•) are compared to the QCD expectation (■) based on the few events predicted by the heavy flavor simulation, normalized to the number of initial dimuons in the data and implemented with the probability that hadronic tracks mimic a muon signal. The detector efficiency for these tracks is close to unity.

cone. Figure 33 plots two-dimensional distributions of the invariant mass of all muons and of the number of tracks with $p_T \geq 2$ GeV/c contained in each cone for the 3016 events containing two cones with two or more muons. Figure 34 shows that the invariant mass distribution

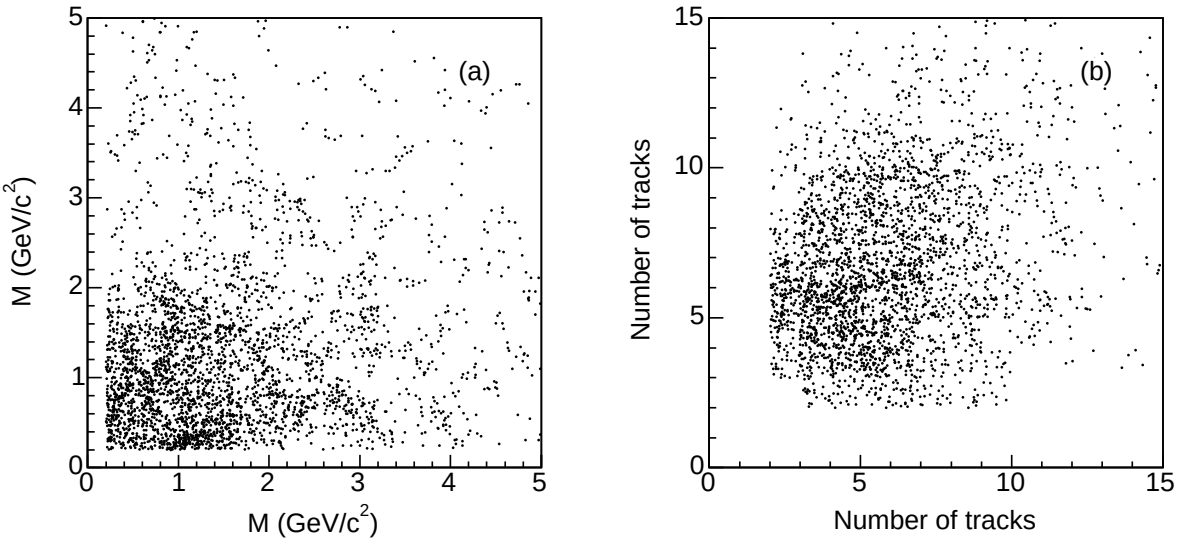

FIG. 33: Two-dimensional distributions of (a) the invariant mass, M, of all muons and (b) the total number of tracks contained in a 36.8° cone when both cones contain at least two muons. The QCD and fake muon contributions have been subtracted.

of all muons contained in the 27990 cones containing at least two muons is consistent with that of the 3016 events in which both cones contain at least two muons. Figure 35 shows the invariant mass distribution of all muons and all tracks with $p_T \geq 2$ GeV/c in events in which both cones contains two or more muons.

Following the procedure outlined in Sec. VII A, we count the number of secondary vertices of two-track systems in events with two cones containing at least two muons. Figure 36 shows the average number of secondary vertices in one cone as a function of the number of secondary vertices in the other cone.

VIII. CONCLUSIONS

We have studied a sample of events containing at least two central muons with $p_T \geq 3$ GeV/c and invariant mass $5 \leq m_{\mu\mu} \leq 80$ GeV/c^2. The data sets were collected with the CDF II detector at the Fermilab Tevatron collider, and correspond to integrated luminosities up to 2100 pb^{-1}. Similar data samples have been previously used by the CDF and DØ collaborations to derive measurements of the correlated $\sigma_{b\to\mu,\bar{b}\to\mu}$ cross section that are inconsistent with the NLO theoretical prediction. A similar data set was used by the

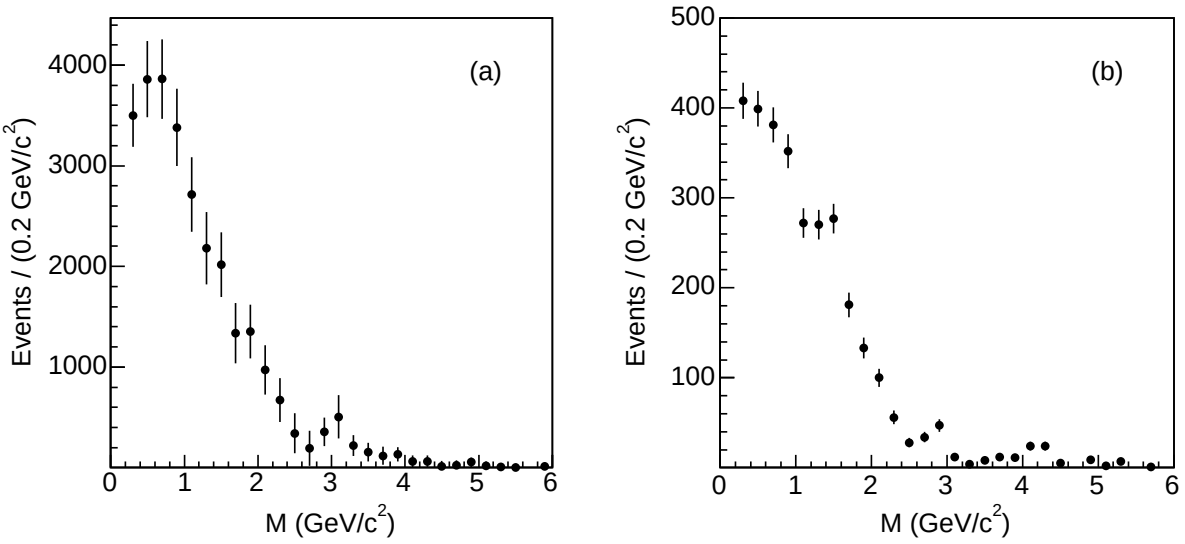

FIG. 34: Distributions of invariant mass, M, of all muons contained in (a) the 27990 36.8° cones with two or more muons and (b) in each cone of the 3016 events in which both cones contain two or more muons. The QCD and fake muon contributions have been subtracted.

CDF collaboration to extract a value of $\bar{\chi}$, the average time-integrated mixing probability of b-flavored hadrons, that is appreciably larger than that reported by the LEP experiments. This analysis extends a recent study [6] by the CDF collaboration which has used a dimuon data sample to re-measure the correlated $\sigma_{b\to\mu,\bar{b}\to\mu}$ cross section. In Ref. [6], the value of $\sigma_{b\to\mu,\bar{b}\to\mu}$ is measured using the sample composition as determined by fitting the impact parameter distribution of these primary muons with the expected shapes from all known sources. The data are well described by contributions from the following QCD processes: semileptonic heavy flavor decays, prompt quarkonia decays, Drell-Yan production, and instrumental backgrounds from hadrons mimicking the muon signal. Reference [6] reports $\sigma_{b\to\mu,\bar{b}\to\mu} = 1549 \pm 133$ pb for muons with $p_T \geq 3$ GeV/c and $|\eta| \leq 0.7$. That result is in good agreement with the NLO prediction as well as with analogous measurements that identify b quarks via secondary vertex identification [26, 27]. The study in Ref. [6] uses a subset of dimuon events in which each muon track is reconstructed in the SVX with hits in the two inner layers and in at least four of the inner six layers. These tight SVX requirements select events in which both muons originate within 1.5 cm from the nominal beam line. According to the simulation, approximately 96% of the dimuon events contributed by known QCD processes satisfy this condition. This study reports the presence of a much

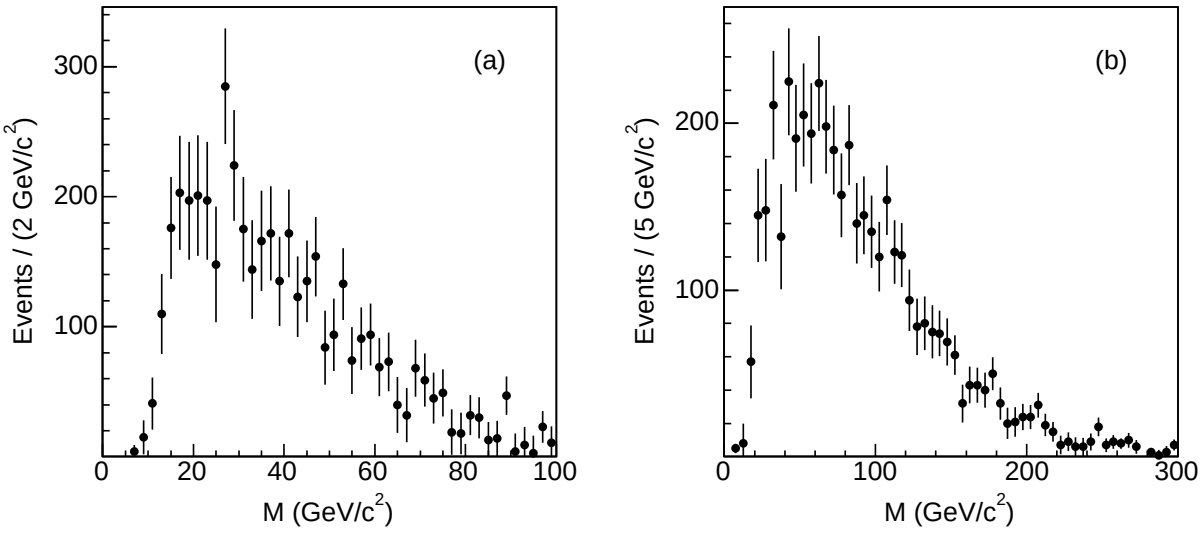

FIG. 35: Invariant mass distribution of (a) all muons and (b) all tracks for events in which both cones contain at least two muons. The QCD and fake muon contributions are subtracted. The data correspond to an integrated luminosity of 2100 pb^{-1}.

larger than expected sample of events, referred to as ghost events, that does not satisfy this condition. This component was present in previous $\sigma_{b\to\mu,\bar{b}\to\mu}$ [7, 8] and $\bar{\chi}$ [4] measurements in which this decay-radius requirement was not made. When applying the tight SVX criteria to initial muons, the invariant mass spectrum of combinations of an initial muon with an additional accompanying muon is well described by known QCD sources and is dominated by sequential semileptonic heavy flavor decays. In contrast, without any SVX requirement the invariant mass spectrum is not well modeled by the QCD simulation and the inconsistencies at low invariant mass reported in Ref. [3] are reproduced. Our study shows that ghost events offer a plausible resolution to these long-standing inconsistencies related to $b\bar{b}$ production and decay. A large portion of these events is due to muons arising from in-flight-decays of pions and kaons or punchthrough of hadronic prongs of K^0_S and hyperon decays. However, a significant fraction of these events has features that cannot be explained with our present understanding of the CDF II detector, trigger and event reconstruction. The nature of these events is characterized by the following properties. Impact parameters of initial muons are distributed differently from those of QCD events. After subtracting the contribution of hadrons mimicking a muon signal, an angular cone of 36.8° around the direction of an initial muon contains a rate of additional muon candidates that is approximately

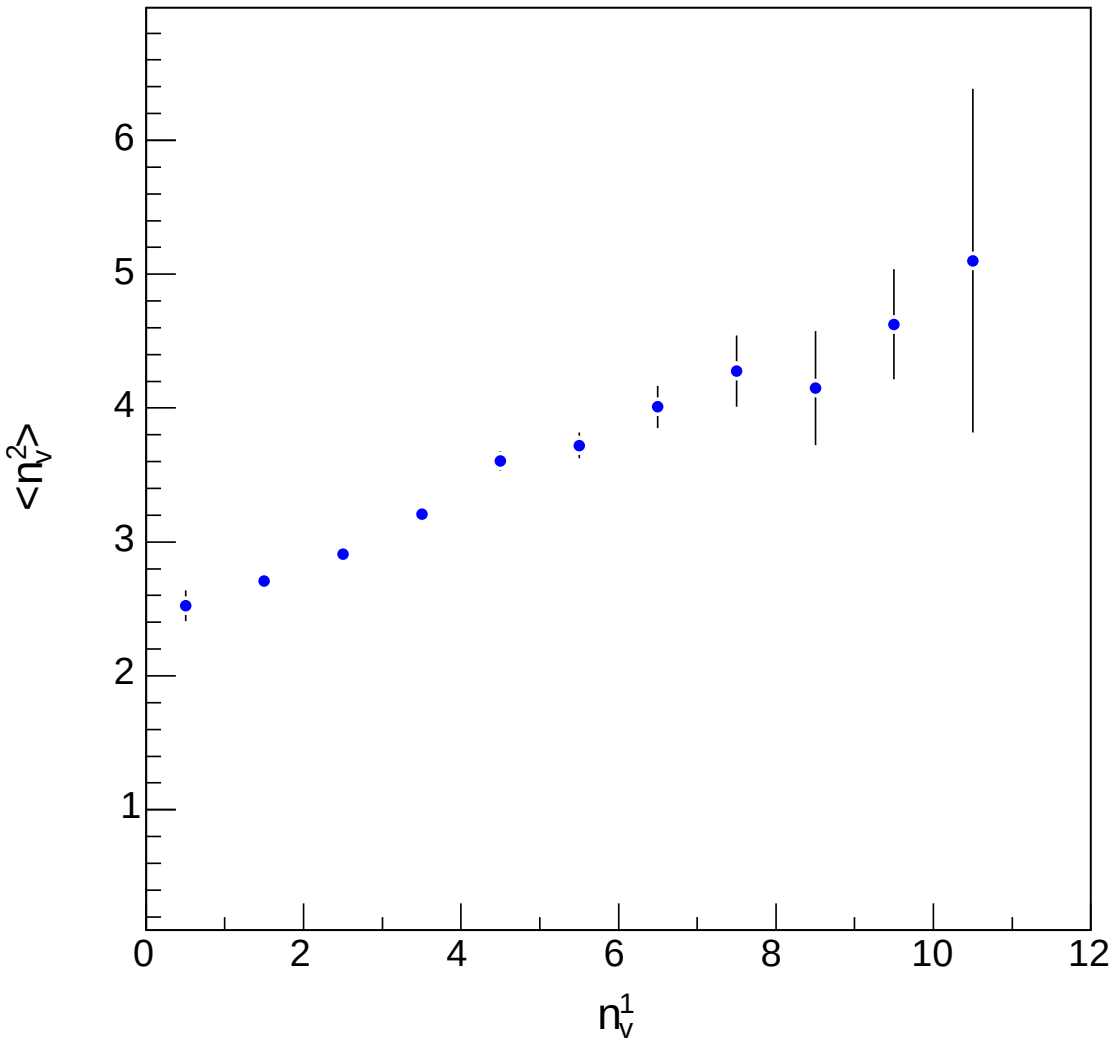

FIG. 36: Average number of secondary vertices, $< n_v^2 >$, in one cone as a function of the number of secondary vertices, n_v^1, observed in the recoiling cone. Both cones contain at least two muons.

four times larger than that of cascade semileptonic decays of b quarks. In contrast with sequential semileptonic decays of b hadrons, initial and additional muon candidates have the same or opposite charge with equal probability. The impact parameter distribution of additional muon candidates, as well as that of secondary vertices reconstructed using tracks contained in a 36.8°, have shapes different from what is expected if they were produced by known long-lived particles. The average number of tracks contained in a 36.8° cone is also two times larger than that of QCD events. We have verified these findings using stricter

analysis selections and several control samples of data. We are continuing detailed studies with longer timescales for completion to better understand the cause of these effects.

IX. ACKNOWLEDGMENTS

We thank the Fermilab staff and the technical staffs of the participating institutions for their vital contributions. This work was supported by the U.S. Department of Energy and National Science Foundation; the Italian Istituto Nazionale di Fisica Nucleare; the Ministry of Education, Culture, Sports, Science and Technology of Japan; the National Science Council of the Republic of China; the Swiss National Science Foundation; the A.P. Sloan Foundation; the Korean Science and Engineering Foundation and the Korean Research Foundation; the Science and Technology Facilities Council and the Royal Society, UK; the Institut National de Physique Nucleaire et Physique des Particules/CNRS; the Russian Foundation for Basic Research; the Ministerio de Ciencia e Innovación, Spain; the European Community's Human Potential Programme; the Slovak R&D Agency; and the Academy of Finland.

APPENDIX A: DETECTOR LEVEL DISTRIBUTIONS IN QCD AND GHOST EVENTS

This appendix presents a few of many detector-level distributions that have been investigated looking for pathologies in track reconstruction, muon reconstruction, detector response, and in the observed properties of the ghost events. The assumption is that detector and pattern recognition failures are not an issue if detector-level distributions for ghost events are similar to those for QCD events, which in turn are correctly modeled by a simulation based on the HERWIG and GEANT Monte Carlo programs.

1. Quality of reconstructed tracks

A visual investigation of the display of reconstructed muon tracks and associated COT and SVX hits has not shown any indication of detector or track-reconstruction program failures. COT tracks reconstructed using hits in at least 20 COT layers are considered well

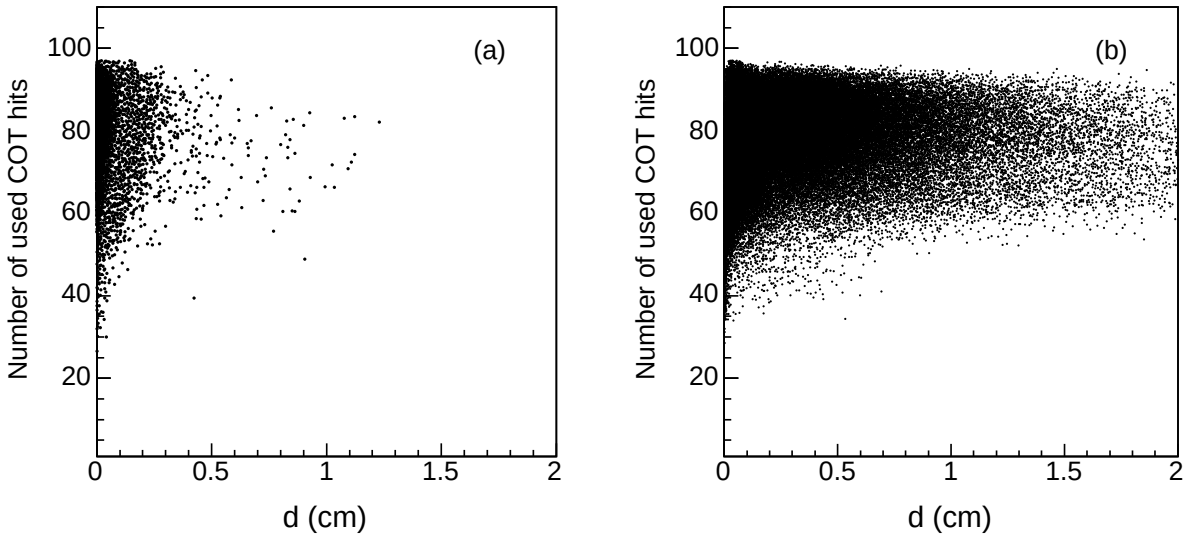

FIG. 37: Number of COT hits associated with initial muon tracks as a function of the track impact parameter for (a) QCD and (b) ghost events.

measured tracks and are used in most CDF analyses. Figure 37 shows the number of COT hits used to reconstruct initial muon tracks as a function of the track impact parameter. In both QCD and ghost events, muon tracks are associated with an average of 75 hits, and the average number of associated hits does not depend on the impact parameter value.

As also shown by cosmic muons in Fig. 3 (b), the impact parameter of COT tracks associated with at least three silicon hits is measured with a rms resolution of approximately 30 μm [6]. We have studied the impact parameter resolution of COT tracks without silicon hits, which populate ghost but not QCD events, by using muons from Υ decays included in our data sample. The impact parameter distribution is shown in Fig. 38. The rms resolution is approximately 230 μm, and the impact parameter distribution is exhausted beyond 0.15 cm. Therefore, the large impact parameter tail characteristic of muons in ghost events is not due to tracks reconstructed without silicon hits. We have studied a large sample of K^0_S mesons reconstructed in the dimuon sample by using COT tracks with and without silicon hits, and with small or very large impact parameters (see Fig. 29). The observed L_{xy} distribution is correctly modeled by the value of the K^0_S lifetime [5]. As shown in Figs. 4, 27, and 28, initial muons in ghost events are not accompanied by D^0 mesons and muons in events acquired with the request of a D^0 meson do not exhibit any large impact parameter tail. It is therefore unlikely that a significant fraction of ghost events arises from detector

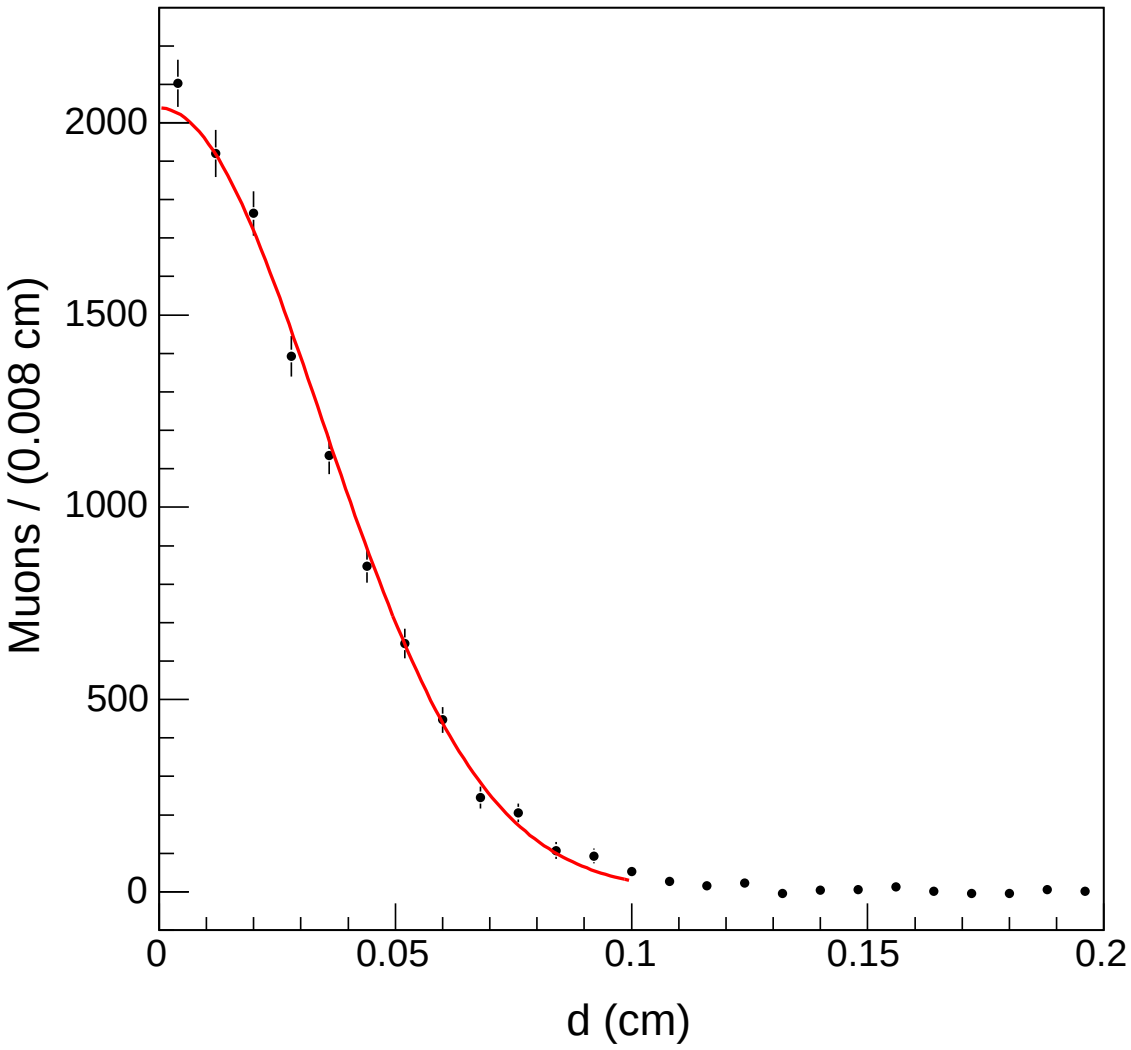

FIG. 38: Impact parameter distribution of tracks corresponding to muons from Υ decays. Tracks are not associated with silicon hits. The combinatorial background under the Υ signal has been removed with a sideband subtraction technique. The solid line is a fit to the data with a Gaussian function.

or pattern recognition failures in standard QCD events.

2. Quality of reconstructed muons

A track is accepted as a muon if the $r-\phi$ distance between its projection onto a muon detector and a muon stub is $\Delta x \leq 30$, 40, and 30 cm for the CMU, CMP, and CMX detector,

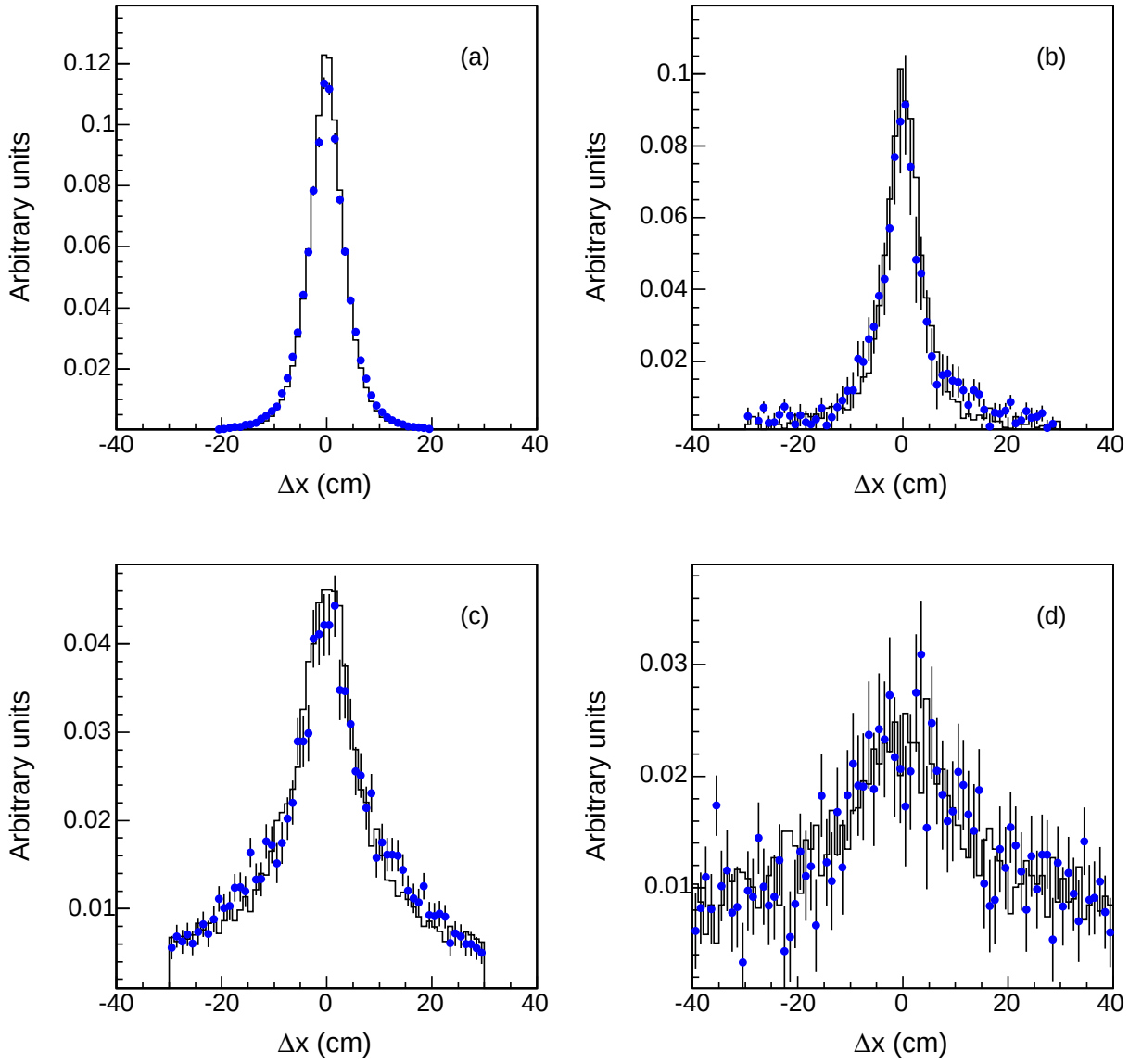

FIG. 39: Distributions of Δx (see text) for (a) initial and (b) additional CMUP muons, and additional (c) CMU or (d) CMP muons in QCD (histogram) and ghost (•) events.

respectively. For CMX or CMU muons, we also construct the quantity $\chi^2 = (\Delta x/\sigma)^2$, where σ is a rms deviation that includes the effect of muon multiple scattering and energy loss. These quantities are compared in Figs. 39 and 40 for initial and additional muons in QCD and ghost events. Table XI shows the fraction of additional muons identified by the different detectors in QCD and ghost events. These matching distributions, as well as the fractional usage of different muon detectors, in ghost events are not significantly different to those of QCD events. Since we are able to predict the rate of additional muons in QCD events,

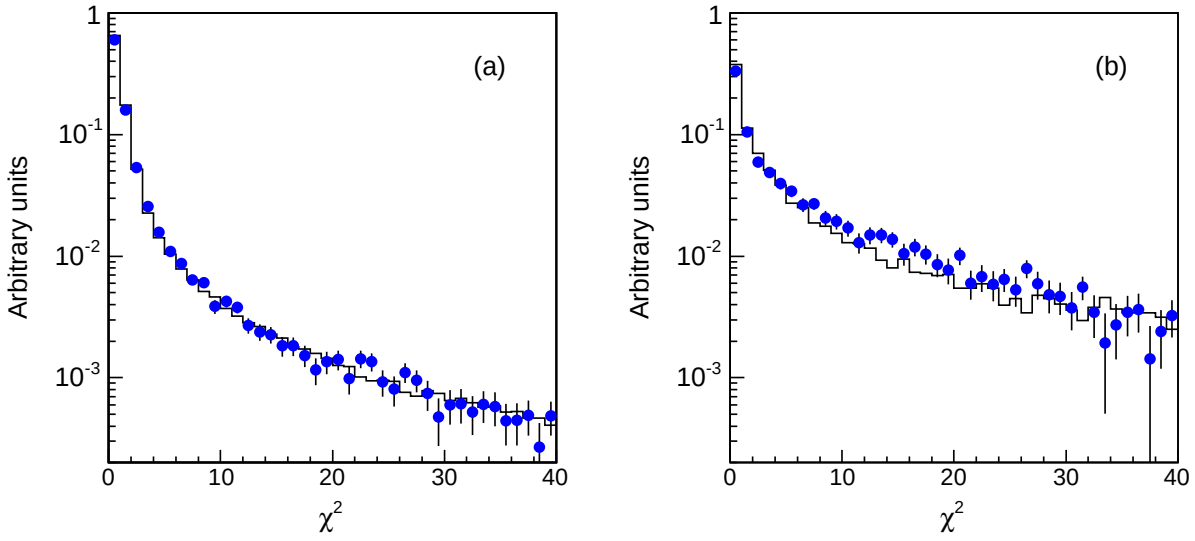

FIG. 40: Distributions of χ^2 (see text) for (a) initial and (b) additional muons in QCD (histogram) and ghost(•) events.

TABLE XI: Fractional contributions (%) to additional muons of different detectors in QCD and ghost events.

Sample	CMUP	CMU	CMP	CMX
QCD	17.0 ± 0.4	53.0 ± 0.7	26.0 ± 0.5	4.0 ± 0.2
Ghost	14.0 ± 0.8	60.0 ± 1.4	24 ± 1	2.0 ± 0.4

the response of the muon detector is an unlikely candidate to explain the large excess of additional muons in ghost events.

The Δx distributions for CMU and CMP muons in Fig. 39 show a significant quasi-flat contribution due to random track-stub matches under the Gaussian signal of real muons. This contribution is negligible for CMUP muons. These features are consistent with the fake muon prediction based on the fake probability per track derived using the decay products of D^0 mesons. For CMUP muons, the fake probability has been verified using the data in Ref. [6]. Ref. [6] estimates the fraction of dimuons due to heavy flavor production that are faked by hadrons from heavy flavor decays in two complementary ways. This fraction is estimated by applying the fake probability per track to simulated hadrons from heavy flavor decays. This fraction is also estimated by simultaneously fitting the impact parameter

distributions of dimuon events selected with loose and tight χ^2 requirements, and therefore containing different fractions of fake muons. The fit result shows that the fraction of fake muons is negligible, and slightly overestimated by the fake probability prediction. This conclusion is also supported by the fact that, when using initial CMUP muons no wrong-sign μD^0 candidates are observed in Fig. 4. The fit to the muon impact parameters in Ref. [6] yields the rate of dimuons due to $b\bar{b}$ and bg production (BB and BP component in Table I, respectively). In the latter case, the muon signal is mimicked by a prompt hadron in the gluon jet. The ratio of these components returned by the fit is 0.194 ± 0.013. When applying the fake probability per track to simulated bg events normalized to the observed $b\bar{b}$ cross section, Ref. [6] predicts this ratio to be 0.21 ± 0.01. These comparisons show that the fake CMUP probability per track cannot be underestimated by more than 10%. Since the rate of fake CMUP muons predicted in Table IX is approximately 4% of the signal, it seems unlikely that the additional CMUP signal in ghost events can be explained by an underestimate of the fake rate. In turn, this supports the main findings of our study that uses all muon detectors since they are consistent with the result based on CMUP muons only. As mentioned in Sec. VI A, the multi-muon signal in ghost events is not affected by selections based on stricter track-stub matching, whereas the fake probability per track models correctly the number of additional muons observed in events in which one initial muon is mimicked by the hadronic leg of a K^0_S decay.

APPENDIX B: ADDITIONAL DATA DISTRIBUTIONS

Figure 41 shows the invariant mass distribution of several combinations of muon and tracks with $p_T \geq 2$ GeV/c and contained in a 36.8° cone around an initial muon.

Figures 42 and 43 show the L_{xy} distributions of three-track systems in ghost and QCD events, respectively. We search for tracks with $p_T \geq 1.0$ GeV/c and $|\eta| \leq 1.1$ in a 36.8° cone around the direction of each initial muon. Track systems with total charge of ± 1 are constrained to arise from a common space point. Three-track combinations are discarded if the three-dimensional vertex fit returns a χ^2 divided by three degree of freedom larger than five.

Similar distributions can be constructed by pairing initial muons with any additional muon contained in a 36.8° cone. The two-track systems are constrained to arise from a

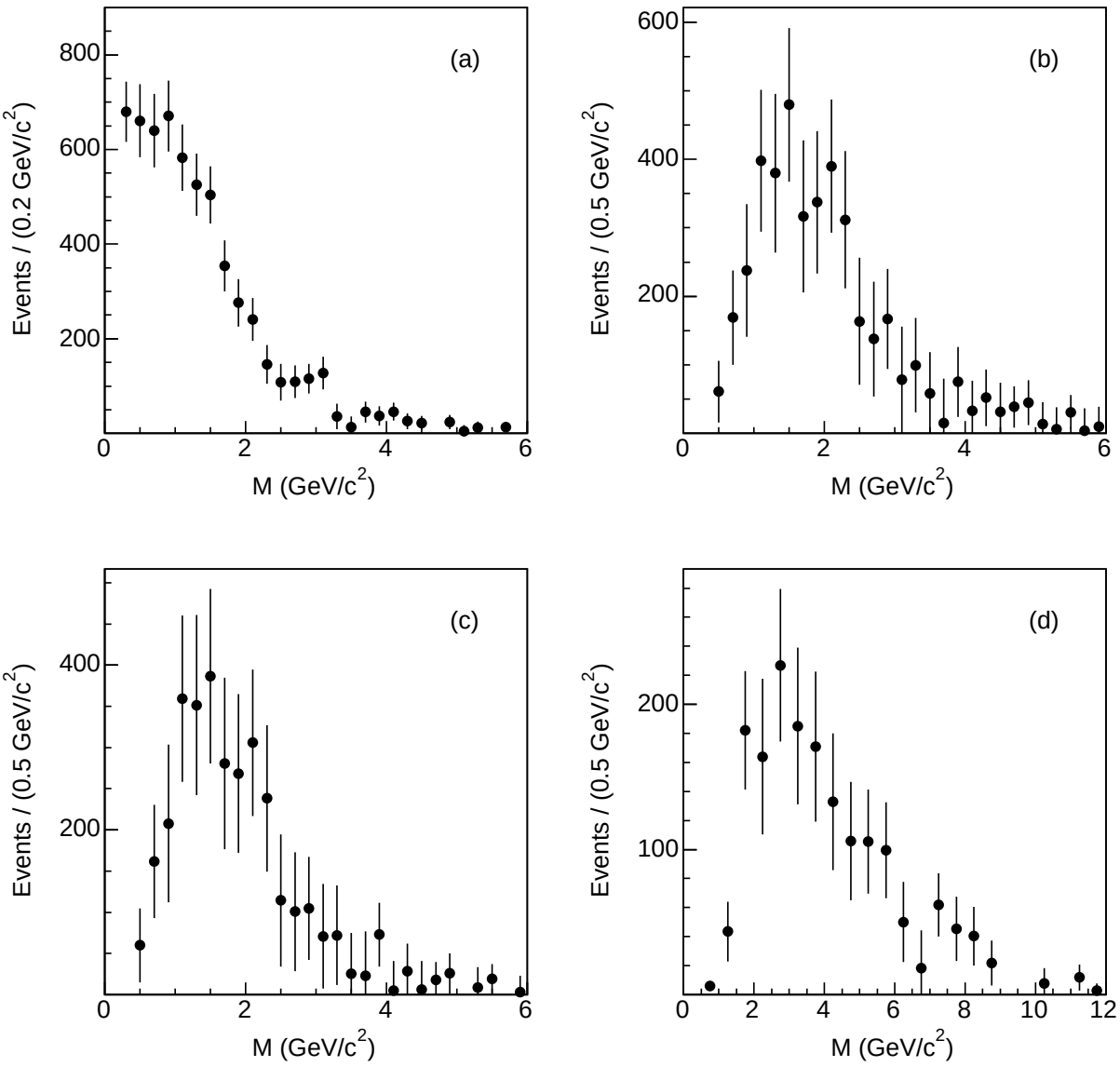

FIG. 41: Invariant mass, M, distributions of all muons in a 36.8° cone when (a) both cones contain at least two muons, (b) a cone contains three or more muons, (c) a cone contains three muons, and (d) of muons and tracks for cones containing 5 to 6 tracks and three or more muons. QCD and fake muon contributions have been subtracted.

common space point, and combinations are discarded if the three-dimensional vertex fit returns a χ^2 larger than 10. The L_{xy} distributions for ghost and QCD events are shown in Fig. 44.

We also select events in which a cone around the direction of an initial muon contains only three tracks with $p_T \geq 1$ GeV/c. Three-track systems with total charge of ± 1 are

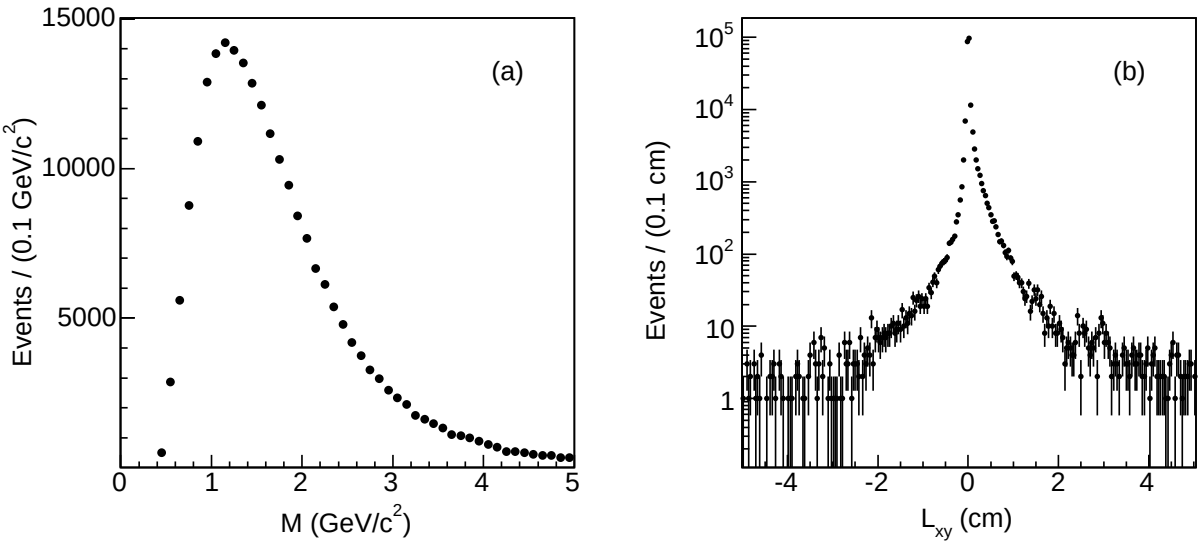

FIG. 42: Distributions of (a) the invariant mass and (b) the distance L_{xy} of three-track systems in QCD events.

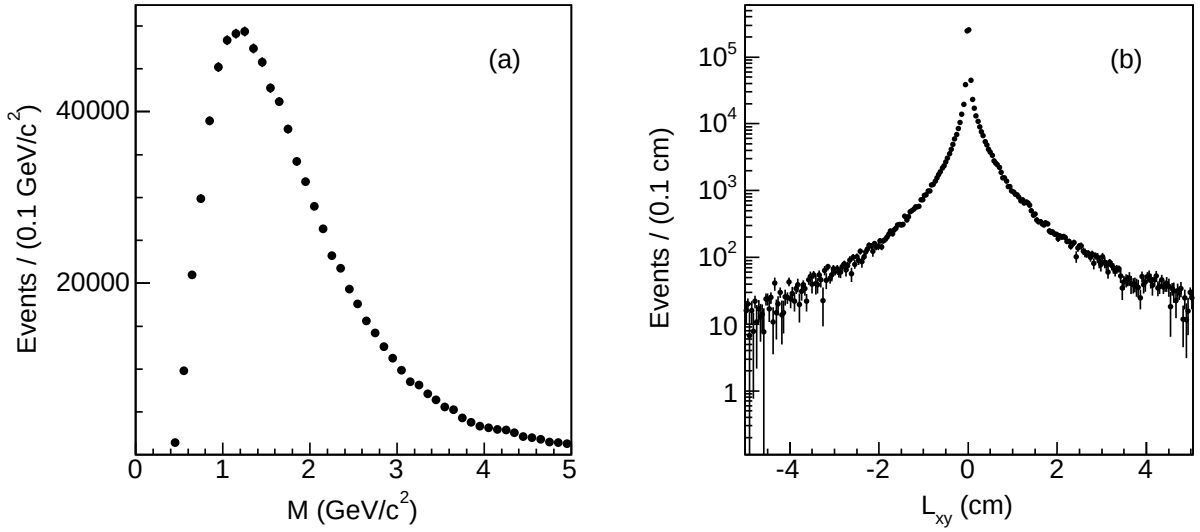

FIG. 43: Distributions of (a) the invariant mass and (b) the distance L_{xy} of three-track systems in ghost events.

constrained to arise from a common space point. Three-track combinations are discarded if the three-dimensional vertex fit returns a χ^2 divided by three degree of freedom larger than five. Figure 45 shows the resulting L_{xy} distribution for ghost and QCD events. Figure 46 compares the invariant mass distribution of the three-track systems for positive and negative

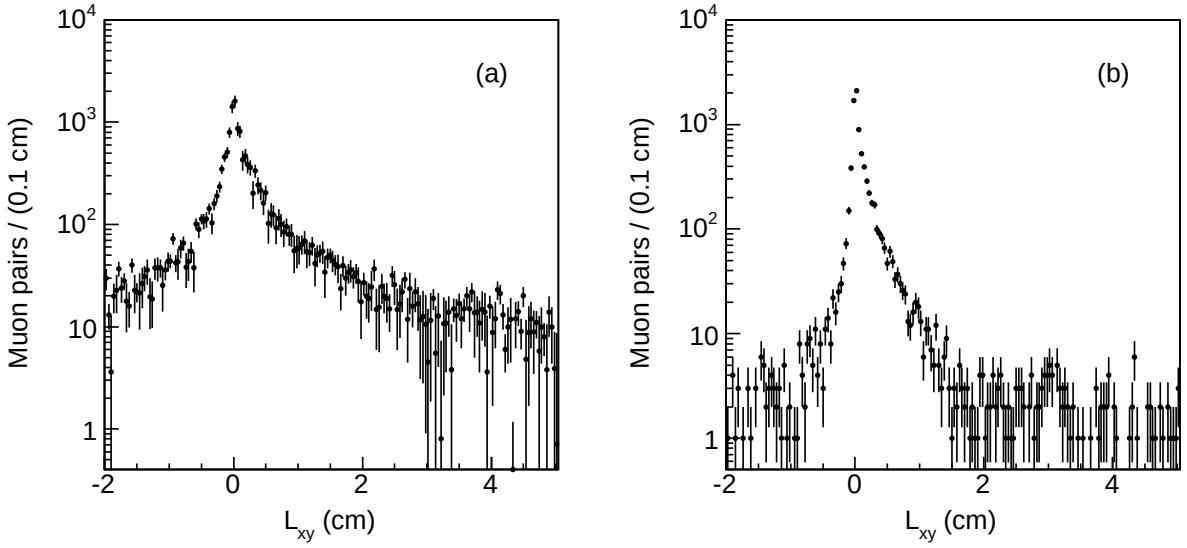

FIG. 44: Distribution of the distance L_{xy} of the fit-constrained vertices of muon pairs contained in a 36.8° cone for (a) ghost and (b) QCD events.

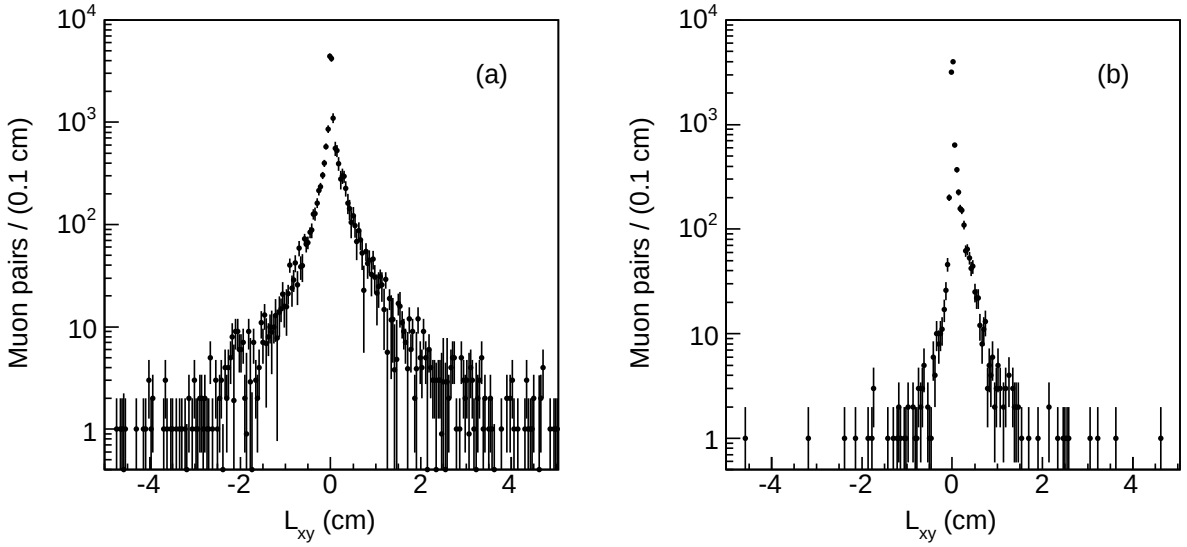

FIG. 45: Distribution of the distance L_{xy} of fit-constrained vertices of three-track systems contained in a 36.8° cone around the direction of an initial muon for (a) ghost and (b) QCD events. We select cases in which angular cones contain only three tracks.

L_{xy} values.

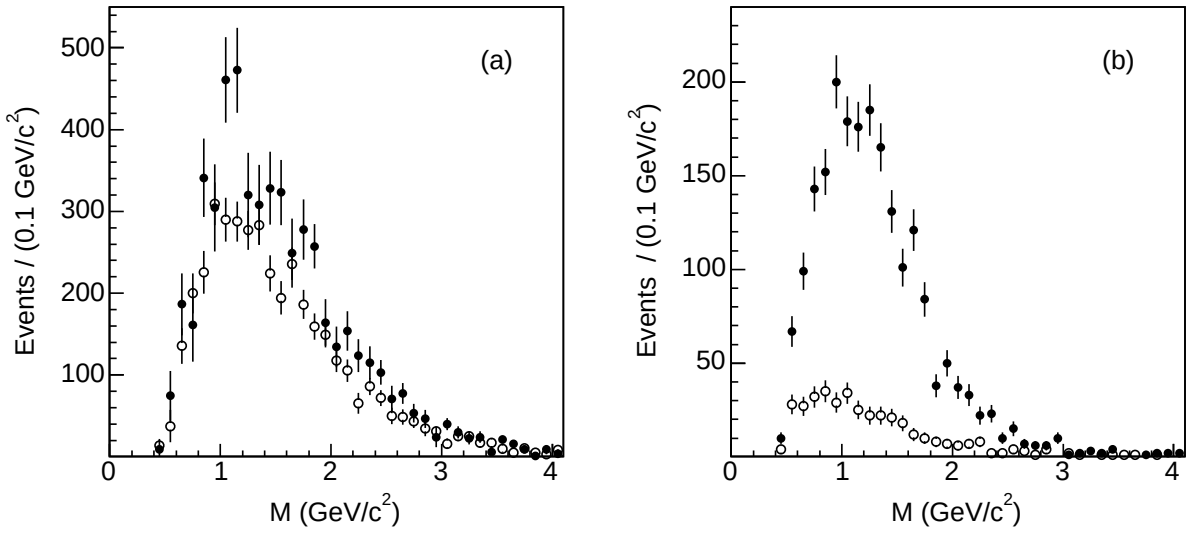

FIG. 46: Distributions of the invariant mass, M, of three-track systems in (a) ghost and (b) QCD events. Systems with distance $L_{xy} \geq 0.04$ cm (•) are compared to those with $L_{xy} \leq -0.04$ cm (○).

[1] M. L. Mangano, P. Nason, and G. Ridolfi, Nucl. Phys. **B373**, 295 (1992).

[2] F. Happacher *et al.,* Phys. Rev. D **73**, 014026 (2006); F. Happacher, *Status of the Observed and Predicted $b\bar{b}$ Cross Section at the Tevatron*, `www − conf.kek.jp/dis06/doc/WG5/hfl20 − happacher.ps`, to appear in the Proceedings of DIS 2006, Tsukuba, Japan.

[3] G. Apollinari *et al.,* Phys. Rev. D **72**, 072002 (2005).

[4] D. Acosta *et al.,* Phys. Rev. D **69**, 012002 (2004).

[5] W.-M. Yao *et al.,* J. Phys. G **33**, 1 (2006).

[6] T. Aaltonen *et al.,* Phys. Rev. D **77**, 072004 (2008).

[7] F. Abe *et al.,* Phys. Rev. D **55**, 2546 (1997).

[8] B. Abbott *et al.,* Phys. Lett. B **487**, 264 (2000).

[9] F. Abe *et al.,* Nucl. Instrum. Methods Phys. Res., Sect. A **271**, 387 (1988).

[10] R. Blair *et al.,* Fermilab Report No. FERMILAB-Pub-96/390-E (1996).

[11] C. S. Hill *et al.,* Nucl. Instrum. Methods Phys. Res., Sect. A **530**, 1 (2004).

[12] A. Sill *et al.,* Nucl. Instrum. Methods Phys. Res., Sect. A **447**, 1 (2000).

[13] T. Affolder *et al.,* Nucl. Instrum. Methods. Phys. Res., Sect. A **453**, 84 (2000).

[14] T. Affolder *et al.,* Nucl. Instrum. Methods Phys. Res., Sect. A **526**, 249 (2004).

[15] G. Ascoli *et al.,* Nucl. Instrum. Methods Phys. Res., Sect. A **268**, 33 (1988).

[16] J. Elias *et al.,* Nucl. Instrum. Methods. Phys. Res., Sect. A **441**, 366 (2000).

[17] D. Acosta *et al.,* Nucl. Instrum. Methods Phys. Res., Sect. A **461**, 540 (2001).

[18] R. Downing *et al.,* Nucl. Instrum. Methods Phys. Res., Sect. A **570**, 36 (2007).

[19] M. M. Block and R. N. Cahn, Rev. Mod. Phys. **57**, 563 (1985).

[20] S. Klimenko *et al.,* Fermilab Report No. FERMILAB-FN-0741 (2003).

[21] B. Ashmanskas *et al.,* Nucl. Instrum. Methods Phys. Res., Sect. A **518**, 532 (2004).

[22] G. Marchesini and B. R. Webber, Nucl. Phys. B **310**, 461 (1988); G. Marchesini *et al.,* Comput. Phys. Commun. **67**, 465 (1992).

[23] D. J. Lange, Nucl. Instrum. Meth. A **462**, 152 (2001). We use version V00-14-05 downloaded from `http://www.slac.stanford.edu/BFROOT/dist/packages/EvtGen/`.

[24] R. Brun *et al.,* CERN Report No. CERN-DD-78-2-REV; R. Brun *et al.,* CERN Programming Library Long Write-up W5013 (1993).

[25] F. Abe *et al.,* Phys. Rev. D **50**, 2966 (1994); T. Affolder *et al.,* Phys. Rev. D **64**, 032002 (2001); D. Acosta *et al.,* Phys. Rev. D **72**, 032002 (2005).

[26] D. Acosta *et al.,* Phys. Rev. D **69**, 072004 (2004).

[27] T. Shears, *Charm and Beauty Production at the Tevatron*, Proceedings of the Int. Europhys. Conf. on High Energy Phys., PoS (HEP2005), 072 (2005).

[28] F. Abe *et al.,* Phys. Rev. Lett. **64**, 157 (1990).